

https://dspace.org/

Synthesis of DI- and trialkylthiourea complexes of Cd, Mn and Ni as precursors for phosphonoacetic acid (PAA)-capped metal sulphide nanoparticles

Mlambo, Mbuso

2010-08-03
http://hdl.handle.net/10539/8347

Downloaded from a DSpace repository. https://dspace.org/

SYNTHESIS OF DI- AND TRIALKYLTHIOUREA COMPLEXES OF Cd, Mn AND Ni AS PRECURSORS FOR PHOSPHONOACETIC ACID (PAA)-CAPPED METAL SULPHIDE NANOPARTICLES

SUBMITTED TO THE FCULTY OF SCIENCE IN FULFILLMENT OF THE REQUIREMENTS FOR THE AWARD OF THE DEGREE OF MASTER OF SCIENCE IN THE SCHOOL OF CHEMISTRY, UNIVERSITY OF WITWATERSRAND

BY

MBUSO MLAMBO

335896

Supervisor

Dr. M. J. MOLOTO

DECLARATION STATEMENT

"I hereby declare that the work on "Synthesis of di- and trialkylthiourea complexes of Cd, Mn and Ni as precursors for PAA-capped metal sulphide nanoparticles is my own work and that all the sources I have quoted have been indicated and acknowledged by means of complete references."

M. MLAMBO (335896)

……

TABLE OF CONTENTS

TITLE PAGE.....I

DECLARATION STATEMENT.....II

ACKNOWLEDGEMENTS…….……VII

CONFERENCE ATTENDED.....VIII

LIST OF TABLES.....IX

LIST OF FIGURES.....X

LIST OF ABBREVIATIONS.....XII

ABSTRACT.....XIII

1. INTRODUCTION.....1

1.1 General background on substituted thioureas. 1

1.2. General background on nanoparticles 3

1.2.1. Electronic properties of semiconducting nanoparticles..... 6

1.2.2 Preparative methods for the synthesis of nanoparticles 8

1.2.2.1 Colloidal route..... 8

1.2.2.2 Synthesis in confined matrices..... 9

1.2.2.3 Metal-organic routes..... 9

1.3.3 Applications of nanoparticles 10

1.3.3.1 Molecular Electronic and Nanoelectronics..... 11

1.3.3.2 Biological Applications 12

1.3.3.3 Textile applications 14

1.3.3.4 Catalytic Application..... 15

1.4 Background on thermal analysis 16

1.4.1 Thermogravimetric analysis..... 18

1.4.2 TGA Instrumentation..... 19

1.4.3 Analytical applications of thermogravimetry 24

1.5 General background on spectroscopy..... 24

1.5.1 Theory of infrared spectroscopy. 25

1.5.2 Theory of NMR spectroscopy..... 25

1.6 Theoretical background to instrumentation use to characterize nanoparticles..... 26

1.6.1 Ultraviolet-visible spectrophotometry..... 26

1.6.1.1 General introduction..... 26

1.6.1.2 Theory of UV-visible spectrophotometry 27
1.6.1.3 Absorbing by organic species 28
1.6.1.4 Absorption by Inorganic species 29
1.6.1.5 Charge-transfer absorption 29
1.6.1.6 Instrument components 30
1.6.1.7 Applications 30
1.6.1.7 (a) Qualitative application of UV/visible spectrophotometry 30
1.6.1.7. (b) Quantitative applications 31
1.6.2 Photoluminescence 32
1.6.2.1 General introduction 32
1.6.2.2 Theory of photoluminescence 32
1.6.2.3 Deactivation processes 34
1.6.2.3 (a) Vibrational relaxation 34
1.6.2.3 (b) Internal conversion 34
1.6.2.3 (c) External conversion 35
1.6.2.3 (d) Intersystem crossing 35
1.6.2.4 Limitations of luminescence measurements 35
1.6.2.5 Applications of photoluminescence 36
1.6.2.6 Application in organic and biochemical species 36
1.6.2.7 Instrument components 36
1.6.3 Electron microscopy 38
1.6.3.1 General introduction 38
1.6.3.2 Theory of transmission electron microscopy 38
1.6.3.3 Limitations 40
1.7 Statement of Objective 41
2. EXPERIMENTAL SECTION 42
2.1 Materials 42
2.2 Instrumentation 42
2.2.1 The following were used for characterization of complexes. 42
(a) Microanalysis 42
(b) NMR and FT-IR spectroscopy 42
(c) Thermogravimetry 43
2.2.2 The following were used for characterizing the nanoparticles. 43

(a) Optical characterization 43
(b) Electron microscopy 43
(c) X-Ray diffraction 43
2.3 Preparation of the complexes. 44
(a) $Mn[SC(NH_2)NH(C_6H_5)]_4Cl$ (I) 44
(b) $Mn[(CH_3)HNCSNH(CH_3)]_2Cl_2$ (II) 45
(c) $Mn[SCN(CH_2CH_2CH_2CH_3)_2NH(CH_2CH_2CH_2CH_3)]_2Cl_2$ (III) 45
(d) $Cd[(CH_3)HNCSNH(CH_3)]_2Cl_2$ (IV) 45
(e) $Cd[(C_6H_5)HNCSNH_2]_2Cl_2$ (V) 46
(f) $Ni[(CH_3)HNCSNH(CH_3)]_2Cl_2$ (VI) 46
(g) $Ni[(SCN(CH_2CH_2CH_2CH_3)_2NH(CH_2CH_2CH_2CH_3)]_2Cl_2$ (VII) 46
2.4 Synthesis of organically-capped nanoparticles 47
2.4.1. Synthesis of PAA-capped nanoparticles 47
2.4.2. Synthesis of PAA/TOPO-capped nanoparticles 47
2.4.3 Synthesis of HDA-capped CdS nanoparticles 48
3. RESULTS AND DISCUSSION 49
3.1 Characterization of the new complexes 49
3.1.1 Spectroscopic studies 50
3.1.1.1 FTIR spectral analysis 50
3.1.1.2 NMR spectral analysis 55
3.1.1.3 Thermal analysis 57
3.2 Characterization of nanoparticles 60
3.2.1 PAA-capped nanoparticles 60
3.2.2 Optical properties of PAA-capped nanoparticles 63
3.2.3 Structural characterization 72
3.3 HDA-capped nanoparticles 76
3.3.1 Optical properties 76
3.3.1.1 HDA-capped CdS nanoparticles 76
3.3.1.2 HDA-capped NiS nanoparticles 78
3.3.2 Structural characterisation 78
3.4 PAA\TOPO-capped nanoparticles 82
3.4.1 Optical properties 82

3.4.2 Structural characterisation 85

3.5 CONCLUSIONS 88

3.6 RECOMMENDATIONS FOR FUTURE WORK 89

3.7. REFERENCES 90

ACKNOWLEDGEMENTS

I would like to pass my words of gratitude to my supervisor Dr M. J. Moloto for his guidance, support and motivation throughout the study. I would also like to be thankful of all the opportunities that he sent on my way. My gratitude goes to the; School of Chemistry at University of Witwatersrand for allowing me to do this work on their premises, CATOMAT group all your support that is highly appreciated and also the technical staff . My research group members Poslet, Nosipho, Nobathembu, Ben, Thandeka and Phindile, guys I would not make it without you.

My deepest gratitude goes to my Family who has been supportive all the way, Mom, late sister Phumlile, Lungi, Xolo, Ronnie, Sibongakonke, my nephews, my little princesses Simphiwe and Slindo. I would also thank my friends, who have been encouraging me Khehla Chili, Phumlani Mdluli, Ndabenhle Sosibo, Sbusiso Mlondo, Sboniso Goqo, Sihle Mnqondo, Simphiwe Msomi, and Sphamandla Ncube. I cannot leave the greatest Almighty, I would not be where I am right now beside your strength!

Lastly, I would to be grateful to NRF, University of Zululand and University of Witwatersrand for a financial support and laboratory space and equipment used for research.

CONFERENCE ATTENDED

1. Inorganic Chemistry Conference (Poster)

Title: Synthesis of *N,N,N'*-trialkylthiouea of Cd, Mn and Ni as precursors to the PAA-capped nanoparticles. Club Mykonos, Western Cape, South Africa 8 - 12 July 2007

2. International Conference of Materials Research held at Richards Bay Science centre hosted by the Jackson State University and University of Zululand, July 29-August 1, 2007. (Poster).

Title: Synthesis of *N,N,N'*-trialkylthiouea of Cd, Mn and Ni as precursors to the PAA-capped nanoparticles.

3. NanoAfrica 2009 International conference. (Oral)

Title: Synthesis of substituted thioureas complexes of Cd and Mn as precursors for PAA-capped metal sulphide nanoparticles. Held on 1 to 4 February 2009 at CSIR ICC, Pretoria.

LIST OF TABLES

Table 1: Absorption of ultraviolet and visible light and colour. 27
Table 2 : Selected IR data for all metal complexes and free ligands 54
Table 3: Band edges and corresponding emission peaks of CdS at different temperature 67
Table 4: Band edges and corresponding emission peaks of MnS nanoparticles at different temperatures 69
Table 5: Band edges and corresponding emission peaks of NiS nanoparticles at different.... 71

LIST OF FIGURES

Figure 1: Structure of phosphonoacetic acid. 6
Figure 2: The spatial electronic state diagram showing the quantum confinement effect in bulk semiconductor (a) and nanoparticles (b)..... 7
Figure 3: Typical compositional analysis..... 18
Figure 4: Block diagram of TGA system. 21
Figure 5: Energy diagram for the transitions in UV region. 29
Figure 6: Example of UV-Vis double beam instrument. 30
Figure 7: Photoluminescence energy diagram 33
Figure 8: Schematic diagram of a fluorimeter. 37
Figure 9: Layout of optical components in a basic TEM 40
Figure 10 : Infrared spectrum of complex V 51
Figure 11: Infrared spectra of free phenylthiourea ligand..... 52
Figure 12: Infrared spectra of complex VI 52
Figure 13: Infrared spectrum of free dimethylthiourea ligand 53
Figure 14: NMR spectra of ^{1}H (a) ^{13}C (b) of $Mn[(C_6H_5)HNCSNH_2]_2Cl_2$ 56
Figure 15: NMR spectra of ^{1}H (a) and ^{13}C (b) of $Cd[(C_6H_5)HNCSNH_2]_2Cl_2$..... 56
Figure 16: TGA spectrum of complexes II, IV, V and VII. 58
Figure 17 : TGA curve of complex I..... 60
Figure 18: Schematic diagram showing the effect of reaction parameters on the morphology of nanoparticles. 61
Figure 19: TEM image of CdS nanoparticles synthesized at 150 °C (a) and 240 °C (b)..... 62
Figure 20: TEM (a) and HRTEM (b) image of HDA-capped CdS nanoparticles at 180 °C. . 63
Figure 21: Absorption spectra of PAA-capped CdS from complex V at different temperatures, 120 (a), 160 (b) and 200 °C (c). 65
Figure 22: Emission spectra of PAA-capped CdS nanoparticles from complex V at different temperatures 120 (a), 160 (b) and 200 °C (c). 66
Figure 23: Absorption spectra of PAA-capped MnS from complex III at different temperatures 120 °C (a), 160 °C(b) and 200 °C(c). 67
Figure 24: Emission spectra of PAA-capped MnS nanoparticles from complex III at different temperatures 120 °C(a), 160 °C(b) and 200 °C(c). 69
Figure 25: Absorption spectra of PAA-capped NiS nanoparticles from complex VII at different temperatures 160 °C (a) and 200°C(b). 70

Figure 26: Emission spectra of PAA-capped NiS nanoparticles from complex VII at different temperatures 160 °C (a) and 200°C(c). 71
Figure 27: TEM image (a) of PAA-capped CdS nanoparticles at 160 °C, (b) corresponding particle size distribution histogram and TEM image at 200 °C(c)..... 73
Figure 28: TEM image of PAA-capped MnS nanoparticles from complex III prepared at 200 °C..... 74
Figure 29: TEM micrograph of PAA-capped NiS from complex VII at (a) 160 °C. 75
Figure 30: Absorption spectra of HDA-capped CdS from complex IV at different temperatures 120 °C (a), 160 °C (b) and 200 °C(c). 76
Figure 31: Emission spectra of HDA-capped CdS nanoparticles from complex IV at different temperatures 120 °C (a), 160 °C (b) and 200 °C(c). 77
Figure 32: Absorption (a) and emission (b) spectra of HDA-capped NiS nanoparticles synthesized from complex VI at 160 °C..... 78
Figure 33: TEM images and corresponding particle size distribution histograms of HDA-capped CdS nanoparticles from complex IV, prepared at 120 °C (a), (b), and at 160 °C (c), (d). 79
Figure 34: TEM micrographs of HDA-capped MnS nanoparticles from complex I, prepared at 120 °C (a), 160 °C (b) and 200 °C (c). 80
Figure 35: The XRD pattern of HDA-capped CdS nanoparticles from complex VI..... 81
Figure 36: The XRD pattern of HDA-capped MnS nanoparticles from complex I 81
Figure 37: Absorption (a) and Emission (b) spectra of TOPO/PAA-capped CdS nanoparticles synthesized from complex V at 160 °C. 83
Figure 38: Absorption (a) and emission (b) spectra of TOPO/PAA-capped MnS nanoparticles synthesized from Complex II at 160 °C. 84
Figure 39: Absorption (a) and emission (b) spectra of TOPO/PAA-capped NiS nanoparticles synthesized from Complex VI at 160 °C..... 85
Figure 40: TEM image of TOPO\PAA-capped CdS nanoparticles from complex V at 160 °C 86
Figure 41: TEM image of TOPO\PAA-capped NiS nanoparticles from complex VI, at 160 °C..... 86

LIST OF ABBREVIATIONS

Chemical reagents

PAA	**phosphonoacetic acid**
HDA	**hexadecylamine**
TOPO	**trioctylphosphine oxide**
TOP	**trioctylphosphine**

Instrumentation

IR	**infrared spectroscopy**
NMR	**nuclear magnetic resonance spectroscopy**
PL	**photoluminescence spectroscopy**
SEM	**scanning electron microscope**
TEM	**transmission electron microscope**
TGA	**Thermogravimetric analysis**

Symbols

a.u.	**arbitrary units**
v	**frequency**

ABSTRACT

Many studies on thiourea and its derivatives in different metal (II) complexes have confirmed that coordination is through the sulphur atom. The bonding of substituted thioureas to different metals was confirmed with a combination of spectroscopic studies such as IR and NMR spectroscopy and elemental analysis. A series of metal (II) di- and trialkylthioureas complexes have been synthesized and characterized. Their bonding through sulphur atoms rendered these complexes good precursors for the preparation of metal sulphide nanoparticles. Thermogravimetric analysis on the complexes was undertaken to check their suitability as precursors for the synthesis of nanoparticles and their potential as precursors for metal sulphide thin films using the chemical vapour deposition (CVD) technique and their general chemical and thermal stability.

All the complexes reported in this work were used as single source molecular precursors for the synthesis of cadmium, manganese and nickel sulphide nanoparticles. In this study the investigation on the influence of capping agent and temperature on the size and morphology of nanoparticles was undertaken. Nanoparticles obtained by thermolysis of precursors in phosphonoacetic acid (PAA) were bigger in size and rod-shaped compared to smaller rods obtained in hexadecylamine (HDA). CdS nanoparticles prepared using PAA as a capping agent showed a huge blue-shift of the band edge from the bulk of 515 nm, compared to CdS nanoparticles obtained using HDA as a capping agent. When PAA was mixed with trioctylphosphine oxide (TOPO), a blue shift of band edges in all the bulk materials of different metal sulphides prepared was observed and the rod-shaped nanoparticles changed to spherical particles.

1. INTRODUCTION

1.1 General background on substituted thioureas.

Thioureas and their derivatives are potentially very versatile ligands, there are able to coordinate to a range of metal centers as either neutral ligands,[1] monoanions,[2] or dianions[3, 4]. In addition, the hard nitrogen and soft sulphur donor atoms provide a multitude of bonding possibilities. Previously the most attractive feature of their chemistry was their ease of synthesis, and the ready modification of the substituent's on nitrogen and hence their physical and chemical properties.

In modern days more interest is on their use as a sulphur source and their binding ability through sulphur atoms for complex formation. Many studies have shown that thioureas and their derivatives are capable of binding through the sulphur atom rather than nitrogen atom. There have been many studies on substituted thioureas coordinated to metals through sulphur. For example, Moloto *et al*[5,6] has reported the reaction between a number of N-alkyl substituted thioureas and lead, copper and cadmium. Thiourea complexes have been used as staring materials in chemical spray pyrolysis (CSP) processes which are used to produce thin films of binary and tertiary sulphides.[7, 8] Also, Moloto[9] and Nair[10] have reported the use of thioureas and their substituted constituents for the preparation of metal sulphide nanoparticles.

The study of N-benzoyl-N'-alkylthioureas and N-benzyl-*N', N'*-dialkylthioureas has recently attracted much interest in the view of their potential use as highly selective reagents for the concentration and separation of metal cations. Some of these complexes have been synthesized and studied[11-14]. One of the specific uses for these compounds is their coordination with harmful compounds; organism can be bound to one of the several ligands that have been synthesized to

date. This is an important aspect and in future more attention will be devoted to the design and synthesis of new agents able to coordinate these toxic metal ions with a view of forming complexes that can be readily eliminated from the host environment. Another specific use of these compounds is as an extraction agent which can be used to extract metal cations.[15] Platinum-thiourea complexes have also attracted interest for their biological activity.[11] Metal cluster complexes with coordinated thiourea monoanions are also well known.[16] However, there are relatively few examples of mononuclear metal complexes of simple alkyl- or aryl-substituted thiourea monoanions, containing N,S-chelated ligands; examples of chromium(III),[17] rhodium(III),[18] technetium(III),[19] rhenium(V),[20,21] aluminium,[22] ruthenium,[23,24] osmium,[24] and iridium.[24] Aliphatic and aromatic thiourea compounds have demonstrated antimicrobial behavior against different micro-organisms. Thioureas have strong antifungal activities comparable to the activity observed for common antifungal antibiotic, ketoconazole,[25] and their antimicrobial and insecticidal properties have been documented in the past 56 years.[26] Thioureas can be used not only in the control of plant pathogenic fungi[27,28] but also they have been shown to possess antitubercular, antithyroid, anthelmintic, antibacterial, insecticidal and rodenticidal properties.[26,29-31]

In our work the interest is on studying the interaction of di- and trialkylthiourea molecules with metals such as cadmium(II), manganese(II) and nickel(II). The binding of di- and trialkylthiourea ligands through the sulphur atom of the CS group suggest that they could be used as a potential single source precursor for nanoparticle preparation. Thermal analysis can be used to give information about the possibility of formation of metal sulphide formation which is usually in small percentage. Most complexes of thioureas are characterized by amongst other techniques

FTIR and NMR spectroscopy and thermal stability from TGA studies. TGA studies provide information to evaluate the use in chemical vapour deposition for deposition of thin films.

1.2. General background on nanoparticles

Research on nanoparticles has become a major interdisciplinary area of science and has attracted significant scientific and industrial interest during the last decade.[32-36] These materials are current of interest, and have a huge potential to develop as important classes of materials for electronics and photonics in the current century. This field of research has been widely recognized as one of the most promising and rapidly emerging research areas in various scientific disciplines. The functional materials for information storage have stimulated a great interest in recent years, with metal sulfide semiconductor nanomaterials being an area of intense activity.[37-39] The ultimate scientific and technological impact of these materials mainly depend on their electronic, optical, and catalytic properties. Hence, the studies concerning quantum and electronic confinement observed in these materials are of exceptional importance.

Semiconductor nanoparticles are generally considered to be particles of about 1-20 nm diameter. As a result a whole lot of emphasis has been put into the production of nanoparticles of the highest quality. Nanotechnology is the development and utilization of structures and devices with size range from 1 nm (molecular size) to about 50 nm where new physical, chemical and biological properties occur as compared to bulk materials. Particulate semiconducting materials with small dimensions in the order of nanometers are often referred to as quantum dots, Q particles or nanoparticles. Nanoparticles have a large ratio of surface atoms to those located in

the crystal lattice.[9] Strong confinement is most readily achieved in narrow band-gap semiconductors, in which the excitons have large Bohr radii.[40]

Over the past 25-30 years, remarkable progress has been made in synthesis of nanomaterials using various methods. The II-VI semiconductor quantum dots are materials of immense interest since they exhibit a wide range of electrical and optical properties that are tunable by tailoring the sizes and shapes of nanocrystals. Consequently they find potential applications in optoelectronic devices.[41, 42] One of the first attempts to produce II-VI nanoparticles by Spendel, *et al*.[43, 44] was the synthesis of the colloidal suspensions where CdS was formed by precipitation of Cd^{2+} in aqueous solution by adding H_2S. Growth was controlled conveniently by using heterogeneous media, which was pioneered by Steigerwald and Brus, [45] and Petit, *et al*.[46] Subsequent interest was devoted to the study on the synthesis of II-VI quantum dots using an organometallic route developed by Bawendi, [47] Alivisatos[48] and their co-workers. The resultant nanoparticles prepared by this method were made from metal alkyls at elevated temperatures, which was clearly undesirable for the health and safety reasons. A significant breakthrough was established when Trinidade and O'Brien [49, 50] investigated the dithio- and diselenocarbamate cadmium complexes as single source molecular precursors for the preparation of TOPO-capped II-VI materials.

The use of a single-source molecular precursor is a better route since it avoids problems encountered by employing the organometallic route, since the metal chalcogenide bond is already in place in this route. Revaprasadu *et al*.[51] also reported the synthesis of many metal chalcogenide nanoparticles using single source precursors. Thiourea, xanthate and the

thiosemicarbabazide complexes of cadmium and zinc were also used by Revaprasadu *et al*.[51] and Nair, *et al*.[10, 52] as the single source precursors to synthesize the nanoparticles that displayed both isotropic and anisotropic morphologies. The HDA-capped CdS nanoparticles prepared by the single-source precursor method has been reported,[9, 53] where the control of the shape and size of nanocrystals was affected by the reaction conditions such as reaction temperature, monomer concentration and reaction time. It is well known that strong intermolemolecular forces, such as van der Waals attraction and π-π interactions contribute to the aggregration of nanoparticles. This it is challenge to obtain monodispersed nanopartilces. Different ligands, such as polymers and surfactants, have been used to modify the surface of nanoparticles fro stabilization and the growth control. Murray *et al*[54] synthesized CdS nanoparticles by pyrolysis of organometallic reagents by injection into a coordaniting solvent, TOPO. Particle size control with stabilizers like thiols [55.56] and mercaptopropionic acid [55] have been reported.

This work reported the synthesis of phosphonoacetic acid (PAA) (Figure 1) capped metal sulphides nanoparticles of Cd, Ni, and Mn using a single-source precursor method from their substituted thiourea complexes. Due to their small sizes, nanoparticles are highly unstable; therefore they require a stabilizing chemical environment.

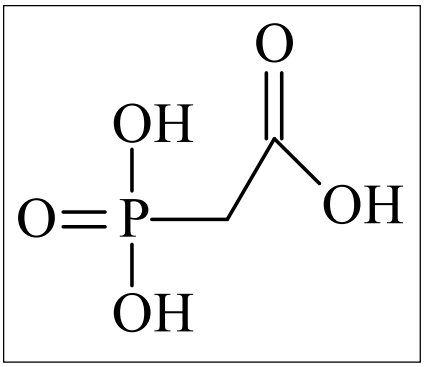


Figure 1: Structure of phosphonoacetic acid.

Ligands such as PAA used in the preparation of nanoparticles may lead to multifunctional adsorption on the surface. There are two possible adsorption sites in PAA, the COOH functional group and the phosphate functional group. PAA has a melting point ranging from 143 - 146 ^{o}C. This molecule has many biological actions. For example it is known to be active against the herpes simplex virus in mice and rabbits[54], and related virus in vitro and in vivo[55, 56]. It selectively inhibits herpes virus induced polymerase[57]. Since the PAA anion is a chelating agent, many biological actions of PAA might be related to its metal complexing ability. It has also been used as a chelating agent in Cu-PAA and Zn-PAA with glycinate (Gly) and histidine (His) which have shown stability. PAA used in this work was found to be insoluble in most solvents like alcohols, it was only slightly soluble to tetrahydrofuran (THF) and water.

1.2.1. Electronic properties of semiconducting nanoparticles

One of the defining features of a semiconductor is the energy gap separating the conduction and the valence energy bands, which is influenced by the size of the particles. The color emitted by a semiconductor material is determined by the width of the gap. Generally with nanoparticles the smaller the particle size the higher the band gap.

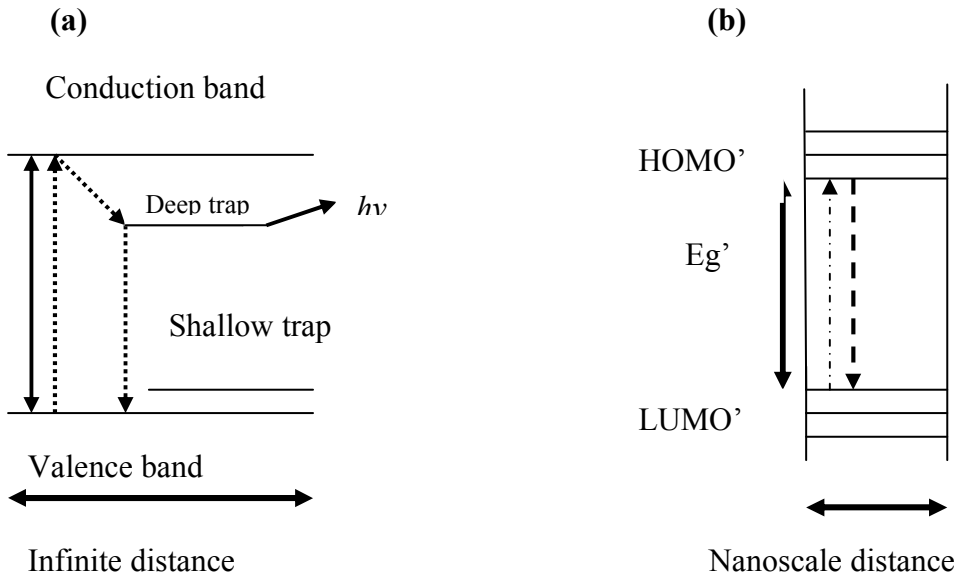


Figure 2: The spatial electronic state diagram showing the quantum confinement effect in bulk semiconductor (a) and nanoparticles (b)[40]

For a semiconductor crystal, electronic excitation consists of a loosely bound electron-hole pair usually delocalized over a length much longer than the lattice constant. For the exciton to occur, *hν*(excitation energy or light) > energy gap. Pumping energy into a semiconductor can excite an electron, e^-, into the conduction band (Figure 2), leaving behind the hole, h, in the normally filled valence band, and thus an electron-hole pair is created. The electron and the hole each relax to the respective band edge states by non-radiative processes. During the band edge transition a photon is emitted as the excited electron spontaneously recombines with the hole. The band edge is due to the direct recombination of charge carriers from atom-like orbitals. Charge carriers in bulk semiconductor recombine from the deep shallow traps giving the emission at different wavelengths from the band edge.[34] In the case of nanoscale semiconductor particles with smaller sizes (<10 nm), the situation changes. As the diameter of the crystalline material approaches the exciton Bohr diameter, its electronic properties start to change. This size range corresponds to

the regime of the so-called quantum confinement effect, which can be observed as a blue shift in the band gap or exciton energy. The charge carriers are confined in all three dimensions in a quantum dot and thus the exciton has a zero degrees of freedom for its motion, with the result that the electron exhibits a discrete atomic like spectrum. As a result of these geometrical constrain and an electron feels the particle boundaries and responds to particle size by adjusting their properties. This phenomenon is known as the quantum size effect.

1.2.2 Preparative methods for the synthesis of nanoparticles

Compound semiconductor nanoparticles of materials such as metals, metals oxides, carbides, borides, nitrides and other elemental semiconductors has been reported.[59-66] Ideally, the synthetic method employed should lead to samples of crystalline nanoparticulates of high purity, narrow size distribution and that can be surface derivatized. A number of different techniques have been reported for the preparation of nanoparticles.

1.2.2.1 Colloidal route

The first reported routes to small particles involved the controlled precipitation of dilute colloidal solutions and the cessation of growth immediately after nucleation. La Mer, *et al*.[67-68] reported the synthesis of highly monodispersed micrometric colloids in which it was shown that if nucleation and growth are properly controlled, particles with dimensions of the order of nanometers can be synthesized. Small crystals, which are less stable dissolve and then re-crystallize on larger more stable crystals, a process known as Ostwald ripening. For such methods to be effective quantum dots must have low solubility, which can be achieved by correct

choice of solvent, pH, temperature and passivating agent. Highly monodispersed samples are obtained if the process of nucleation and growth are distinctly separated that fast nucleation and slow growth. The colloidal stability can be improved by using solvents with a low dielectric constant or by using stabilizers such as styrene/maleic acid polymer.

1.2.2.2 Synthesis in confined matrices

A number of matrices have been used for the preparation of semiconductors nanoparticles and those include; zeolites,[69] layered solids,[70] molecular sieves[71-73] micelles/microemulsions, [74-78] gels, [79-81] polymers [82-86] and glasses[87] . These matrices can be viewed as nanochambers, which limit the size to which crystals can grow. Their properties are not only determined by the confinements of the host material but also by the properties of the system, which include the internal/external surface properties of zeolites and the lability of micelles. Growing particles in the internal cavities of zeolites limits the particle size of materials usually to less than 20 nm. CdS has been synthesized in two different zeolites by ion exchange from the sodium cationic form to the cadmium cationic form, followed by exposure to H_2S gas. Depending on the amount of cadmium ions utilized, different particles size were obtained.[69]

1.2.2.3 Metal-organic routes

A popular method for preparing high quality, crystalline monodispersed nanoparticles was first reported by Murray, *et al*.[88] in 1993. In this method a volatile metal alkyl (dimethylcadmium) and a chalcogen source TOPSe (trioctylphosphine selenide) were mixed in tri-n-octylphosphine (TOP) and injected into hot TOPO (tri-n-octylphosphine oxide), a polar coordinating Lewis base

solvent. Nucleation of the nanoparticulate CdSe was achieved by the sudden introduction of concentrated reagents resulting in abrupt supersaturation and the formation of the nuclei, followed by slower growth and annealing, consistent with an Ostwald ripening process. The nanoparticles were passivated by a monolayer of the solvent ligands and hence could be isolated by solvent/non-solvent interactions. The size distribution of the nanoparticles is controlled by the temperature at which the synthesis is undertaken, with larger particles being obtained at higher temperature. The combination of TOP/TOPO allowed for slow steady growth conditions above 280 °C. This method has advantage over other methods including, the generating near mono-disperse particles. Gram scales of materials can be produced. One of limitations of this method is the use of hazardous compounds such as dimethylcadmium, $Cd(CH_3)_2$ especially at high temperature. An approach to overcome this problem involves the use of single molecule precursors, a single compound containing all the elements required for within the nanocrystal, such as alkyldiseleno- or alkyldithiocarbamato complexes.[49, 50]

1.3.3 Applications of nanoparticles

Due to the unique phenomenon which occurs in nanoparticles, their properties (electrical, optical, chemical, mechanical, magnetic, etc.) can be selectively controlled by engineering the size, morphology, and composition of the particles. These new substances will have enhanced or entirely different properties from their parent material. Nanoparticles can make metals stronger and harder, gives ceramics enhanced ductility and formability, enables normally insulating materials to conduct heat or electricity, and make protective coatings transparent. Hence industries can reengineer many existing products and design novel new product/processes to function at unprecedented levels. Below are some of the applications of nanoparticles:

1.3.3.1 Molecular Electronic and Nanoelectronics

The last few years have been witnessing a tremendous progress in the molecular electronic and nanoelectronics[89]. In molecular electronics, single molecules are designed to control electron transport, which offers the promise of exploring the vast variety of molecular functions for electronic devices. The control over electronic energy levels at the surface of conventional semiconductors and metals is achieved by assembling on the solid surfaces and molecules can be designed into a working circuit. If molecules are biologically active, then bioelectronic devices could be developed[90].

Many nanoelectronic devices have been developed which includes tunneling junctions, electrically configurable switches, carbon nanotube transistors, single molecular transistors [91, 92]. Various techniques have been used in the fabrication of nanoelectronics such as focused ion beam (FIB), electron beam lithography and imprint lithography [93,94]. The fundamental path way for enhancing the conversion efficiency can be accessed through photovoltaic cells composed of nanocrystal arrays, through the dispersion of nanoparticles in organic semiconductor polymer matrices or through nanocrystal-sensitized TiO_2 solar cells also known as Gratzel cells. The ideal material used in the cell must have a high surface are for light absorption and charge separation. Nanoparticles, having a comparable surface area to volume ratio, provides for just that. Titanium dioxide nanoparticles are used to make nanoporous thin film supported upon a glass substrate. The material obtained has optical transparency, excellent stability and good electrical conductivity. The benefit of these novel photoelectrical solar cells is that they can be fabricated from cheap, low purity materials by simple and low cost procedures. Contrary to expectation,

some of the new devices also have strikingly high conversion efficiency. The size-tunable band-gaps of the semiconductor nanoparticles, due to size quantization, also means more efficient solar cells can be produced (electricity production) and water splitting (hydrogen production) processes.

1.3.3.2 Biological Applications

One of the important biological applications of colloidal nanocrystals is molecular recognition [95]. Living organisms are built of cells that are approximately 10 microns in size, with the cell parts a fraction of this. Proteins, which are about 5 nanometers, are even smaller. One could imagine nanoparticles which are 1-3 nanometers in size which can acts as probes within the cells causing much interference. In order for nanoparticles to function as biological labels or tags, the particles have to interact with the biological targets, which can be done through the attachment of a molecular coat or layer which act as a bioinorganic interface. Antibodies, biopolymers or monolayers of small molecules that make nanoparticles compatible are examples of biological coatings. Control of the average size and size distribution tune the wavelength of the emission in wide a range of wavelengths, making them very efficient probes. The nanoparticles are brighter and last longer than the conventional fluorescent dyes making them potentially useful for diagnosing cancers. Recent animal studies conducted showed that nanoparticles can be used to map a lymph node near a breast cancer. The fluorescent properties of the particles also could make them an energy source for certain therapies. Inactivated drugs could be attached to nanoparticles and once they have reached to a tumor they could be activated by a flash of light. Insoluble nanoparticles of varying sizes and colours could be packed inside a bead the size of a virus. Subsequently each microbead has that a distinctive optical signature could be used as a

barcode to label individual cells and proteins. The use of multifunctional probe built around gold nanoparticles to identify protein-protein interactions has also been reported.

The majority of commercial nanoparticle applications in medicine are focused on drug delivery. Magnetic nanoparticles have properties which would render them useful in biomedicine. The magnetic nature of the particles implies that they could be manipulated by an external magnetic field gradient. This almost 'remote control' action means that they could deliver a package such as an anticancer drug to a targeted region of the body. The nanoparticles could also be heated through transfer of energy from an exciting field to the nanoparticles thereby making them useful as hyperthermia agents, delivering toxic amounts of thermal energy to tumours or as chemotherapy and radiotherapy enhancement agents.

Recently a variety of magnetic nanoparticles have been developed to deliver to specific sites in *vivo*. The magnetic component of the particle is coated by a biocompatible polymer such as PVA (polyvinyl alcohol) or dextran. The coatings protect the magnetic particle from the surrounding environment. Functional groups such as carboxyl groups, biotin, carbodi-imide could be attached. These molecules could then be used as attachment points for coupling of cytotoxic drugs or targeted antibodies to the carrier complex. This advancement overcomes a major disadvantage for impreciseness of most chemotherapies, in which intravenous administration of the drug results in side effects as the drug attacks healthy cells in addition to the target tumor cells. Another breakthrough has been the transportation of the drugs bound to nanoparticles across the blood brain barrier (BBB). The nanoparticles/drug systems are coated with a surfactant The drugs are attached to the surface of the nanoparticles and/or incorporated into

poly(butylcyanoacrylate) particles (PBCA). This almost "Trojan horse" drug delivery mechanism allows for efficient delivery of the drug specifically in the central nervous system (CNS).

1.3.3.3 Textile applications

The recent development of nanotechnology in textile areas has included textile formation and textile finishing. Carbon nanofibers and carbon black nanonoparticles are among the most commonly used nanosized filling materials. Carbon nanofibers can effectively increase the tensile strength of composite fibers due to its high aspect ratio, while carbon black nanoparticles can improve their abrasion resistance and toughness. Both of them have high chemical resistance and electric conductivity. Clay nanoparticles or nonoflakes are composed of several types of hydrous aluminosilicates. Each type differs in chemical composition and crystal structure. Clay nanoparticles possess electrical, heat and chemical resistance and an ability of blocking ultraviolet (UV) light. Therefore, composite fibers reinforced with clay nanoparticles exhibit flame retardant, anti-UV and anti-corrosive behavior. For example nanopaticles of montmorillonite, one of most commonly used clays, have been applied as a UV blocker in a nylon composite fiber.

Nanosized particles of TiO_2, Al_2O_3, ZnO and MgO are a group of metal oxides that possess photocatalytic ability, electrical conductivity, and UV absorption and photo-oxidizing capacity against chemical and biological species. Intensive research has been focused on antimicrobial, self decontaminating and UV blocking functions for both military protection gear and civilian

health products. Nylon fiber filled with ZnO nanoparticles can provide a UV shielding function and reducing static electricity on nylon fiber. A composite fiber with nanoparticle of TiO_2/MgO can provide a self-sterilizing function. The most important of use nanotechnology in the textile finishing area had brought up innovative finishes as well as new application techniques. Particular attention has been paid in making chemical finishing more controllable and more thorough. Ideally, discrete molecules or nanoparticles of finishes can be brought individually to designated sites on textile materials in a specific orientation and trajectory through thermodynamic, electrostatic or other technical approaches.

1.3.3.4 Catalytic Application

Any material to show good catalytic activity must possess high surface area. Nanomaterials have tremendous implications in catalysis since the surface area of nanomaterials markedly increases with the reduction of their size. For example, a nanocrystal of 10 nm diameter will have ~15 % of its atoms on the surface while nanocrystal of 1 nm diameter will have ~100 %. Thus, a small nanocrystal with a higher surface area would be more catalytically active. Furthermore, the change in electronic properties arising due to quantum confinement in small nanocyrstals will also bestow unusual catalytic properties on these particles [96]. Yates *et al*. demonstrated that the decrease in catalytic activity per unit surface area of nickel with the increase in particle size in the hydrogenation reaction of ethane [97]. In a series of papers, Corrolleur, Gault and their co-workers demonstrated that the effect of particle size on mechanisms and product distributions of hydrogenolysis reactions over platinum catalysts 98. There have been quite a few interesting examples of nanostructured metal oxides and sulfides exhibiting unusual catalytic properties [99].

1.4 Background on thermal analysis [100]

When matter is heated, it undergoes certain physical and chemical changes. Physical changes include phase changes such as melting, vaporization, crystallization, transitions between crystal structures, changes in microstructure in metal alloys and polymers, volume changes (expansion and contraction), and changes in mechanical behavior. Chemical changes include reactions to form new products, oxidation, corrosion, decomposition, dehydration, chemisotropin, and the like. The physical and chemical changes take place over a wide temperature range. The rates of chemical reactions vary with temperature and properties of some materials, such as semicrystalline polymers and metal alloys, depend on the rate at which they are cooled. Materials are used over a wide range of temperatures, from Arctic cold to tropical heat, in corrosive environments, variable humidity, and under load. It is necessary to characterize materials and their behavior over the a range of temperatures to determine what materials are suitable for specific uses and to determine what temperature range materials or chemicals can withstand without changing. The sort of information is used to predict safe operating conditions for a product, such as which type of tyre material is best for vehicle types in extremely cold or hot climates, the average expected lifetime of materials such as paints and polymers exposed to temperature changes, processing conditions for materials and the curing times and temperatures needed for dental filling material, among other uses.

The physical changes and chemical reactions a sample can undergo when heated are characteristic of the material being examined and the atmosphere in which heating occurs. By

measuring the temperature at which such a reaction occurs and the heat involved in the reaction, we can determine a great deal about the material. The composition of pure compounds and mixtures, including polymer blends, can be determined from such experiences. The purity of pharmaceutical compounds can also be determined. Rate of reaction, rate of crystallization, glass transition temperatures, decomposition temperatures and catalysis can be studied. The effectiveness of additives and stabilizers in materials to be evaluated. Percent crystallinity of polymers, which greatly affects the mechanical properties of polymers, can be determined. By heating materials under load (stress), mechanical properties such as modulus, ductility, yield point (the point at which nonpermanent elastic deformation changes to permanent plastic deformation), and volume change as a function of the load can be measured.

These parameters are very important in engineering design to ensure safe and functional products. The analytical techniques used to study changes in physical properties with temperature are called thermal analysis techniques. They include thermogravimetric analysis (TGA), differential thermal analysis (DFA), differential scanning calorimetry (DSC), and thermometric titration (TT), direct injection enthalpimetry, dynamic mechanical analysis (DMA), and thermochemical analysis (TMA). Thermal analysis techniques are used in the characterization of inorganic and organic compounds, polymers, cosmetics, pharmaceutical, metals, alloys, geological samples, ceramics, glasses, and many manufactured products.

1.4.1 Thermogravimetric analysis

Thermogravimetric analysis (TGA) measures the mass (weight) of a sample in a specified atmosphere as the temperature of the sample is programmed. The most common temperature program is a linear increase in the temperature with time, although isothermal programs, stepped temperature programs, and so on can be used. In most common TGA experiments, the sample temperature is increased linearly over a time period and the mass of the sample is constantly measured. The output from a TGA experiment is a plot of mass or weight % vs. temperature. The TGA plot is called the thermal curve. An example of a TGA curve is shown in Figure 3. Weight or weight % is plotted along the *y-axis* and the temperature (or time linear temperature ramp) along the *x-axis*.

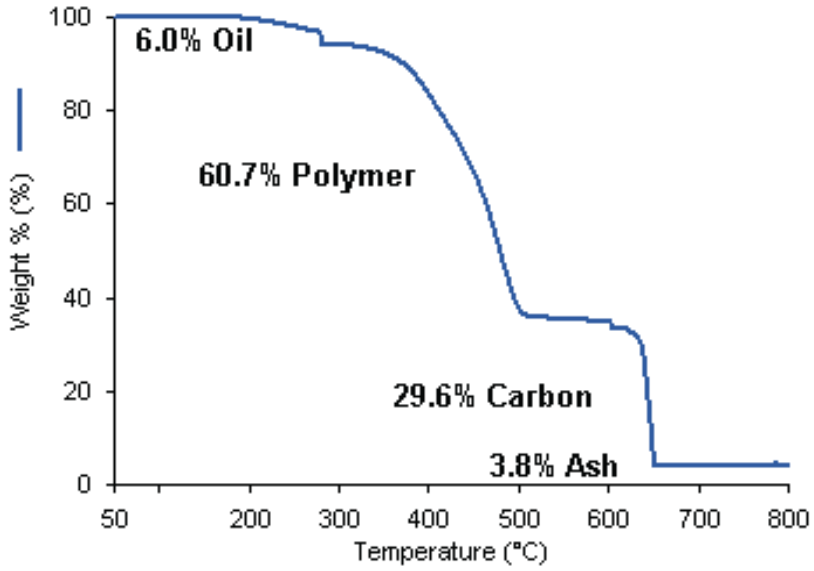


Figure 3: Typical compositional analysis.[100]

The change in weight of the sample as the temperature changes gives out a lot of information. First, the plot determines the temperature at which the material loses (or gains) the weight. Loss of weight indicates decomposition or evaporation of the sample. A gain in weight can indicate adsorption by the sample of the component in the atmosphere or a chemical reaction with the atmosphere. Second, the temperatures at which no weight change takes place are determined, which indicate the temperature stability range of the material. These weight changes at certain temperatures are physical properties of chemical compounds under the conditions of the experiment. This information can be used to determine if a sample is the same as the standard or a good material in a production process. The weight lost by a sample heated to a given temperature helps the inorganic or analytical chemist to determine the composition of a compound and follow the reactions involved in its decomposition. It also enables the analytical chemist to identify crystals of unknown composition or determine the percentage of a given compound in a mixture of compounds.

1.4.2 TGA Instrumentation

Modern TGA equipment has a sensitive balance, usually a microbalance, for continuously measuring the sample weight, a furnace surrounding a sample holder, and a purge gas system for providing inert or reactive atmosphere. A computer generally controls the furnace and the data (weight vs. sample temperature) is collected and processed by the computer. Intelligent autosamplers are available the most instruments that permit the unattended analysis of samples. Modern analytical microbalances of several different designs are commercially available: torsion balances, spring balances, and electrobalances and have been used in TGA instruments. In

general, the general, the balance is designed so that a change in a sample weight generates an electrical signal proportional to the weight change. The electrical signal is transformed into weight or weight loss by the data processing system and plotted on the *y*-axis of the thermal curve. TGA balances are available for samples masses from 1 to 1000 mg, with the usual sample weighing 5 and 20 mg. There are specialized high-capacity TGA systems available that can accommodate samples up to 100 g and systems that can handle microgram quantities of sample. Figure 4 shows a schematic of a TGA electrobalance. The usual sample size for TGA is very small, so care must be taken to obtain a homogeneous or representative sample. The balance itself must be thermally isolated from the furnace, although the sample holder and sample must be in furnace. There are two possible configurations of the balance and furnace, a horizontal furnace or a vertical furnace. Both types of configuration suffer from the drift as the temperature increases. Vertical configurations suffer from buoyancy effects due to the change in gas density with temperature. The horizontal configuration was designed to minimize buoyancy effects, but horizontal configurations experience changes in the length of the quartz rod connecting the sample to the balance as the temperature changes. Buoyancy effects and changes in the quartz rod result in errors in determining the mass of the sample.

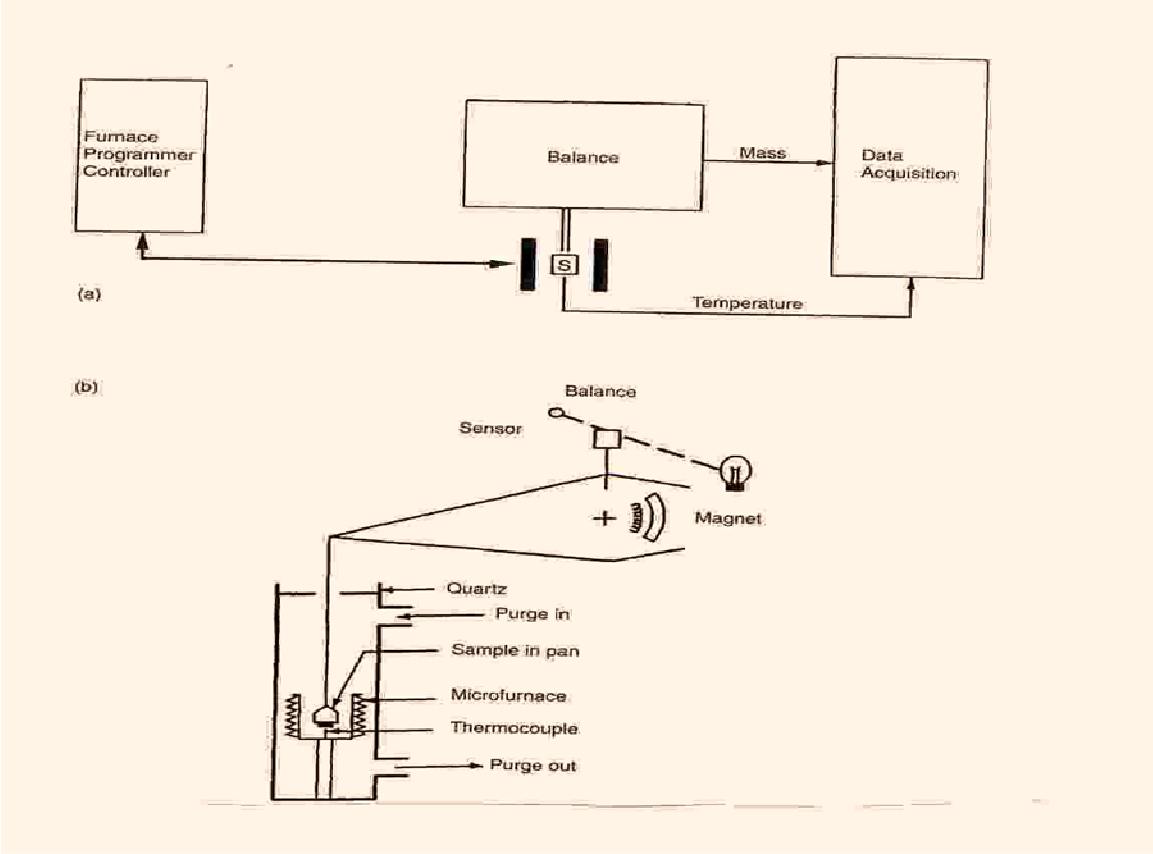


Figure 4: (a) Block diagram of TGA system. S represents the sample pan hanging from the balance arm in the position in the furnace. (b) Schematic of a commercial TGA, showing the purge gas inlet and outlet and the thermocouple position beneath the sample pan. [100]

The furnace surrounds the sample and sample holder. It must be capable of being programmed for a linear heating rate. Modern instruments can be heated and cooled rapidly, which increases sample throughout. Instruments that heat up to rate of a 1000 °C/min are available. There are furnaces available that can heat up to 1500, 1700, or 2400 °C; these higher temperatures are useful in studying refractory materials and engineering materials. The furnace must be able to be purged with a desired gas, to provide the correct atmosphere for the experiment and to remove gaseous products from the sample compartment. Argon or nitrogen is used when an inert atmosphere is desired. Reactive gas atmospheres can be used for certain studies. Air is often used for oxidation and combustion studies. Hydrogen gas may be used to provide a reducing

atmosphere, with the appropriate precautions to prevent explosions. Modern instruments permit the purge gas to be switched automatically, so that the sample can start heating in an inert atmosphere and be switched to air or other reactive gas at high temperatures.

The sample holder and any instrument parts inside the furnace, such as thermocouple for measuring temperature, must be able to withstand high temperature and be inert at these temperatures. Quartz, platinum, and various ceramics are used for the sample holder and other parts. The sample is placed is a small pan or crucible made of platinum, quartz or ceramic. Ideally, the temperature recorded is the exact temperature of the sample. This entails measuring the temperature of the sample while the analysis is carried out. It is particularly important to measure the temperature of the sample rather than that of the furnace. This is difficult because the temperature is measured with the thermocouple which is near but not in the sample.

The temperature of the sample inside the furnace is measured with a thermocouple, either a chromel/alumel thermocouple or one made of platinum alloy. The thermocouple is never inserted directly into a sample because of possible sample contamination, inadvertent initiation of a catalytic reaction, particle size effects, sample packing effects, and possible weighing errors. The thermocouple is made as small as possible and placed close to the sample holder, sometimes in contact with the bottom of the sample pan. The temperature actually recorded may be slightly different from the sample temperature; the sample temperature generally is lower than the recorded temperature in the thermocouple. This is due to factors such as the rate of heating, gas flow, thermal conductivity of the sample, and the sample holder. Modern instruments have a

temperature-voltage control program in the computer software that permits reproducible heating of the furnace. With precise, reproducible heating, thermocouple can be calibrated to provide accurate furnace temperatures, but the relationship between actual sample temperature and the recorded temperature is complex. The problem is compounded by the fact that at temperatures below 500 °C, where the furnace is red-hot, most of the energy is transferred by radiation. The switch from conduction-convection to radioactive energy transfer makes choosing the position of the thermocouple to obtain accurate temperature measurements of the sample quite a complicated problem.

Temperature calibration of TGA instruments with samples of pure materials with well characterized weight losses can be done, but often is not satisfactory. A more accurate calibration method uses the Curie temperature of various ferromagnetic standard materials. The materials undergo specific and reversible changes in magnetic behavior at their Curie temperature. Standards are available covering the temperature range of 242 - 771°C. A ferromagnetic material is magnetic under normal conditions, but at a characteristic temperature (the Curie temperature) its atoms become disoriented and paramagnetic and the material loses its magnetism. An advantage of this phenomenon, ferromagnetic materials is weighed continuously, with a small magnet placed above the balance pan. The standard's apparent weight is then its gravitational weight minus the magnetic force it experiences due to the magnet immediately above. At the Curie temperature, the standard loses its magnetism and the effect of the magnet is lost. There is a change in apparent weight of the standard, and this can be recorded. The temperatures of the Curie transitions of ferromagnetic materials are well known and therefore can be used for calibration purposes.

1.4.3 Analytical applications of thermogravimetry

One of the first important applications of thermogravimetry was the determination of the correct drying temperatures for precipitates used in gravimetric analysis. This knowledge was of vital importance if accurate and reproducible results were obtained from gravimetric analysis. A second important application was the identification of the gases given off while a sample's temperature is increased. In addition, the composition of the residue can be determined using the techniques such as XRD, XRF, and others. This information reveals the chemical decomposition process occurring when materials are heated and permits identification of the formulas of the starting materials. TGA is very important in determining the upper temperatures of materials such as polymers by identifying the temperature at which oxidative degradation occurs on heating in air. TGA can also be used for the identification of compounds present in mixtures of materials.

1.5 General background on spectroscopy

Infrared (IR) and nuclear magnetic resonance (NMR) spectroscopy are most useful techniques available for studying the structure of molecules. Infrared provides information on molecular vibrations and rotations while the NMR technique provides information about the molecular structure based on the nuclear spin of atoms present. Both instruments were used to characterize all the prepared complexes to confirm the formation of the metal sulphide bond and the presence of the number of ligands bonded to a metal.

1.5.1 Theory of infrared spectroscopy.[101]

Infrared spectroscopy involves absorption of electromagnetic radiation in the infrared region of the spectrum, normally 4000 to 200 cm^{-1}. The energy associated with a quantum of light may be transferred to the molecule if work can performed on the molecule in the form of displacement of charge. A molecule will absorb infrared radiation if the change in vibration states is associated with a change in dipole moment of the molecule. As the molecule vibrates, the charge distribution may or may not change with respect to that origin, depending on the relative displacements of atoms. Only the vibration that causes the electric dipole to change will be associated with the absorption of infrared radiation.

1.5.2 Theory of NMR spectroscopy

NMR involves the absorption of radiowaves by the nuclei of some combined atoms in a molecule that is located in a magnetic field. NMR spectroscopy can be considered a type of absorption spectroscopy, not unlike UV/vis absorption spectroscopy. Radiowaves are low energy electromagnetic radiation. Their frequency is on order of 10^7. The energy (E) of radiofrequency (RF) radiation can be calculated from:

$$E = hv \qquad (1)$$

where the Planck's constant h is 6.626 X 10^{-34} Js and v (frequency) is between 4 and 1000 MHz. The quantity of energy involved in RF radiation is very small. It is too small to vibrate, rotate, or electronically excite an atom or molecule. It is great enough to affect the nuclear spin of atoms in a molecule. As a result, the spinning nuclei of some atoms in a molecule in a magnetic field can

absorb RF radiation and change the direction of the spinning axis. In principle, each chemically distinct atom in a molecule will have a different absorption frequency (or resonance) if its nucleus possesses a magnetic moment.

1.6 Theoretical background to instrumentation use to characterize nanoparticles

1.6.1 Ultraviolet-visible spectrophotometry[101]

1.6.1.1 General introduction

The increasing demand for the need of identification and determination of inorganic, organic as well as biochemical species has called upon the use of molecular spectroscopy such as UV-visible spectrophotometry. The utilization of molecular ultraviolet and visible absorption spectroscopy is primarily used for quantitative analysis and therefore is probably the single most used analytical method in chemical and clinical laboratories throughout the world. Molecular absorption spectroscopy can be considered as based on the measurement of transmittance (T) or absorbance (A) of solutions contained in transparent cells having the path length *b* cm where, the concentration *c* , and ε is molar absorptivity of an absorbing analyte. The term P_o and P refers to the power of radiation after it has passed through the cells containing the solvent and analyte respectively:

$$A = -\log T = \log P_o/P = \varepsilon bc \qquad (2)$$

1.6.1.2 Theory of UV-visible spectrophotometry

Absorption of ultraviolet and visible radiation by molecules generally occurs in one or more electronic absorption bands, each of which is made up of numerous closely packed but discrete lines. Each line arises from the transition of an electron from the ground state to one of the many vibrational and rotational energy states associated with each excited energy state. The absorption of ultraviolet or visible radiation results from excitation of bonding electrons, therefore the wavelengths of absorption peaks can be correlated with types of bands in the species being analyzed as shown in Table 1. Molecular absorption spectroscopy is, therefore valuable for identifying functional groups in a molecule.

Table 1: Absorption of ultraviolet and visible light and colour.

Wavelength (nm)	Colour (absorbed)	Colour (transmitted
<380	Ultraviolet	
380-435	Violet	Yellowish green
435-480	Blue	Yellow
480-490	Greenish blue	Orange
490-560	Bluish green	Red
500-560	Green	Purple
560-580	Yellowish green	Violet
580-595	Yellow	Blue
595-650	Orange	Greenish blue
650-780	Red	Bluish green
>780	Near-infrared	

1.6.1.3 Absorbing by organic species

Electronic transitions in organic molecules are characterized by the promotion of electrons in ground-state bonding or non-bonding molecular orbitals to excited-state antibonding molecular orbitals. If molecular structure is the dominant factor in determining the electronic energies of the ground and excited states, then the photon energy required for n-π*, π- π*, and n-σ* would vary from molecule to molecule depending on the structural and environmental variations as shown in Figure 5. When the radiation of a frequency corresponding to one of the fundamental frequencies of the molecule interacts with that molecule, radiant energy is absorbed to increase the energy content of the molecule by an equal amount of energy of the quantum absorbed, in accordance with the relation:

$$\Delta E = h\nu = hc / \lambda \qquad (3)$$

The wavelength at which an organic molecule absorbs depends upon how tightly its several electrons are bound. Electrons involved in double and triple bonds of organic molecules are not strongly held and are therefore more easily excited by radiation, thus species with unsaturated bonds generally exhibit useful absorption peaks. Unsaturated organic functional groups that absorb in the ultraviolet or visible regions are known as chromophores.

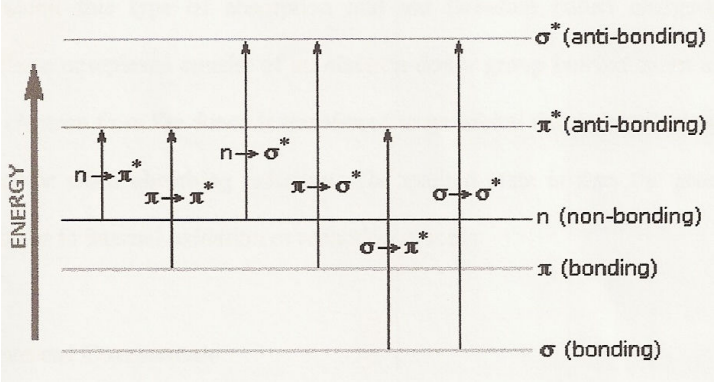


Figure 5: Energy diagram for the transitions in UV region.[101]

1.6.1.4 Absorption by Inorganic species

The ions and complexes of the elements in the first two transitions series absorb broad bands of visible radiation in at least one of their oxidation states and are, as a consequence coloured. Here absorption involves transitions between filled and unfilled d-orbitals with energies that depend on the ligands bonded to the metal ions. The ions of most lanthanide and actinide elements absorb in the ultraviolet and visible regions. The transitions responsible for absorption by elements of the lanthanide series appear to involve the various energy levels of 4*f* electrons, while it is the 5*f* electrons of the actinide series that interact with radiation.

1.6.1.5 Charge-transfer absorption

Charge-transfer absorption plays an important role due to its unusually large molar absorptivities (<10000), which leads to high sensitivity. Many inorganic and organic complexes exhibit this type of absorption and are therefore called charge-transfer complexes. These complexes consist of an electron-donor group bonded to an electron acceptor. An electron from the donor is transferred to an orbital that is largely associated with the acceptor when absorbing radiation.

The excited state is thus the product of something similar to internal oxidation or reduction process.

1.6.1.6 Instrument components

Instruments for measuring absorption of ultraviolet, visible radiation are made up of one or more; (1) sources, (2) wavelength, (3) sample containers, (4) radiation transducers, and (5) signal processors and readout devices as shown in an example in Figure 6. There are three different types of sources; i.e. deuterium and hydrogen lamps, tungsten filament and xenon arc lamps. The cells or cuvettes are used as sample containers. The best cells have windows perpendicular to the direction of the beam in order to minimize reflection losses. There are different types of instruments; (1) single-beam, (2) double-beam, (3) double-beam in time, and (4) multichannel.

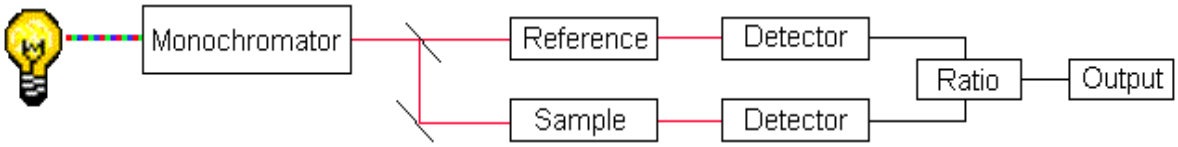


Figure 6: Example of UV-Vis double beam instrument.

1.6.1.7 Applications

1.6.1.7 (a) Qualitative application of UV/visible spectrophotometry

Ultraviolet and visible spectroscopy have somewhat limited application for qualitative analysis because the number of absorption maxima and minima are relatively few. Spectrophotometric measurements with ultraviolet radiation are useful for detecting chromophic groups. Ultraviolet

spectra for qualitative analysis are most commonly derived for dilute solutions of an analyte. For volatile compounds, however, more useful spectra often result when the sample is examined as a gas. A solvent for ultraviolet/visible spectroscopy must be transparent throughout this region and should dissolve a sufficient quantity of the sample to give well-defined peaks. Polar solvents such as alcohols, water, esters, and ketones tend to obliterate vibration spectra and thus should be avoided when spectral detail is desired. Non-polar solvents, such as cyclohexane, often provide spectra that more closely approach that of a gas.

1.6.1.7. (b) Quantitative applications

Absorption spectroscopy is one of the most useful and widely used techniques available for quantitative analysis to the chemist. The important characteristics of spectrophometric and photometric methods include; (1) wide applicability to both organic and inorganic systems, (2) typical high sensitivity, (3) moderate to high selectivity, (4) good accuracy, (5) ease and convenience for data acquisition. In order to obtain good spectra, the first issue in photometric or spectrophotometric analysis is the development of the conditions that yield a reproducible relationship between absorbance and analyte concentration. To realize maximum sensitivity, spectrophotometric absorbance measurements are ordinarily made at a wavelength corresponding to an absorption peak. The absorption curve is often flat at maximum, which leads to good adherence to Beer's law. Common variables that influence the absorption spectrum of a substance include the nature of a solvent, the pH of the solution, the temperature, high electrolyte concentration and the presence of interfering substances.

1.6.2 Photoluminescence [101]

1.6.2.1 General introduction

Photoluminescence is a general term for fluorescence and phosphorescence in which the two are alike in that excitation is brought about by absorption of photos. In each, molecules of the analyte are excited to give a species whose emission spectrum provides information for qualitative or quantitative analysis. Fluorescence differs from phosphorescence in that the electronic transitions responsible for fluorescence do not involve a change in electron spin, and are therefore short-lived, with luminescence ceasing rapidly in ($< 10^{-5}$ s). Phosphorescence involves a change in electron spin. In most cases photoluminescence emission, is longer in wavelength than the radiation used for excitation. Measurements of the intensity of photoluminescence permit the quantitative determination of trace of amounts in a variety inorganic and organic species. One of the most attractive features of luminescence methods is their inherent sensitivity, with detection limits often being one to three orders of magnitude smaller than those encountered in absorption spectroscopy. Another advantage of photoluminescence is the linear concentration range, which is also significantly greater than those encountered in absorption methods.

1.6.2.2 Theory of photoluminescence

Fluorescence occurs in simple as well as complex gaseous, liquid, and solid chemical systems. Many molecular species also exhibit resonance fluorescence (type of fluorescence, in which the absorbed radiation is re-emitted without a change in frequency). More often, photoluminescence bands are found centered at wavelengths that are longer than the resonance line. The shift

towards (lower energies) is called the Stokes shift. However, an understanding of the difference between the two-photoluminescence phenomena requires a review of electron spin and single/triplet excited states. A deeper understanding of the photoluminescence molecules is shown on the energy level diagram in Figure 1.5.

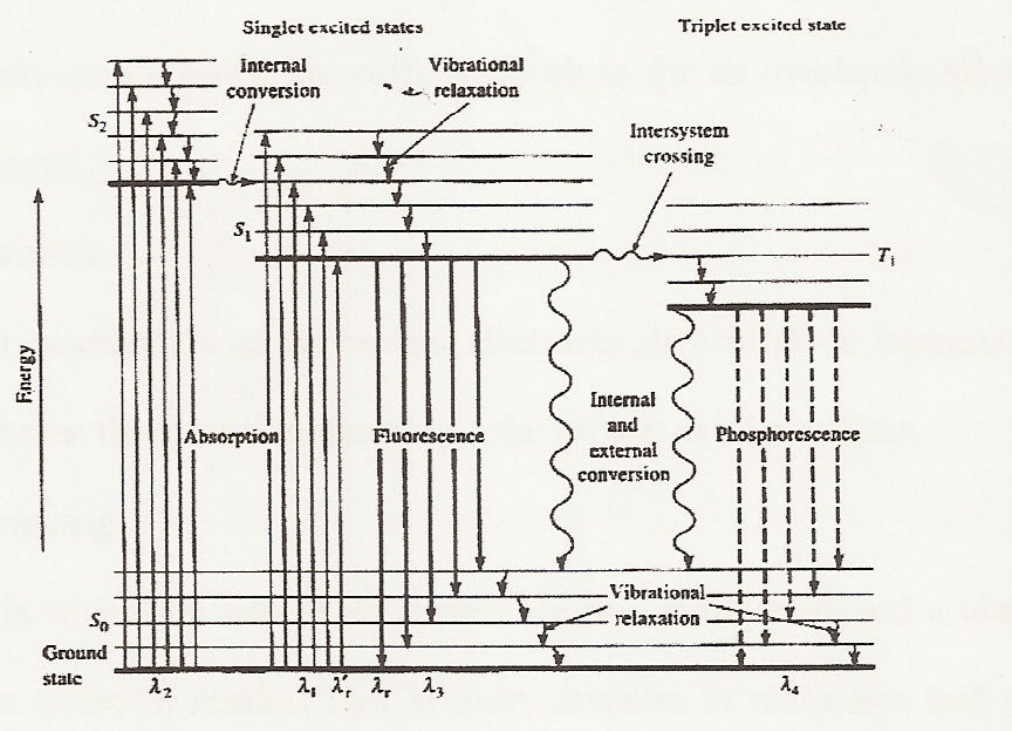


Figure 7: Photoluminescence energy diagram [101]

At room temperature, the ground state represents the energies of essentially all of the molecules in a solution. Numerous vibrational energy levels are associated with each of the four electronic states, as suggested by the horizontal lines as shown in Figure 7. Both molecular structure and environment influence whether a substance will or will not luminescence, which also determines

the intensity of emission when luminescence does occur. Some factors that influence the intensity of emission include; quantum yield, temperature, solvent, pH, and the concentration.

1.6.2.3 Deactivation processes

Excited molecules can return to its ground state by a combination of several mechanistic steps. This is indicated in Figure 7, by straight, vertical and wavy arrows.

1.6.2.3 (a) Vibrational relaxation

In solution the excess vibrational energy is immediately lost as a consequence of collisions between molecules of excited species and those of the solvent. This relaxation process is so efficient that the average lifetime of a vibrational excited molecule is 10^{-12} s or less, which is shorter the average lifetime of an electronically excited state.

1.6.2.3 (b) Internal conversion

This term describes intermolecular process by which a molecule passes to a lower energy electronic state without emission of radiation. Internal conversion is particularly efficient when two electronic energy levels are sufficiently close for overlap in vibrational energy levels to occur.

1.6.2.3 (c) External conversion

This occurs when deactivation of an excited electronic state involves interaction and energy transfer between the excited molecule and solvent or other solutes.

1.6.2.3 (d) Intersystem crossing

This is a process in which the spin of an excited electron is reversed, and a change in multiplicity of the molecule results. This is most common in molecules that contain heavy atoms. The presence of paramagnetic species in solution enhances intersystem crossing and a consequent decrease in fluorescence.

1.6.2.4 Limitations of luminescence measurements

Since the fluorescence measurements are not blank compensated, as in absorption measurements, lack of a blank can be a serious limitation in achieving optimal detection limits. The major factors that contribute to luminescence blank are; (1) Raman scattering from the solvent, (2) luminescence of the sample holder, (3) scattered light from Tyndall and Rayleigh effects, (4) adventitious fluorescence contributed by impurities in the solvent, (5) photo-degradation of the sample, and (6) contributions from other fluorescent species in the sample. Synergistic effects contribute another limitation to luminescence analysis, which results in a diminution of fluorescence intensity in analyte.

1.6.2.5 Applications of photoluminescence

Inorganic fluorometric methods are of two types. The direct method involves the formation of a fluorescing chelate and the measurement of its emission. A second group is based upon the diminution of fluorescence resulting from the quenching action of the substance being determined. Diminution (quenching) is used primarily for the determination of anions. In short the photoluminescence methods are widely used for compound identification. Many transition-metal ions that form fluorescing chelates are paramagnetic; this property increases the rate of intersystem crossing to the triplet state. Non-transition metal ions are less susceptible to the foregoing deactivation processes; it is for these elements that the principal inorganic applications of fluorometry are to be found.

1.6.2.6 Application in organic and biochemical species

The number of applications of fluorometric analysis to organic and biochemical species is impressive. The most important applications of fluorometry are in analysis of food products, pharmaceuticals, clinical samples, and natural products. The sensitivity of selectivity of the method makes it a particularly valuable tool to these fields.

1.6.2.7 Instrument components

There are two basic types of fluorimeters that are commercially available. One is the filter fluorimeter, which usually operates at fixed excitation and emission wavelengths and is relatively inexpensive. The second is the more expensive grating instrument, which is capable of wavelength scanning and produces better resolution than does the filter instrument. The

fluorimeter typically consists of the six major components; (1) the radiation source usually the xenon-arc lamp or mercury-arc lamp which is used for greater excitation, (2) lensing system, (3) sample container, (4) excitation-wavelength selector system, (5) a detector, and (6) the recording device. An example is shown in Figure 8.

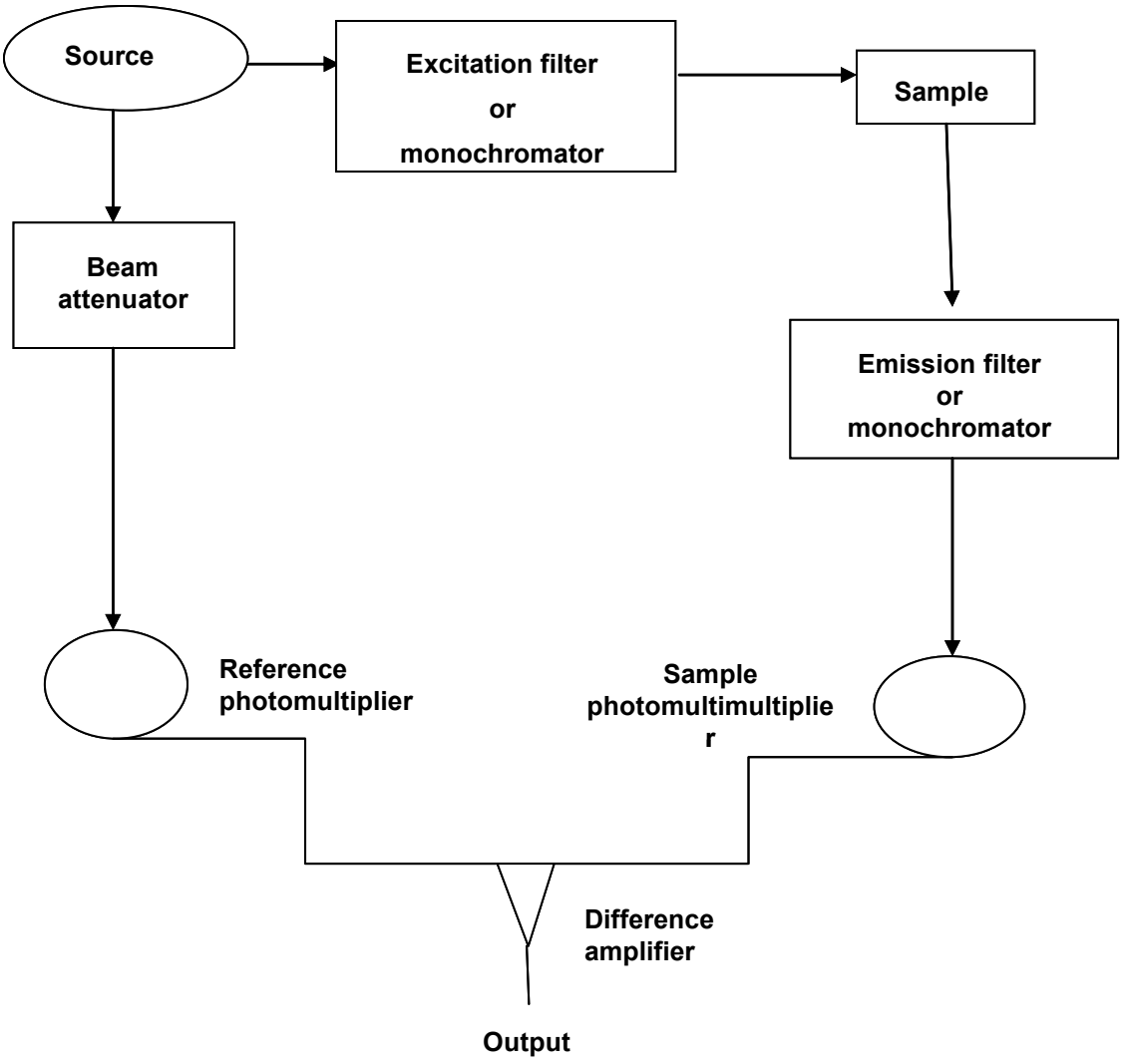


Figure 8: Schematic diagram of a fluorimeter.

1.6.3 Electron microscopy

1.6.3.1 General introduction

In order to determine the morphology and the size of nanoparticles, an electron microscope is used. An electron microscope is a type of microscope that uses a particle beam of electrons to illuminate a specimen and create a highly-magnified image. Electron microscopes have much greater resolving power than light microscopes that use electromagnetic radiation and can obtain much higher magnifications of up to 2 million times, while the best light microscopes are limited to magnifications of 2000 times. Both electron and light microscopes have resolution limitations, imposed by the wavelength of the radiation they use. The greater resolution and magnification of the electron microscope is because the wavelength of an electron; (its de Broglie wavelength) is much smaller than that of a photon of visible light.

The electron microscope uses electrostatic and electromagnetic lenses in forming the image by controlling the electron beam to focus it at a specific plane relative to the specimen. This is similar to how a light microscope uses glass lenses to focus light on or through a specimen to form an image. There are four different types of electron microscopes ; Transmission Electron Microscope (TEM), Scanning Electron Microscope (SEM), Reflection Electron Microscope (REM), and Scanning Transmission Electron Microscope (STEM). The only used electron microscope in this work is the TEM.

1.6.3.2 Theory of transmission electron microscopy

The original form of the electron microscope, the transmission electron microscope (TEM) uses a high voltage electron beam to create an image. The electrons are emitted by an electron gun,

commonly fitted with a tungsten filament cathode as the electron source. The electron beam is accelerated by an anode typically at +100 keV (40 to 400 keV) with respect to the cathode, focused by electrostatic and electromagnetic lenses, and transmitted through the specimen that is in part transparent to electrons and in part scatters them out of the beam. When it emerges from the specimen, the electron beam carries information about the structure of the specimen that is magnified by the objective lens system of the microscope. The spatial variation in this information (the image) is viewed by projecting the magnified electron image onto a fluorescent viewing screen coated with a phosphor or scintillator material such as zinc sulfide. The optical layout of the TEM is shown if Figure 9. The image can be photographically recorded by exposing a photographic film or plate directly to the electron beam, or a high-resolution phosphor may be coupled by means of a lens optical system or a fibre optic light-guide to the sensor of a CCD (charge-coupled device) camera. The image detected by the CCD may be displayed on a monitor or computer.

Resolution of the TEM is limited primarily by spherical aberration, but a new generation of aberration correctors have been able to partially overcome spherical aberration to increase resolution. Hardware correction of spherical aberration for the high resolution TEM (HRTEM) has allowed the production of images with resolution below 0.5 Ångström (50 picometres) at magnifications above 50 million times. The ability to determine the positions of atoms within materials has made the HRTEM an important tool for nanotechnology research and development.

1.6.3.3 Limitations

There are a number of drawbacks to the uses of a TEM technique. Many materials require extensive sample preparation to produce a sample thin enough to be electron transparent, which makes TEM analysis a relatively time consuming process with a low throughput of samples. Being almost transparent to electrons, a graphene substrate has been able to show single hydrogen atom and hydrocarbons. The structure of the sample may also be changed during the preparation process. Also the field of view is relatively small, raising the possibility that the region analyzed may not be characteristic of the whole sample. There is potential that the sample may be damaged by the electron beam, particularly in the case of biological materials.

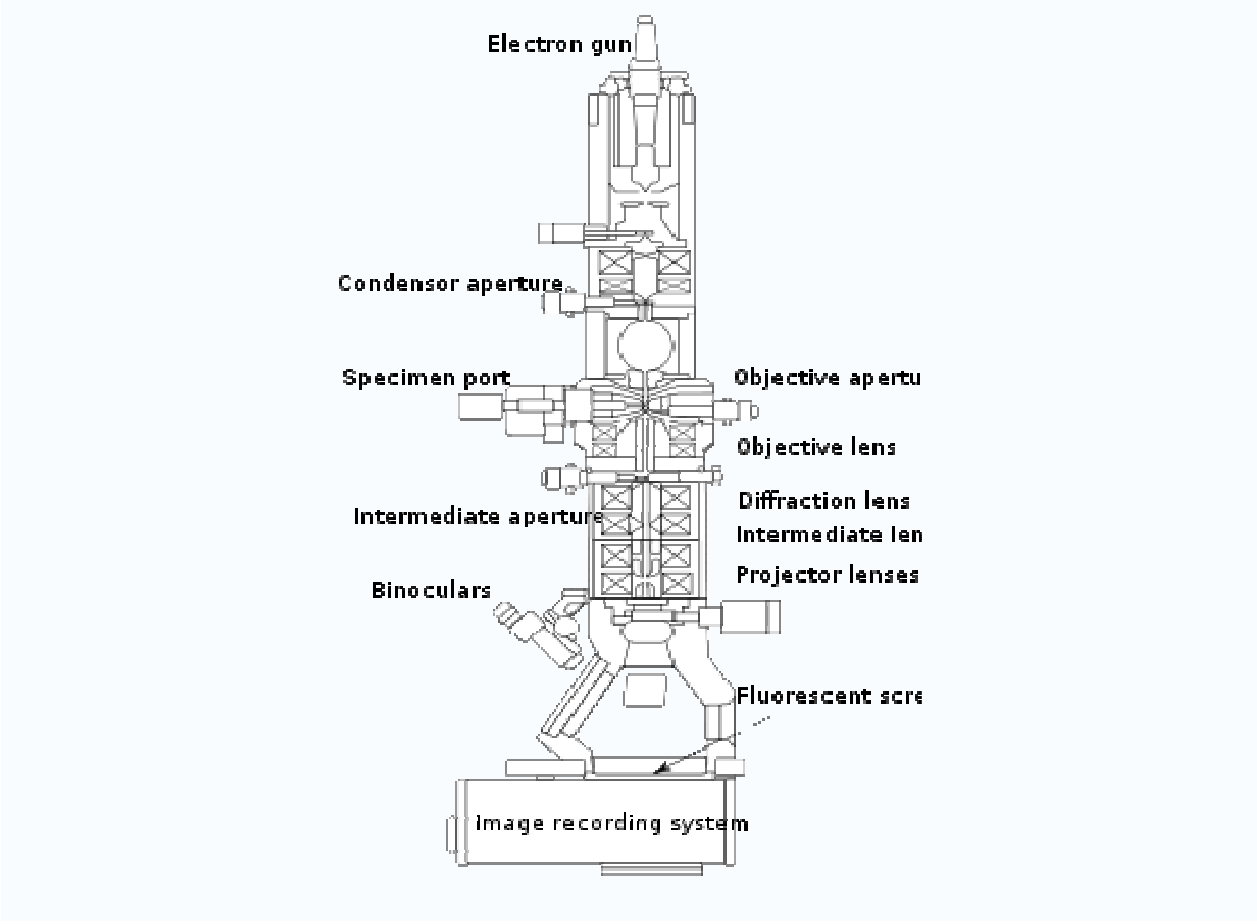


Figure 9: Layout of optical components in a basic TEM [100]

1.7 Statement of Objective

Due to the insoluble nature of the organic capping molecule generally used such as HDA, TOPO and others this makes nanoparticles insoluble in water and hence difficult to use for biomedical applications. In this work the focus is on the phosphonoacetic acid as a water soluble capping molecule which retains organic features as well as having functionalities as P=O, O-H and C=O for the surface interaction with nanoparticles to stabilize them. Hence the objectives include synthesis and characterization of metal sulfide nanoparticles based on Cd, Mn and Ni from their di and trisubstituted alkylthiourea Cd, Mn, and Ni complexes. And also to understand the effect of mixing PAA and TOPO/HDA on the size and morphology of the nanoparticles.

2. EXPERIMENTAL SECTION

2.1 Materials

Cadmium chloride, manganese chloride, nickel chloride, *N,N*'-dimethylthiourea, N-phenylthiourea, *N,N,N'*-tributylthiourea were all obtained from Aldrich and used as purchased. Ethanol and methanol (analytical grade) were used without further purification. TOPO (tri-n-octylphosphine oxide), TOP (tri-n-octylphosphine), PAA (phosphonoacetic acid) and HDA (hexadecylamine) were purchased from Aldrich. Toluene, tetrahydrofuran and methanol were obtained from BDH (British Drug House). Toluene was stored overnight over molecular sieves (40 Å, BDH).

2.2 Instrumentation

2.2.1 The following were used for characterization of complexes.

(a) Microanalysis

Microanalysis was performed on a CARLO ERBA elemental analyzer for C, H, N, S determination.

(b) NMR and FT-IR spectroscopy

Infrared spectra were recorded on FT-IR Perkin-Elmer Paragon 1000 spectrometer. NMR spectra were recorded on a Varian Associates Inova spectrometer (400 and 300 MHz).

(c) Thermogravimetry

Thermogravimetric analysis (TGA) was performed from 50 °C up to 800 °C on a Perkin Elmer Pyris 6 TGA with nitrogen flow and heating rate 10-20 °C.min^{-1}.

2.2.2 The following were used for characterizing the nanoparticles.

(a) Optical characterization

A Perkin-Elmer Lamda 20 UV-Vis spectrophotometer was used to carry out the absorption measurements. Optical absorption measurements were carried out using an Analytikjena SPECORD 50 UV-visible spectrophotometer and the samples were placed in quartz cuvettes (1 cm, path length), using toluene as a reference solvent. The photoluminescence (PL) spectra were recorded on a Perkin-Elmer LS 45 Fluorescence Spectrometer with a xenon lamp at room temperature. The samples were placed in quartz cuvettes (1 cm path length).

(b) Electron microscopy

The TEM micrographs were obtained using JEOL 100S electron microscope operated at 80 kV. The samples were prepared by placing a drop of diluted solution of toluene on a copper grid (400 mesh, agar). The samples were allowed to dry in room temperature.

(c) X-Ray diffraction

X-ray diffraction patterns on powdered samples were measured on a Phillips X'Pert materials research diffractometer using graphite monochromated Cu Kα radiation (λ = 1.54060 Å) at 40 kV/ 50 mA. Samples were supported on glass slides. Measurements were taken at a glancing

angle of incidence detector at an angle of 2°, 2θ values over 2° – 60° in steps of 0.05° with a speed of 0.01° $2\theta.s^{-1}$.

2.3 Preparation of the complexes.

All the complexes were prepared using a similar method as outlined below (Complex **I**). The complexes were prepared by reflux in methanol or ethanol to give a white powder. All the three Mn and Ni complexes were successfully prepared except for cadmium complex based on tributylthiourea, $Cd[SCN(CH_2CH_2CH_2CH_3)_2NH(CH_2CH_2CH_2CH_3))]_2Cl_2$

(a) $Mn[SC(NH_2)NH(C_6H_5)]_4Cl$ (*I*)

In a typical synthesis, $MnCl_2$ (0.81 g, 0.01 mol) was dissolved in a minimum ethanol (30 mL), while phenylthiourea (1.52 g, 0.02 mol) was also dissolved in minimum ethanol (30 mL). Manganese chloride solution was added to a phenylthiourea solution and refluxed for two hours. The hot solution was filtered to remove unreacted impurities and the solution allowed to cool to room temperature to give a colourless precipitate. Yield: 1.41 g, 66%, Anal. Calcd. for $C_{28}H_{32}N_8S_4ClMn$: C 48.10 H 4.61 N 16.02 Found: C 48.73, H 4.80, N 16.07. IR(cm^{-1}) 3340(br), 1559(s), 1525(m), 688(s), 533(w) ^{1}HNMR (DMSO-d_6) ppm: 9.67 (s, 6H, NH, NH_2); 7.33 (d, 2H, J_{HH}=30 Hz); 7.02 (s 1H, C_6H_5). ^{13}C {^{1}H} NMR (DMSO-d_6) ppm; 179.15(s, CS); 137.00, 126.63, 122.39, 121.00 (s, C_6H_5).

(b) $Mn[(CH_3)HNCSNH(CH_3)]_2Cl_2$ (*II*)

$MnCl_2.2H_2O$ (0.39 g, 0.01 mol); 1.3-dimethylthiourea, $[(CH_3)HNCSNH(CH_3)]$ (0.50 g, 0.02 mol); Yield 0.59 g, 74% ; Anal.: Calcd. for $C_6H_{16}N_4S_2Cl_2Mn$: C 21.56 H 4.83 N 16.77 S 19.19 Found : C 21.50 H 4.81 N 16.76 S 19.14.IR (cm^{-1}) 3349(br), 1580(vs), 1449(m), 714(s), 533(w), ^1H NMR (DMSO-d_6) ppm: 7.09 (s, 4H, NH); 2.49 (s, 6H, CH_3)

(c) $Mn[SCN(CH_2CH_2CH_2CH_3)_2NH(CH_2CH_2CH_2CH_3)]_2Cl_2$ (*III*)

$MnCl_{2\cdot2}H_2O$ (1.62 g, 0.01 mol), *N.N'*-dibutyl-N-butylthiourea $[(SCN(CH_2CH_2CH_2CH_3)_2 NH(CH_2CH_2CH_2CH_3)]$ (4.89 g (0.02 mol) ; Yield 3.71 g, 60% Anal. for $C_{26}H_{56}N_4S_2Cl_2Mn$: Calcd. C 56.87 H 10.28 N 10.20 Found : C 56.37 H 11.12 N 10.47.IR (cm^{-1}) 3345(s), 1535(m), 710(s). ^1H NMR (DMSO-d_6) ppm: 7.26(s, 2H, NH); 3.31(s, 12H, CH_2); 1.43 (s, 12H, CH_2); 1.28(d, 12H,J_{HH}=6 Hz); 0.86 (t, 18H, J_{HH}=6 Hz). $^{13}C\{^1H\}$(DMSO-d_6) ppm: 181.68 (s, CS); 42.81 (s, CH_2); 30.63(s, CH_2); 19.26 (s, CH_2); 13.40 (s, CH_3).

(d) $Cd[(CH_3)HNCSNH(CH_3)]_2Cl_2$ *(IV)*

$CdCl_2$ (1.93 g, 0.01 mol), 1.3-dimethylthiourea $[(CH_3)HNCSNH(CH_3)]$ (2.00 g, 0.02 mol) ; Yield 2.34 g, 55%. Anal. for $C_6H_{18}N_4S_2Cl_2Cd$: Calcd. C 18.40, H 4.12, N 16.77, S 16.37 Found : C 19.68, H 4.49 N 15.03 S 17.33. IR (cm^{-1}) 3322(s), 1583(s), 1529(s), 1372(m), 1297(w), 715(m), 539(s). ^{1}HNMR (DMSO-d_6) ppm: 7.51 (s, 2H, NH); 3.32(s, 6H, CH_3). $^{13}C\{^1H\}$(DMSO-d_6) ppm: 181.33(s, CS); (s, CH_3).

(e) $Cd[(C_6H_5)HNCSNH_2]_2Cl_2$ *(V)*

$CdCl_2$ (0.331 g, 0.01 mol) *N*-phenylthiourea $[(C_6H_5)HNCSNH_2]$ (0.50 g (0.02 mol) ; Yield 0.72 g, 82% Anal. for $C_{14}H_{16}N_4S_2Cl_2Cd$ Calcd. C 32.48, H 3.31, N 11.09, S 13.15 Found : C 32.85 H 3.14 N 10.75 S 12.34. IR (cm^{-1}) 3295(br), 1570(s) 1525(vs), 1415(m), 1256(w), 715(s), 539(s). ^1H NMR (DMSO-d_6) ppm: (s, 6H, NH, NH_2);. $^{13}C\{^1H\}$ (DMSO-d_6) ppm: 180.84 (s, CS); 138.97,128,66, 124.43,123,05 (s, C_6H_5).

(f) $Ni[(CH_3)HNCSNH(CH_3)]_2Cl_2$ *(VI)*

$NiCl_2.2H_2O$ (3.42g, 0.01 mol), 1.3-dimethylthiourea $[(CH_3)HNCSNH(CH_3)]$ (3.00 g, 0,02 mol); Yield 5.18 g, 68 %. Anal.for $C_6H_{18}N_4S_2Cl_2Ni$: Calcd. C 21.83, H 4.77, N 15.58. Found: C 22.40, H 5.90, N 14.93. IR (cm^{-1}) 3220(w), 3138(w), 1597(w), 1534(w), 1456(s), 1297(w), 1190(m), 1037(w), 1297(w), 715(w),666(s), 541(m).

(g) $Ni[(SCN(CH_2CH_2CH_2CH_3)_2NH(CH_2CH_2CH_2CH_3)]\ _2Cl_2$ *(VII)*

$NiCl_2.2H_2O$ (1.628 g, 0.01 mol) *N.N'*-dibutyl-N-butylthiourea $[(SCN(CH_2CH_2CH_2CH_3)_2\ NH(CH_2CH_2CH_2CH_3)]$ (3.350 g, 0,02 mol); Yield 5.18 g, 76 %. Anal. for $C_{26}H_{56}N_4S_2Cl_4Ni$ Calculated. C 45. 47. H 8.22, N 8.16 Found: C 44.12, H 8.41, N 11.46. IR (cm^{-1}) 3201(w), 3009(w), 1566(m), 1519(s), 1453(m), 1319(w), 1213(s), 1076(w), 617(m), 547(br).

2.4 Synthesis of organically-capped nanoparticles

2.4.1. Synthesis of PAA-capped nanoparticles

The following complexes were used as precursors to prepare PAA-capped MnS, NiS and CdS nanoparticles, $Mn[SCNH_2NH(C_6H_5)]_4Cl$ (I), $Mn[(CH_3)HNCSNH(CH_3)]_2Cl_2$(II), $Mn[(SCN(CH_2CH_2CH_2CH_3)_2NH(CH_2CH_2CH_2CH_3)]_2Cl_2$ (III), $Cd[(CH_3)HNCSNH(CH_3)]_2Cl_2$ (IV) $Cd[(C_6H_5)HNCSNH_2]_2Cl_2$ (V), $Ni[(SCN(CH_2CH_2CH_2CH_3)_2NH(CH_2CH_2CH_2CH_3)]_2Cl_2$ (VI) and $Ni[(CH_3)HNCSNH(CH_3)]_2Cl_2$ (VII).

In typical experiment, 1.00 g of the precursor was dissolved in approximately 10 ml of TOP. Phosphonoacetic acid (PAA) (5.00 g) was heated in an inert atmosphere until it melted then the temperature was adjusted to a desired reaction temperature. The dissolved precursor in TOP was injected into hot PAA. When the desired reaction temperature was reached, then the reaction was allowed to proceed for an hour. The resultant solution was cooled to about 90 °C, and then THF 30 ml was added. The obtained oily material was dried resulting in formation of a hard solid material was dissolved in toluene for characterization.

2.4.2. Synthesis of PAA/TOPO-capped nanoparticles

In typical experiment, 1.00 g of the precursor was dissolved in approximately 10 ml of TOP. Phosphonoacetic acid (PAA) and TOPO (5.00 g each) in a 1:1 ratio was heated under inert an atmosphere until it melted and then the temperature was adjusted to a desired reaction temperature. The dissolved precursor in TOP was injected into hot mixture of PAA and TOPO. When the desired reaction temperature was reached, the reaction allowed to proceed for an hour.

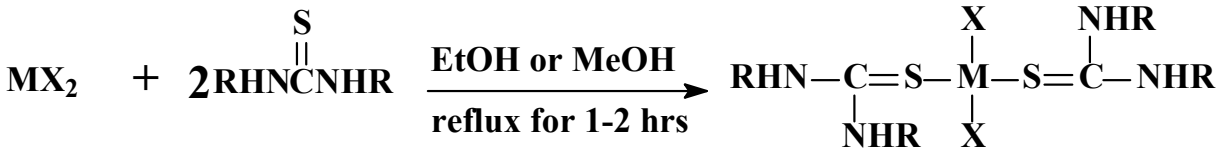
The resultant solution was cooled to about 90 °C, and then added 30 ml of THF. The obtained hard solid material was dissolved in toluene for characterization.

2.4.3 Synthesis of HDA-capped CdS nanoparticles

In typical experiment, 1.00 g of the precursor was dissolved in approximately 10 ml of TOP. Hexadecylamine (HDA) (5.00 g) was heated in an inert atmosphere until it melted then the temperature was adjusted to a desired reaction temperature. The dissolved Cd precursor (Complex IV) in TOP was injected into hot HDA. When the desired reaction temperature was reached, then the reaction was allowed to proceed for an hour. The resultant solution was cooled to about70 °C, and then methanol 30 ml was added to precipitate nanoparticles. The precipitated nanoparticles were further washed with methanol three times to remove excess HDA. The obtained yellow product was dissolved in toluene for characterization.

3. Results and discussion

3.1 Characterization of the new complexes



M= Cd, Mn, Ni

R= H, CH_3, C_6H_5, $CH_3CH_2CH_2CH_2$

X= Cl

(In case of R= C_6H_5, there will be one R-group in the ligand and also in R= $CH_3CH_2CH_2CH_2$ the ligand will have three R-groups)

Thiourea and its derivatives are capable of forming a co-ordinate bond through sulphide and nitrogen atoms. The only reported metals is Ti^{+4} and all others being S-bonded with *ν*(M-S) occurring at 300 - 200 cm^{-1}. Moloto *et al*[5, 6] has reported the reactions of a number of N-alkyl substituted thioureas with lead, copper and cadmium the compound which were formed were to stable for long periods, easy to prepare, inexpensive and gave good crystalline particles. All the prepared complexes were also obtained in reasonable yields but attempts to grow crystals was unsuccessful. The reaction equation for all complexes prepared is as follows:

3.1.1 Spectroscopic studies

3.1.1.1 FTIR spectral analysis

The previous results [5, 6] have shown that upon coordination *v*(NH) bonds of substituted thioureas are not significantly affected which indicates that the ligands are binding through S the atom. The *v*(NH) in complexes I and V showed no significant shifts in the region 3340-3150 cm $^{-1}$. The bands due to *v*(CN) observed at about 1559, 1525, 1449, 1415,1360 cm^{-1} for the complex I and the bands observed at about 1570, 1525, 1415, and 1256 cm $^{-1}$ for complex V (Figure 10) correspond to *v*(CN) of the free phenylthiourea shown in Figure 11. Those due to the *v*(CS) stretching frequency for the ligand at about 719, 638, 538 and 519 cm^{-1} and were shifted to lower frequencies upon coordination to 688 and 533 cm $^{-1}$ for complex I and to 715 and 539 cm^{-1} for complex V respectively. The shift to higher frequencies of *v*(CN) if the complexes and the shift to lower frequencies of *v*(CS) suggest the coordination of the metal is through the sulphur atom. In both complexes some peaks were also observed in the region of 500-200 cm $^{-1}$ which might be due to M-S bond. Also in the dimethylthiourea complexes no significant shifts were observed in the *v* (N-H) regions which suggest that NH's are not involved in binding. The peaks due to *v*(C-N) were observed at 1580, 1529, 1372 and 1303 cm $^{-1}$ for complex II, also those in complex IV were observed at 1583, 1529, 1372, 1297 and for complex VI (Figure 12) were observed at about 1597, 1534, 1456, 1297, 1190 and 1037 cm $^{-1}$ which are the shift to higher frequencies compared to the bands of *v*(C-N) of the free dimethylthiourea shown in Figure 13. The increase of those *v*(C-N) bands in complexes is due to an increase of single character of C-N upon the coordination of a metal through sulphur atom. Those due to *v*(CS) stretching frequencies were observed at 714, 530 cm $^{-1}$ for complexes II and IV were at about 715, 539 cm $^{-1}$, and for complex VI were observed at 715, 666, 541 due to a decrease in double character of C=S bond.

The blue shift of v(CS) bands in complexes III and VII confirms the coordination of metal through sulphur atom, those bands were observed at 710 for complex III, and 617 and 547 cm^{-1} for complex VII in relation to 714 and 530 cm^{-1} observed in ligands. All these bands are summarized in Table 2. There were no significant shifts in the region of v(NH), the bands due to this functional group were observed at 3220, 3138 cm^{-1} and 3201, 3009 cm^{-1}, respectively.

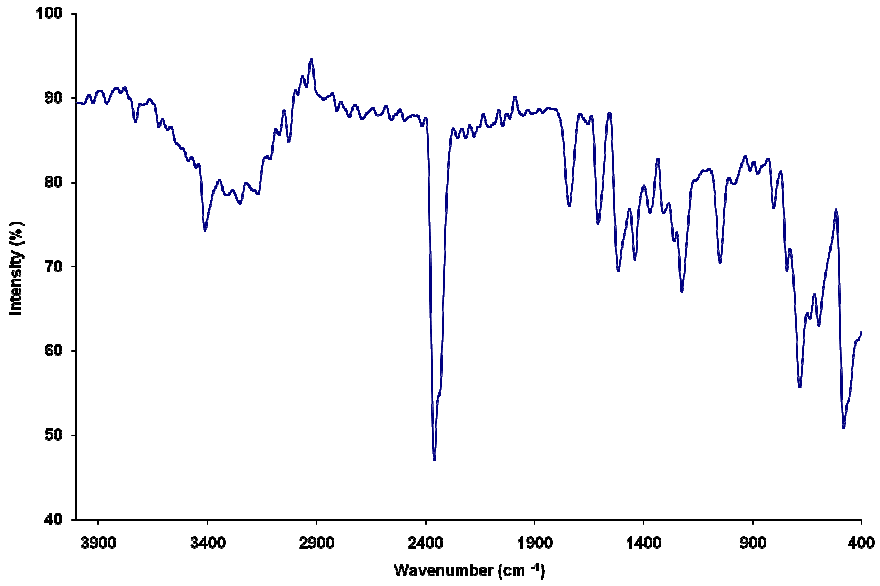


Figure 10 : Infrared spectrum of complex V

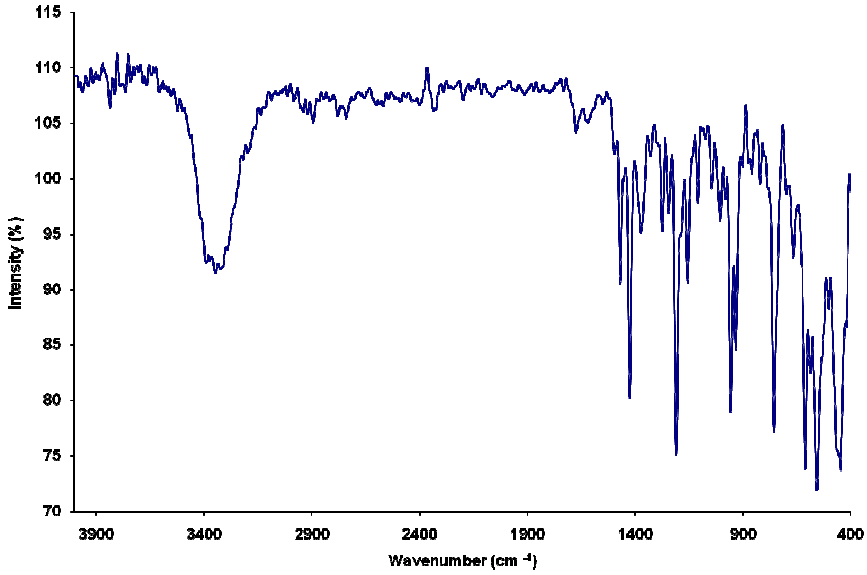


Figure 11: Infrared spectra of free phenylthiourea ligand

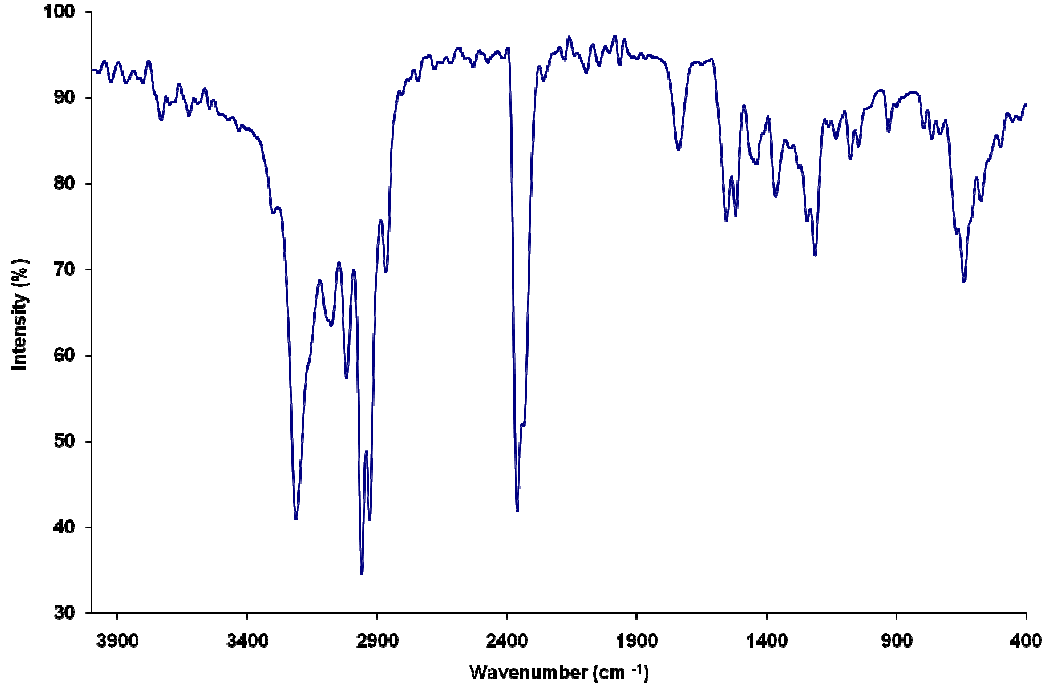


Figure 12: Infrared spectra of complex VI

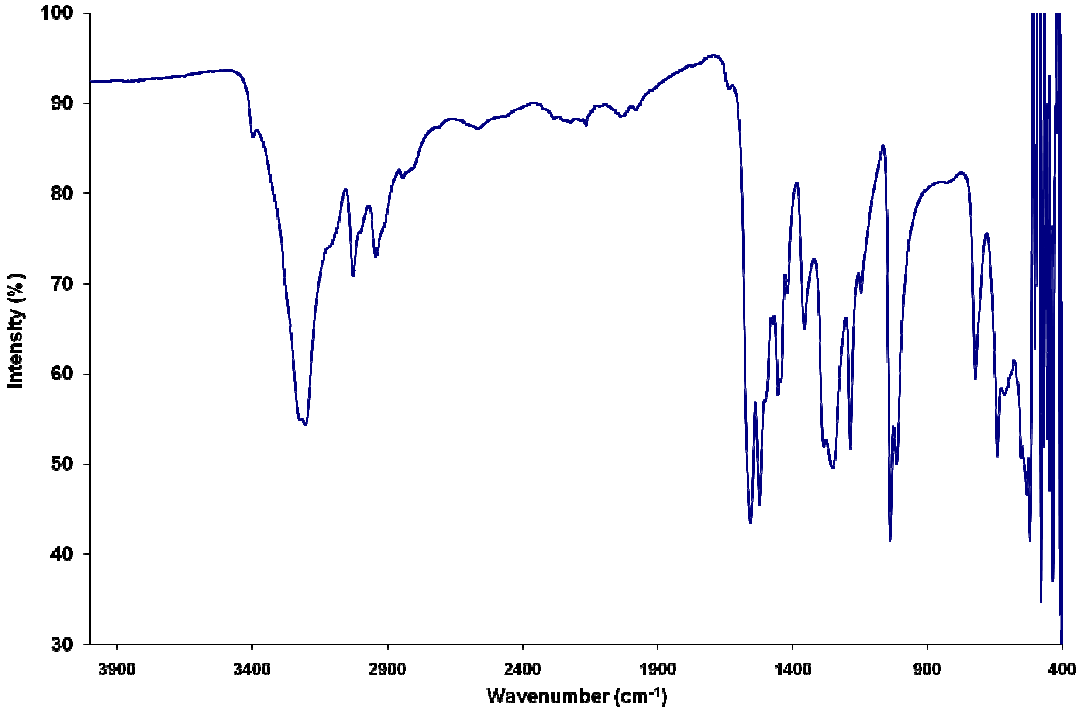


Figure 13: Infrared spectrum of free dimethylthiourea ligand

Table 2 : Selected IR data for all metal complexes and free ligands

Complex	Vibrational modes (cm^{-1})		
	v C=S	*v* C-N	*v* N-H
I	688, 533	1559, 1525, 1449, 1415, 1360	3340
II	714, 530	1580, 1529, 1372, 1303	3349
III	710	1535	3345
IV	715, 539	1583, 1529, 1372, 1297	3322
V	715, 539	1570, 1525, 1415,1256	3295
VI	715, 666, 541	1597, 1534, 1456, 1297, 1190, 1037	3220, 3138
VII	617, 547	1566, 1519, 1453, 1319, 1213, 1076	3201, 3009
PTU	753, 698, 610	1467, 1422, 1368, 1328, 1272, 1240, 1207, 1153, 1109, 1015	3383, 3342, 3308
DMTU	719, 638, 538, 519	1551, 1518, 1440, 1418, 1348, 1273, 1273, 1242, 1182, 1142, 1035	3192, 3019
TBTU	714, 530	1546, 1508, 1420, 1276, 1105	3320, 3205

PTU—Phenylthiourea, DMTU---Dimethylthiourea and TBTU---Tributylthiourea

3.1.1.2 NMR spectral analysis

Nuclear magnetic resonance (NMR) spectroscopy is one the of the most powerful technique available for determining the structure of the molecules. It identifies the number and the type of the proton and carbon atoms in organic and inorganic molecules. It also reveals the positions of nuclei in the molecule relative to each other. NMR spectroscopy is applied to compounds containing heteroatoms.

The ^{1}H NMR spectrum of complex III showed an intense peak at 7.26 ppm due to NH protons. Two singlets were observed at 3.31 and 1.43 ppm corresponding to the first CH_2's nearer the N atom. A doublet at 1.28 ppm assigned to third CH_2 and triplet at 0.86 ppm was also observed corresponding to CH_3 .The ^{13}C $\{^{1}H\}$ NMR spectrum of the same complex showed a small peak assigned to CS group at 181.86 ppm and four singlet peaks 42.81, 30.63, 19.26, 13.40 ppm corresponding to first CH_2's from N atom and the last peak was assigned to CH_3. The ^{1}H NMR spectrum of complex II showed two broad peaks at 7.09 ppm due to NH protons and 2.09 ppm assigned to CH_3 protons.

The ^{1}H NMR spectrum of complex I (Figure 14 (a)) showed a broad peak at 9.67 ppm for NH and NH_2 protons and two doublet at 7.33 and 7.23 ppm corresponding to protons of the first CH's that are in the same chemical environment in benzene ring and protons of the second CH's in the benzene ring respectively. The singlet peak for the last proton in the benzene ring was observed at 7.02 ppm and the $^{13}C\{^{1}H\}$ NMR spectum (Figure. 14 (b))of this complex showed a CS peak at 179.15 ppm and four strong peaks for carbons in the benzene ring at 137.00, 126.23, 122.39 and 121.00 ppm.

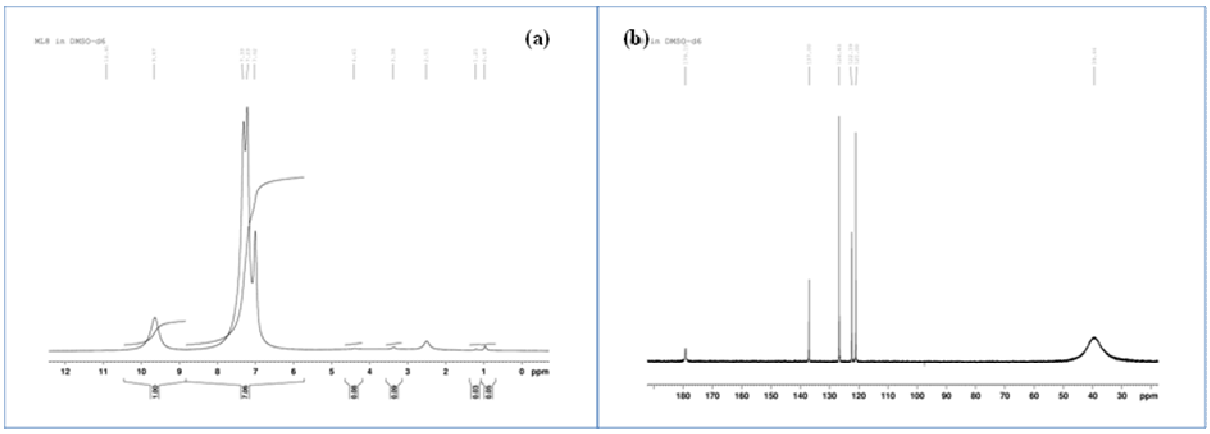


Figure 14: NMR spectra of ^{1}H (a) ^{13}C (b) of $Mn[(C_6H_5)HNCSNH_2]_2Cl_2$

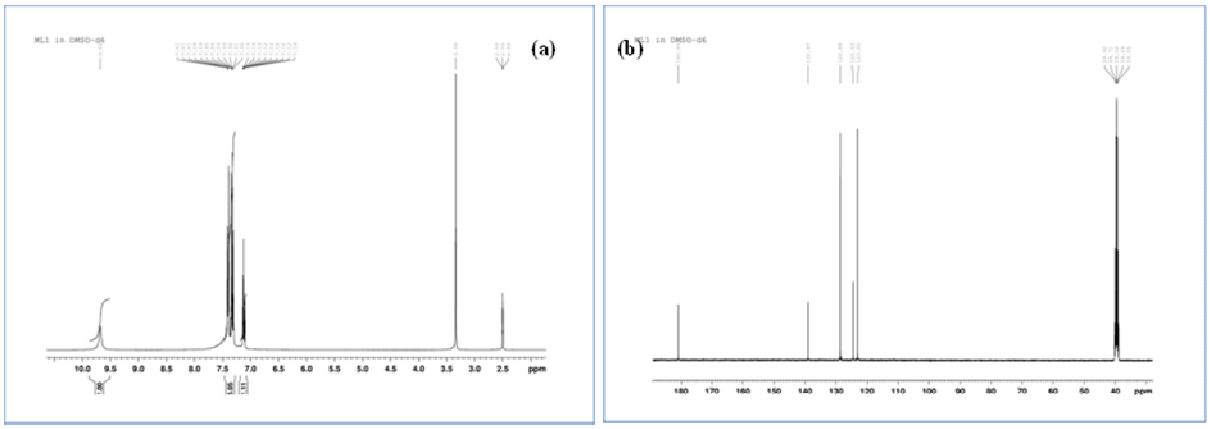


Figure 15: NMR spectra of ^{1}H (a) and ^{13}C (b) of $Cd[(C_6H_5)HNCSNH_2]_2Cl_2$

The H NMR spectrum of complex V showed in Figure 15 (a) displayed a broader peak at 9.68 ppm corresponding to NH and NH_2 protons. While the first protons in benzene where observed at a doublet at 7.41, 7.39 ppm split by two following protons of CH's in phenyl ring. The two protons CH's of phenyl ring showed a triple at 7.35, 7.33 and 7.30 ppm and the last proton in phenyl ring showed a peak at 7.14 ppm. The $^{13}C\{^{1}H\}$ NMR spectrum of complex V (Figure. 15

(b)) showed the CS peak around 180 ppm and also four singlet peaks for carbons in benzene ring were observed at 138.97, 128.66, 124.43 and 123.05 ppm.

3.1.1.3 Thermal analysis

Thermal decomposition studies on metal coordination complexes have shown various correlations of decomposition temperature with metal ion, ligand character, or counter-ion [102-103]. The thermal decomposition has been done as there is an interest in the isolation and identification of the solid decomposition products of complex compounds; interesting decomposition intermediates have been produced [104, 105] and decomposition products have been identified and decomposition schemes suggested.[103, 106] Some investigators have used thermogravimetry as a means of synthesizing new compounds[107, 108].

Metal compounds of thioureas are sulfur bonded complexes with well established structures. Thermal decomposition studies of nickel (II) thiourea compounds have been done by Jona and Sramko[109] and of molybdenum by Spitsyn[110]. For nickel thiourea halides, initial weight loss involved loss of a halogen atom and formation of NiS; however, solid residues have a Ni/S ratio > 1, suggesting some loss of free thiourea. The early stages of decomposition also produced organic products referred to as "melam". While the overall pattern of decomposition was generally similar to that of thiourea itself; coordination clearly has an important influence on the decomposition pattern. The objectives of this study were to consider the decomposition of some substituted thiourea complexes, both to explore stability relationships and to identify the decomposition products formed, including the volatile organic materials.

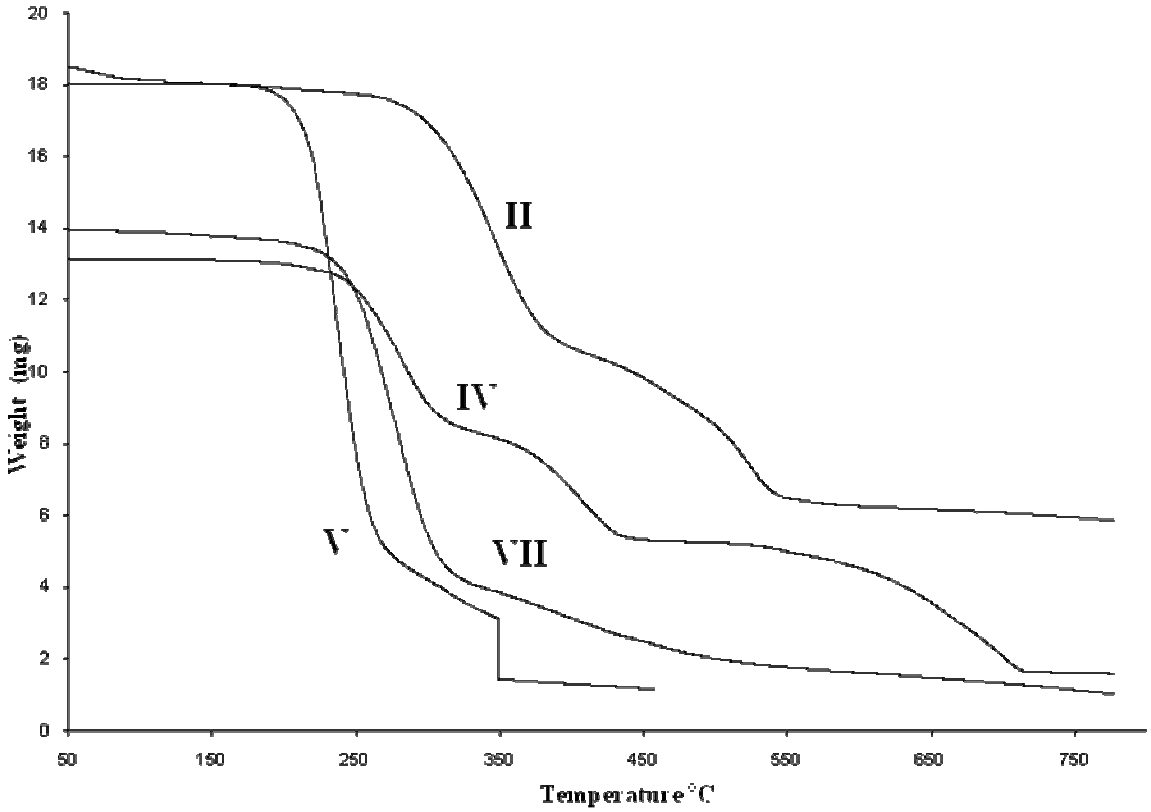


Figure 16: TGA spectrum of complexes II, IV, V and VII.

Bailey *et al*[111] has shown that the decomposition of metal complexes with thiourea and its derivatives yield the metal sulphide compounds, the study were conducted using complexes of cadmium, manganese, cobalt, nickel, iron and chromium. The TGA curves shown in Figure 14 indicate the two-step decomposition of complexes II, IV, and V. Complex IV and V display their first decomposition step at around 250 °C (Figure 16) where both complex loose its organic material from the ligands followed by the loss of the chlorides. Complex II has firstly loose water at about 100 °C, and a second decomposition step of corresponding to the loss of organic

material from the dimethylthiourea at 295 °C. The three complexes their last decomposition step at around 370 °C which correspond to the loss of the .There no exothermic process observed in our TGA curve (Figure 16) which is in contrast to those of copper, tin and zinc thiourea complexes[32], where metal sulphides were converted to metal oxides. The decomposition trend of complex V (Figure 14) displayed the first decomposition temperature at around 240 °C which was due to loss of organic material and the last decomposition step of metal chlorides salts at about 450 °C. Complex VII (Figure 16) showed a clean decomposition at around 260 °C which ended close to 350 C. Figure 17 shows a one clean decomposition step for complex I which starts at 210 °C and ends at 270 °C, displaying their high volatility nature which renders them as good precursors for the preparation of thin films using MOCVD. Complex III displayed the same decomposition trend observed in complex I. All the prepared complexes showed their first decomposition step above 200 °C. Thus the temperature range of 120 °C to 200 °C was chosen for the synthesis of nanoparticles. No such conversion of Cadmium sulphide, nickel sulphide and manganese sulphide into their metal oxides was observed during thermal decomposition of the complexes reported in this work. Such conversion is usually accompanied by an increase of the curve at higher temperatures.

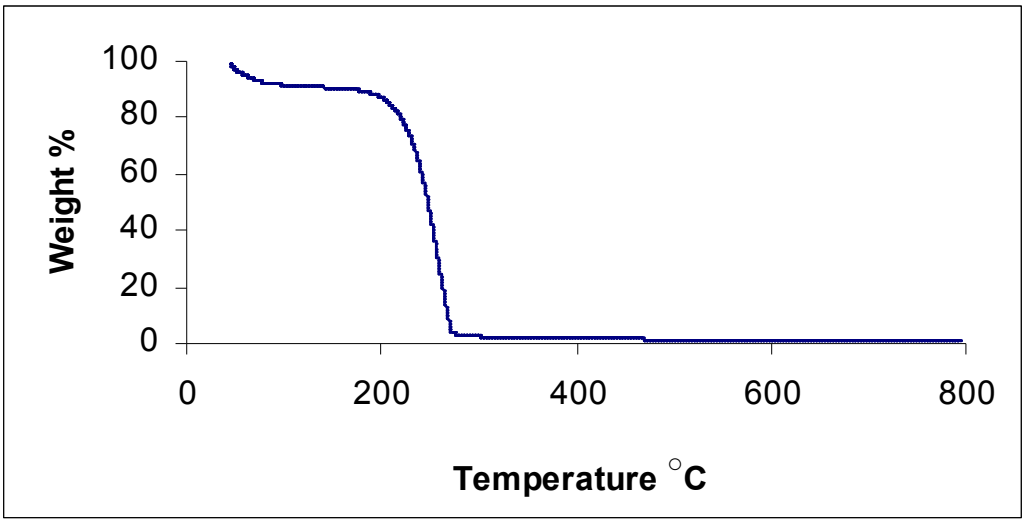


Figure 17 : TGA curve of complex I

3.2 Characterization of nanoparticles

This section covers discussions of all the data from the characterization of particles prepared from these nickel, manganese and cadmium complexes. These were characterized by means of their optical and structural properties. A combination of spectroscopic techniques such as absorption and photoluminescence were used to understand the critical absorption and emission features of the nanoparticles. The structural characterization was carried out using TEM. These include the nanoparticles made with PAA as capping agent and all the characterization data revealed that the effect on the growth and morphology of particles as a function of temperature.

3.2.1 PAA-capped nanoparticles

Generally, there are number of factors which govern the size and shape of nanoparticles i.e, the capping group, concentration of the monomer/precursor, reaction time and the reaction temperature. The monomer/precursor concentration is a factor which affects the morphology and

the size of nanoparticles has been well studied by Cheon *et al*[112] and Moloto *et al*[9]. Both studies elucidated that the monomer concentration influences in the morphology of nanoparticles. Figure 18 shows the relationship between monomer concentration and time. The graph shows the initially constant supply of monomer concentration with increase in time, results in the formation of different morphologies driven by growth parameters and crystalline phases of the nanoparticles. The figure indicates that a decrease in monomer concentration leads to a decrease in particle size.

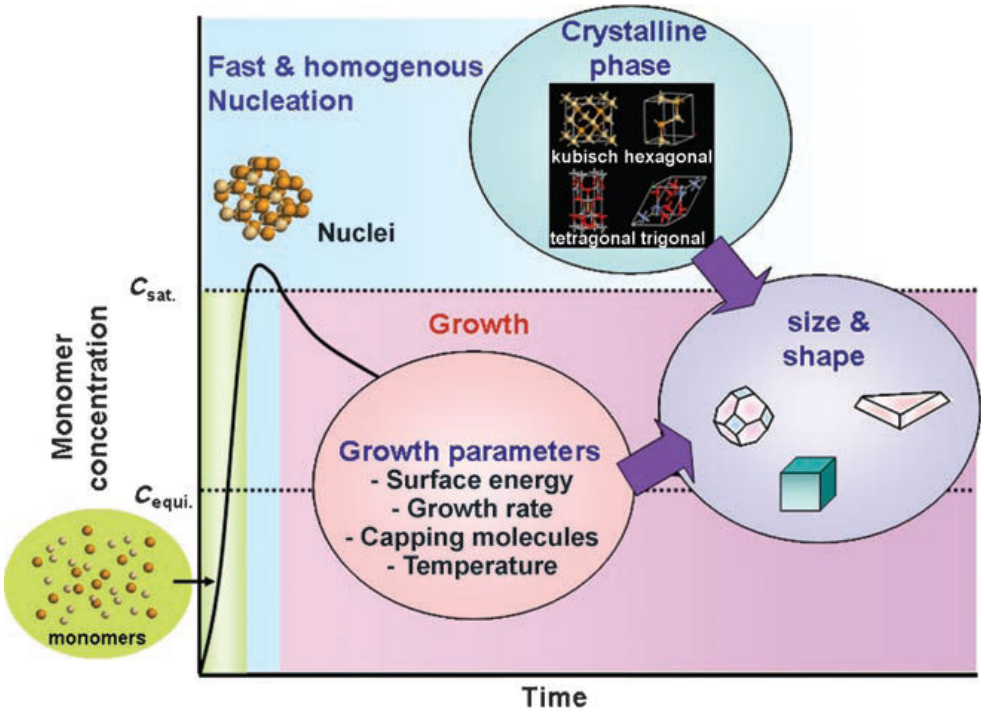


Figure 18: Schematic diagram showing the effect of reaction parameters on the morphology of nanoparticles.

Nair *et al*[40]and Moloto *et al*[9] have also shown the effect of a capping group on the properties of nanoparticles. Nair *et al*[40] prepared TOPO-capped CdS which were spherical with an average diameter of 5.1 nm as shown if Figure 19.

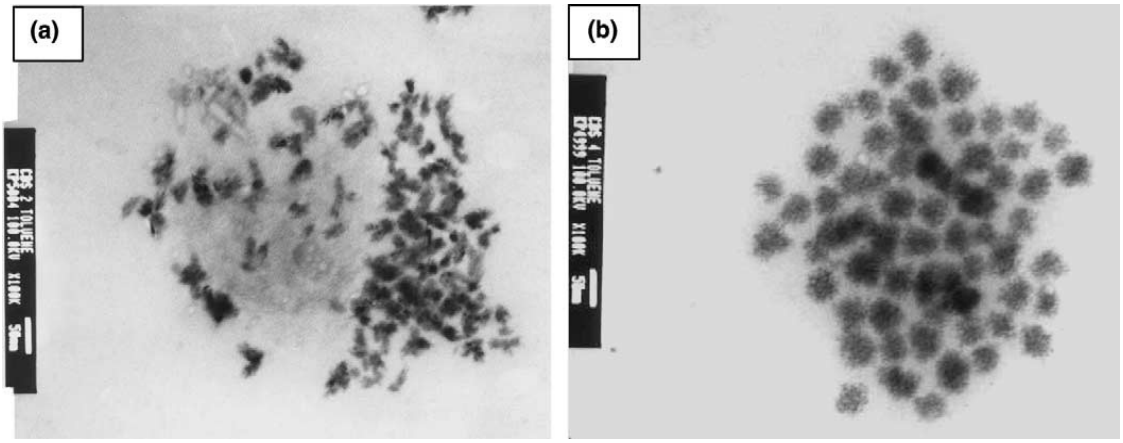


Figure 19: TEM image of CdS nanoparticles synthesized at 150 °C (a) and 240 °C (b).[40]

While Moloto *et al*[10] showed that using HDA as a capping group gave rod-shaped nanoparticles with 5 nm length and 2 nm width, as shown if Figure 20. An increase in particle size with time is consistent with an Ostwald ripening process.

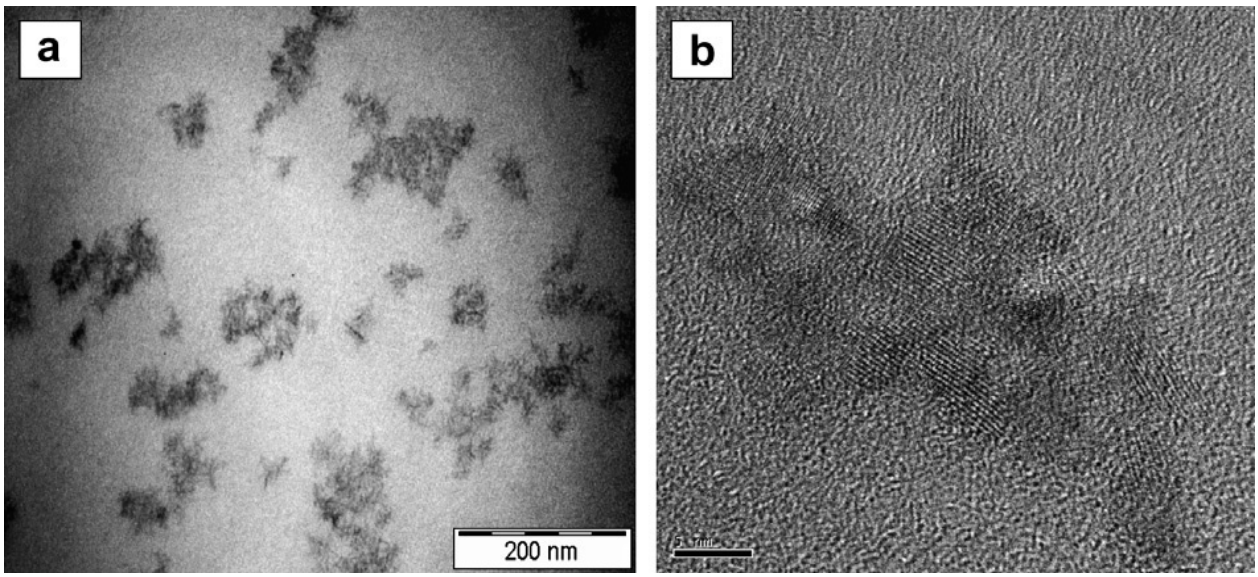


Figure 20: TEM (a) and HRTEM (b) image of HDA-capped CdS nanoparticles at 180 °C.[10]

3.2.2 Optical properties of PAA-capped nanoparticles

The shape control of inorganic nanocrystals has been a hot topic over the past two decades in nanoscience. The shape guiding process for the growth of nanocrystals is as follows.[113] Initially, the presence of the seeds at the nucleating stage is the critical for directing the intrinsic shape of the nanocrystals due to the seeds characteristic unit cell structure. At this stage, the crystalline phase of the seed is highly dependent on its reaction environment, especially the temperature. After the formation of a preferred crystalline-phase seed, the final morphology of the nanocrystals is mainly determined by growth process through a delicate balance between kinetic growth and thermodynamic growth controls. Anisotropic shape control is mainly through the preferential growth of a particular crystallographic surface of nanocrystals during a kinetically controlled growth process. While the isotropic shape control is via the adjustment of total Gibbs

energy of the nanocrystals to close the minimum value during the thermodynamically controlled process.

For the temperature dependence of the growth, the PAA-capped semiconductor nanoparticles synthesis was carried out at constant precursor concentration (1.00 g in 10 ml TOP injected into 5.00 g PAA) at 120, 160 and 200 °C. After the reaction was allowed to proceed for an hour, it was cooled to 90 °C then added THF and dried. The resultant solid material was dissolved in toluene for characterization. The onset absorption of semiconductor nanoparticles is attributed to the band gap absorption, and this will be blue shifted (shift to shorter wavelengths) relative to their bulk materials due to quantum size confinement effects. Figure 21 shows the absorption spectra and the threshold of PAA-capped CdS nanoparticles prepared from complex V which are blue shifted relative to the bulk CdS material (Eg = 515 nm, 2.41 eV), suggesting the formation of nanometer sized material. The PAA-capped CdS nanoparticles showed bang edges at 453 nm (2.74 eV), 402 nm (3.08 eV) and 450 nm (2.76 eV), respectively, with increase in reaction temperature (from 120 °C to 200 °C). At 120 °C, the band gap absorption is much bigger than that observed at higher temperatures. This might be due to the fact that PAA has a melting point of 143- 146 °C. So PAA is not able to interact in its full capacity with CdS. At 160 °C, the absorption of spectrum shows a sharp excitonic peak at 370 nm due to a strong quantum confinement. The shift from the blue to the red region as the temperature increases could be attributed to the decreasing degree of confinement of charge carriers within the excitonic Bohr radius, as a result of the increase in size with increasing temperature.

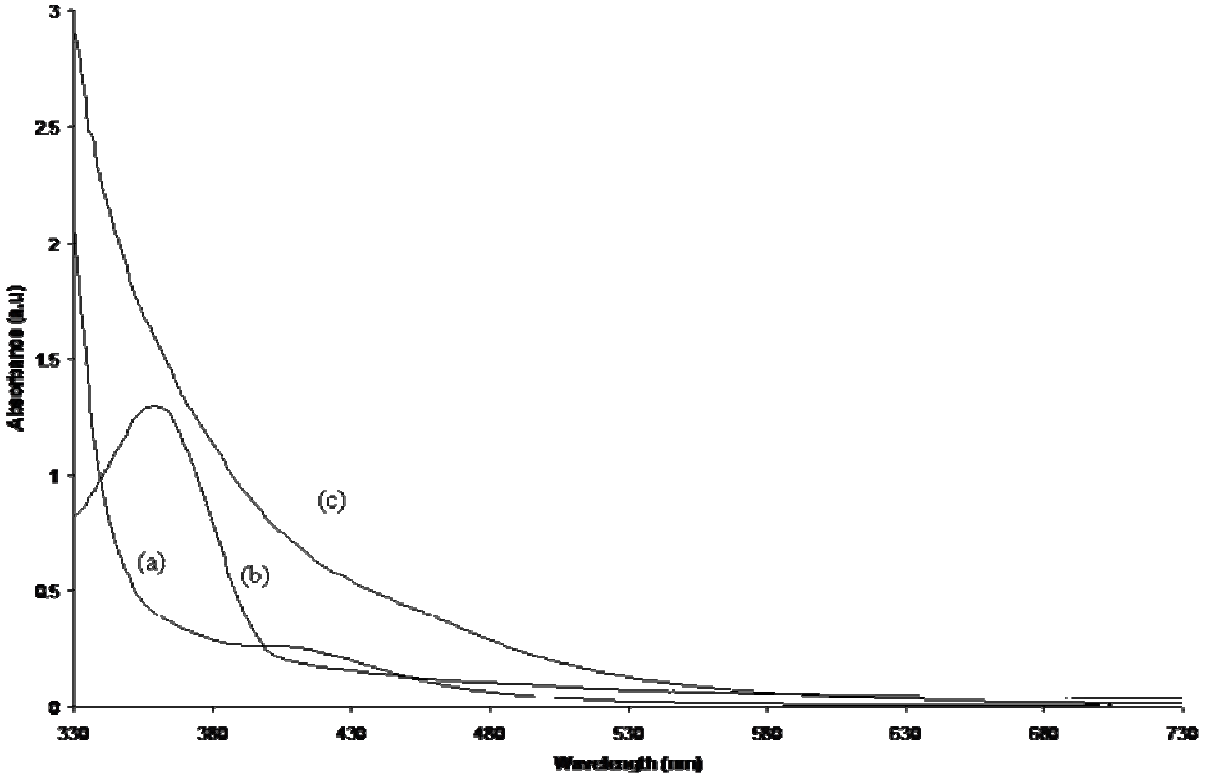


Figure 21: Absorption spectra of PAA-capped CdS from complex V at different temperatures, 120 (a), 160 (b) and 200 °C (c).

The photoluminescence spectra shown in Figure 22 were all red shifted from their corresponding absorption edges with emission maxima of 470 nm, 502 nm and 540 nm, respectively with the increase in reaction temperature. The emission peak at 120 °C is close to its corresponding optical absorption edge, this suggest a near band edge emission (shallow trap emission) is present. The broadness of the emission peaks observed at higher temperatures suggests that particles do not have uniform size. The band edges and emission maxima are summarized in Table 3. It is noted that the increase in particle size is witnessed by the shift of the absorption

edge from the blue to the red region of the absorption spectrum. This can also cause the tailing of spectra towards the red region.

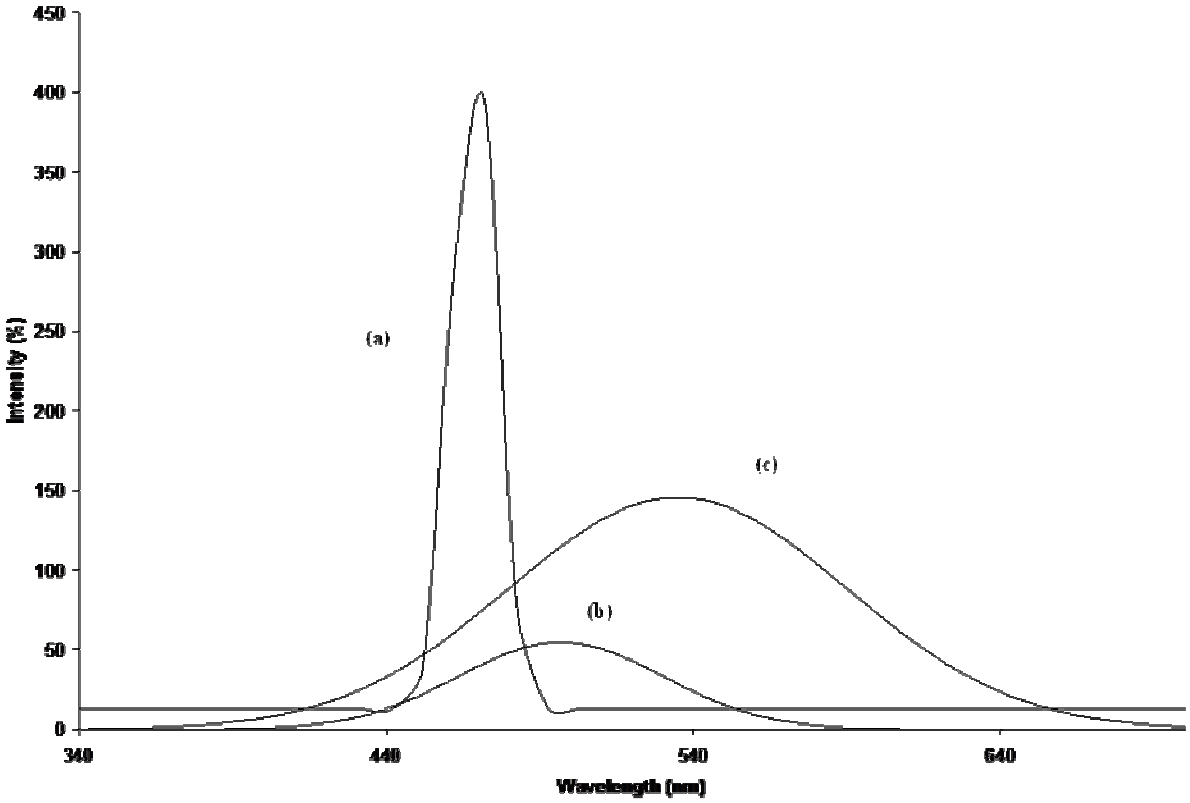


Figure 22: Emission spectra of PAA-capped CdS nanoparticles from complex V at different temperatures 120 (a), 160 (b) and 200 °C (c).

Table 3: Band edges and corresponding emission peaks of CdS at different temperature

Reaction Temperature (°C)	Band edges (nm)	Band edge (eV)	Emission peak (nm)
120	453	2.74	470
160	402	3.08	502
200	450	2.76	540

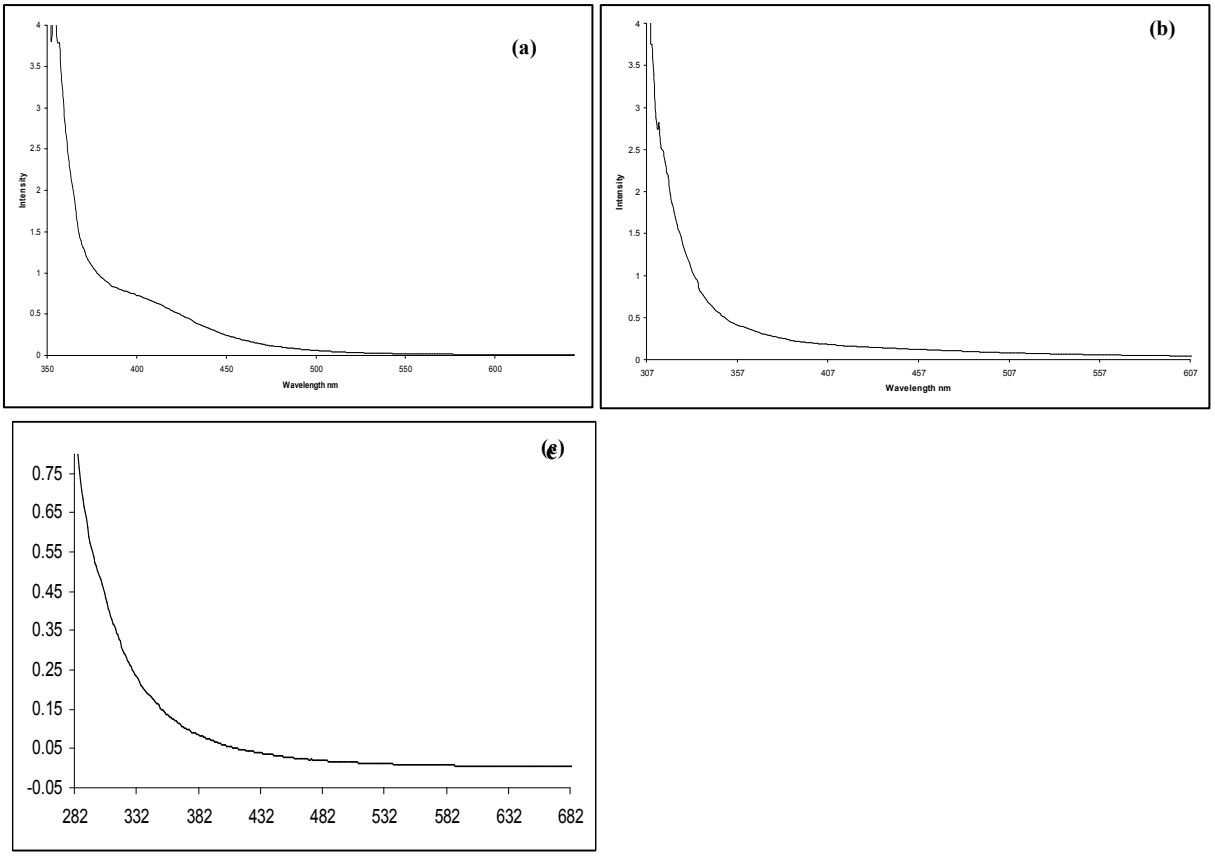


Figure 23: Absorption spectra of PAA-capped MnS from complex III at different temperatures 120 °C (a), 160 °C(b) and 200 °C(c).

The absorption spectra of PAA-capped MnS semiconductor nanoparticles are shown in Figure 23. The absorption band edges are blue shifted from the bulk material of MnS 400 nm (3.1 eV), confirming the existence of a quantum confinement effect. The absorption band edges for 160 °C and 200 °C were observed 337 nm (3.68 eV) and 382 nm (3.24 eV) respectively however the band edge at 120 °C, which was observed at 432 nm (2.87 eV). This bigger bang gap at 120 °C has been also observed in PAA-capped CdS (Figure 21 (a)). However, it is observed that the confinement is rather weak, which could be attributed to larger particle size. Due to this weak quantum confinement, broad emission peaks are observed in Figure 24. The emission peak observed at 120 °C was at 515 nm. The emission peaks from other reaction temperatures were observed at 401 nm and 458 nm respectively with increase in temperature. The absorption band edges and emission maxima are summarized in Table 4.

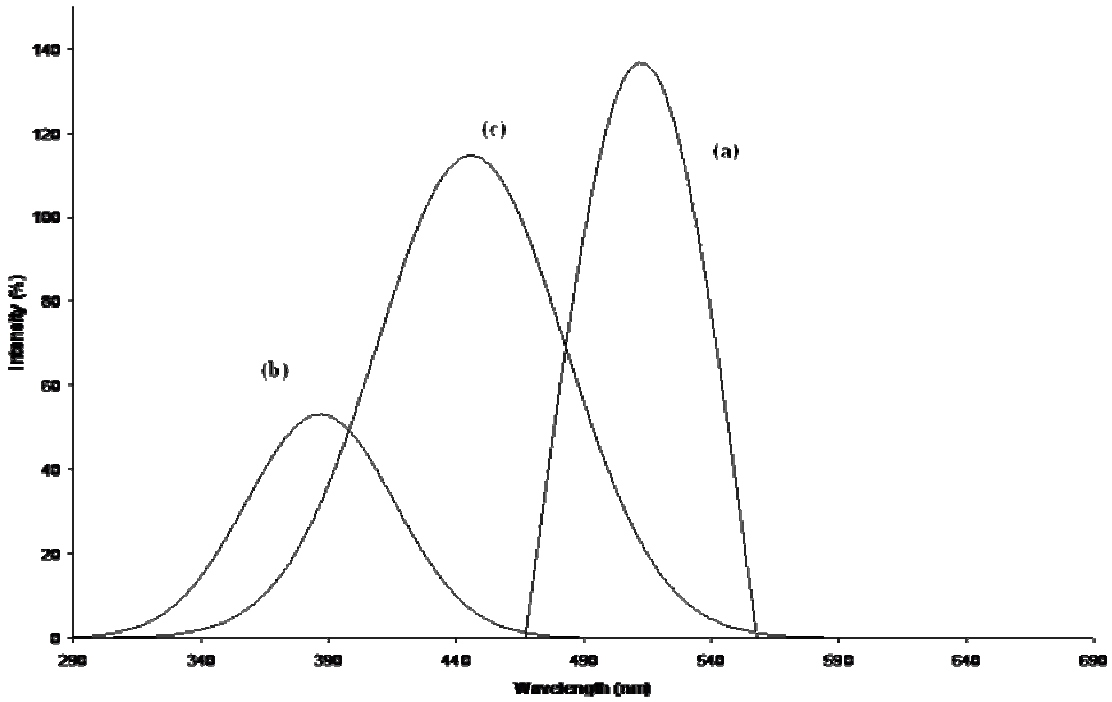


Figure 24: Emission spectra of PAA-capped MnS nanoparticles from complex III at different temperatures 120 °C(a), 160 °C(b) and 200 °C(c).

Table 4: Band edges and corresponding emission peaks of MnS nanoparticles at different temperatures

Reaction Temperature (°C)	Band edges (nm)	Band edge (eV)	Emission peak (nm)
120	432	2.87	515
160	337	3.68	401
200	382	3.24	458

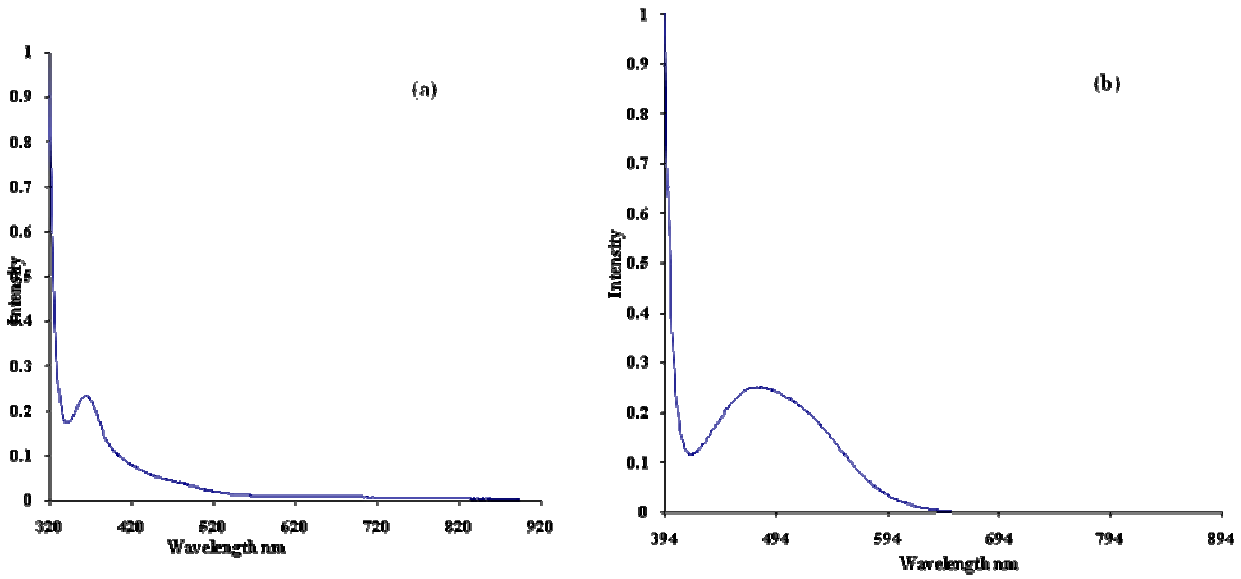


Figure 25: Absorption spectra of PAA-capped NiS nanoparticles from complex VII at different temperatures 160 °C (a) and 200°C(b).

The absorption band edges of PAA-capped NiS nanopartcles prepared form complex VII at different temperatures shown in Figure. 25 also display an increase in band edges from 160 °C to 200 °C. The absorption band edge for the temperature at 160 °C was observed at 415 nm (2.99 eV) and when the temperature was raised to 200 °C, the absorption band edge was observed at 582 nm (2.13 eV). The emission peaks corresponding to these band edges are shown in Figure 26. The emission maxima for the lower temperature observed at 518 nm. The emission for the sample at 200 °C is assigned to deeply trapped surface states because it occurs at lower energy relative to its absorption band edge. The absorption band edges and emission maxima are summarized in Table 5.

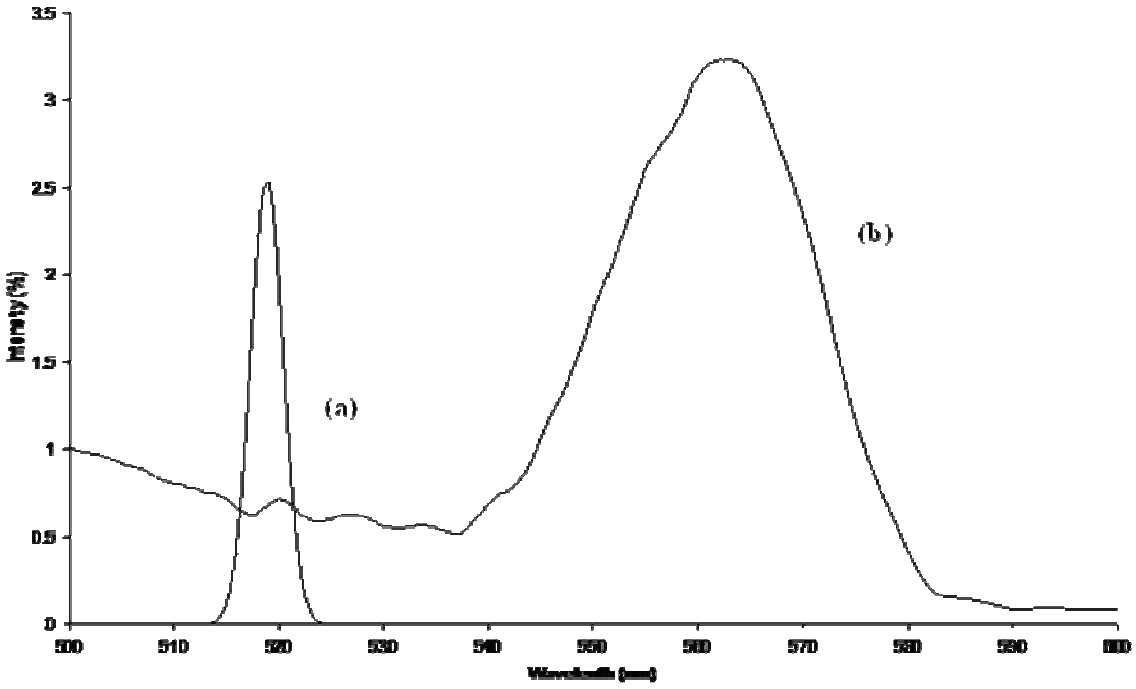


Figure 26: Emission spectra of PAA-capped NiS nanoparticles from complex VII at different temperatures 160 ℃ (a) and 200°C(c).

Table 5: Band edges and corresponding emission peaks of NiS nanoparticles at different

Reaction Temperature (°C)	Band edge (nm)	Band edge (eV)	Emission peak (nm)
160	415	2.99	518
200	582	2.13	562

3.2.3 Structural characterization

The TEM images shown in Figure 27 represent the PAA-capped CdS nanoparticles at the different temperatures at (a) 160 °C and (b) 200 °C. It can be seen that the reaction temperature greatly affects the morphology of PAA-CdS nanoparticles. Figure 27(a) shows the PAA-capped CdS nanoparticles at 160 °C, with smaller but longer rod shaped nanoparticles which have an average width 40 nm width. When the temperature was raised to 200 °C particles formed tubular particles with average width of 90 nm. This might be attributed to the varying potential binding sites on the capping ligand which can either be P=O and COOH functional groups. The polydispersity which was suggested from the absorption peak (Figure 21) is observed in Figure 27(c).

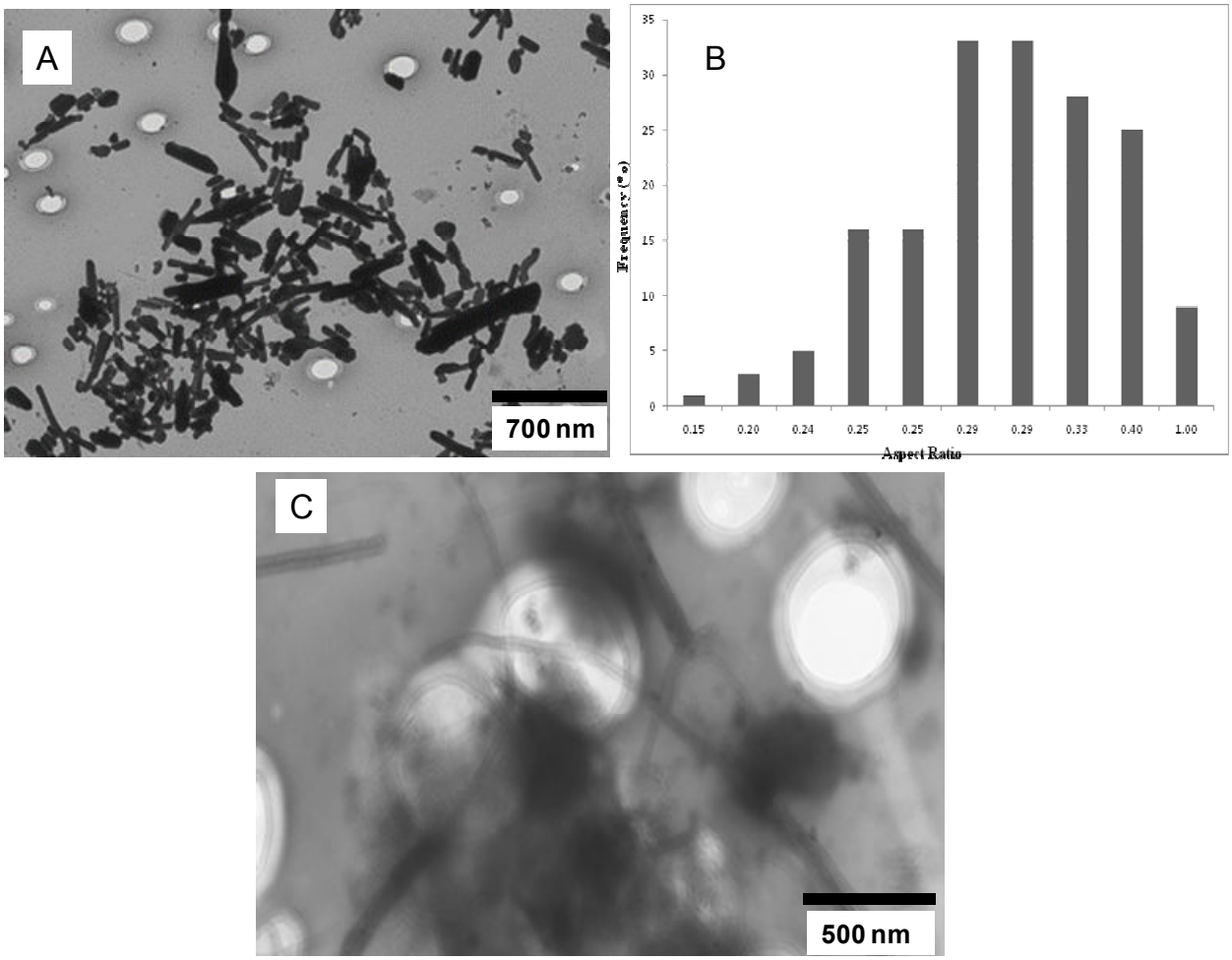


Figure 27: TEM image (a) of PAA-capped CdS nanoparticles at 160 °C, (b) corresponding particle size distribution histogram and TEM image at 200 °C(c)

The shift to higher wavelength of the band edges as the temperature was raised is also signified by the change of the morphology observed in Figure 27. It is not yet established whether PAA uses P=O or the COOH group to bind the surface of nanoparticles. The P=O functional group has been shown to be more prone to the formation of spherical nanoparticles with TOPO as capping ligand , but the effect of the steric hindrance in TOPO compared to PAA might differentiate the two. Obviously the P=O in TOPO is more favoured than the P=O in PAA because of the long alkyl chain in TOPO. The P=O bond is also the favoured one than COOH

group, because of the two –OH functional groups close to the COOH group. The hydrogens in –OH groups diminish the charge on the carboxylic group. Goodwin and Witkop[114] reported the evidence of hydrogen bonding between –OH and the C=O of the carboxylic acid.

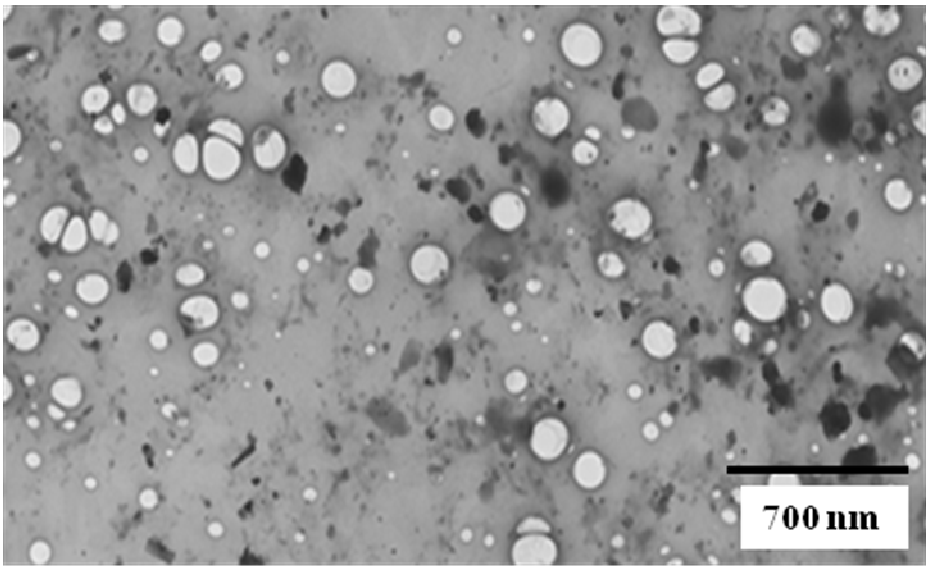


Figure 28: TEM image of PAA-capped MnS nanoparticles from complex III prepared at 200 °C.

The morphology of PAA-MnS was determined by TEM, and its image is shown in Figure 28. The image shows a few spherical particles which have an average size of 40 nm and others that are irregularly shaped. The absorption peak in Figure 23(c) which did not display a sharp excitonic peak or a broad emission peak Figure 24(c) indicates polydispersity of nanoparticles which is also observed in Figure 28.

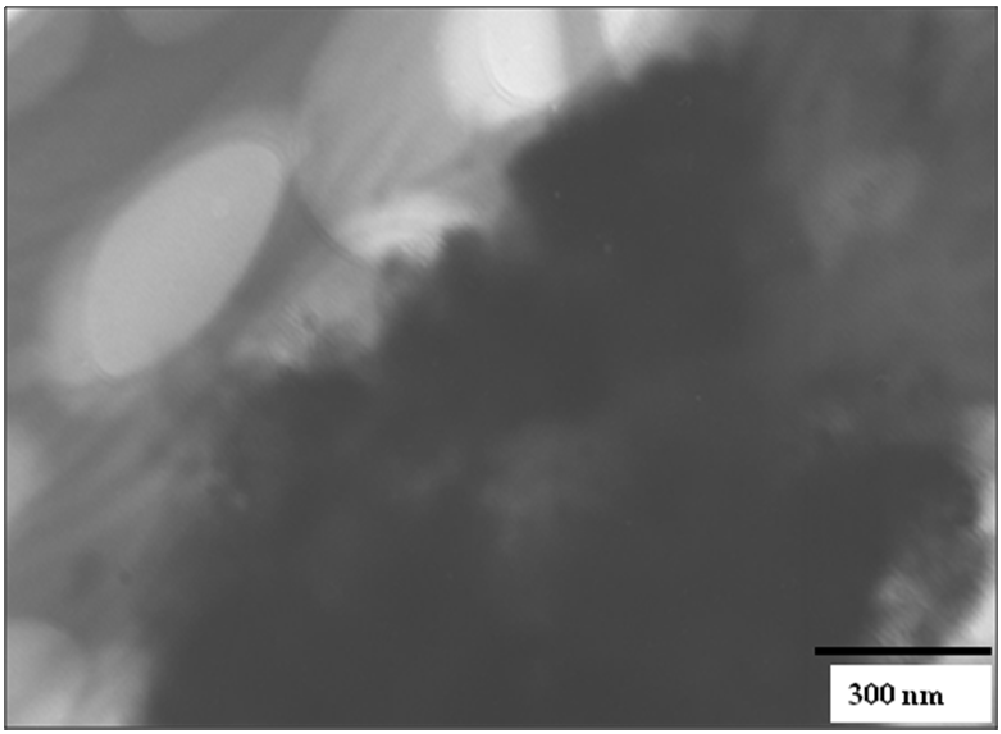


Figure 29: TEM micrograph of PAA-capped NiS from complex VII at (a) 160 °C.

The TEM micrograph of PAA-capped NiS nanoparticles shown in Figure 29 shows agglomeration of particles making it impossible to identify its shape.

3.3 HDA-capped nanoparticles

3.3.1 Optical properties

3.3.1.1 HDA-capped CdS nanoparticles

Figure 30 shows the absorption band edges of HDA-capped CdS nanoparticles prepared from the cadmium complex made with *N,N'*-dimethylthiourea. The nanoparticles were prepared at different temperatures 120 °C, 160 °C to 200 °C. The samples at the different temperatures all displayed a blue shift of the optical band edge in relation to the bulk material of CdS which is observed at 515 nm. As the temperature is increased, an increase in absorption band edge (469 to 496 nm) suggested an increase in the particle size. The sharp excitonic peak observed at 454 nm in Figure. 30(a) suggests particle monodispersity.

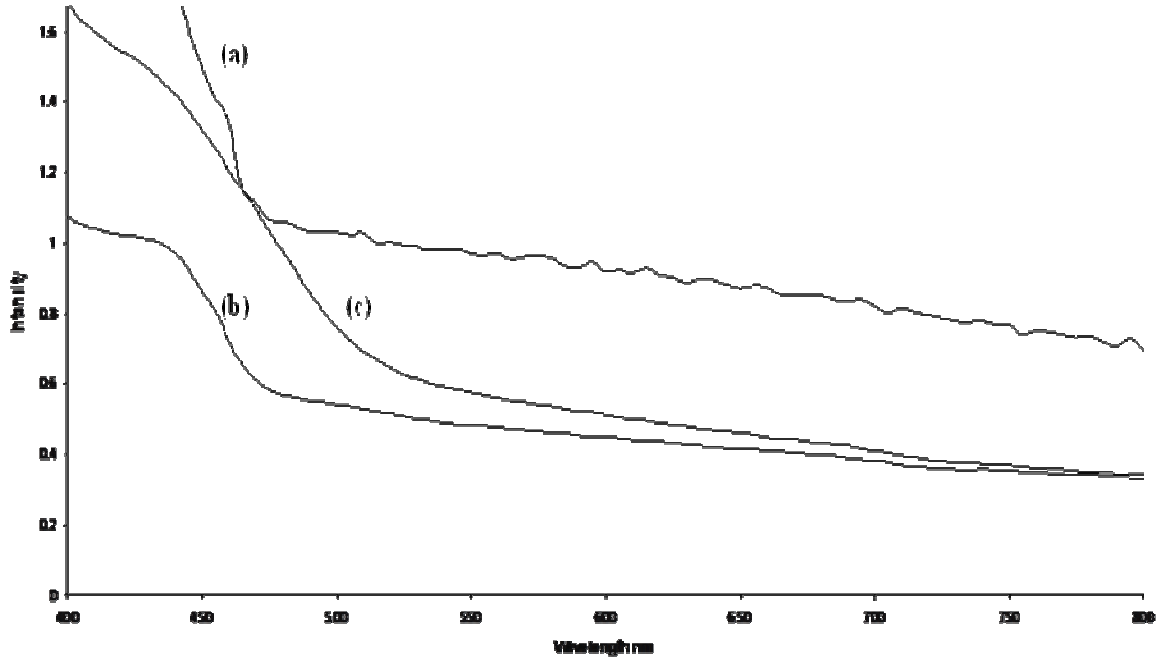


Figure 30: Absorption spectra of HDA-capped CdS from complex IV at different temperatures 120 °C (a), 160 °C (b) and 200 °C(c).

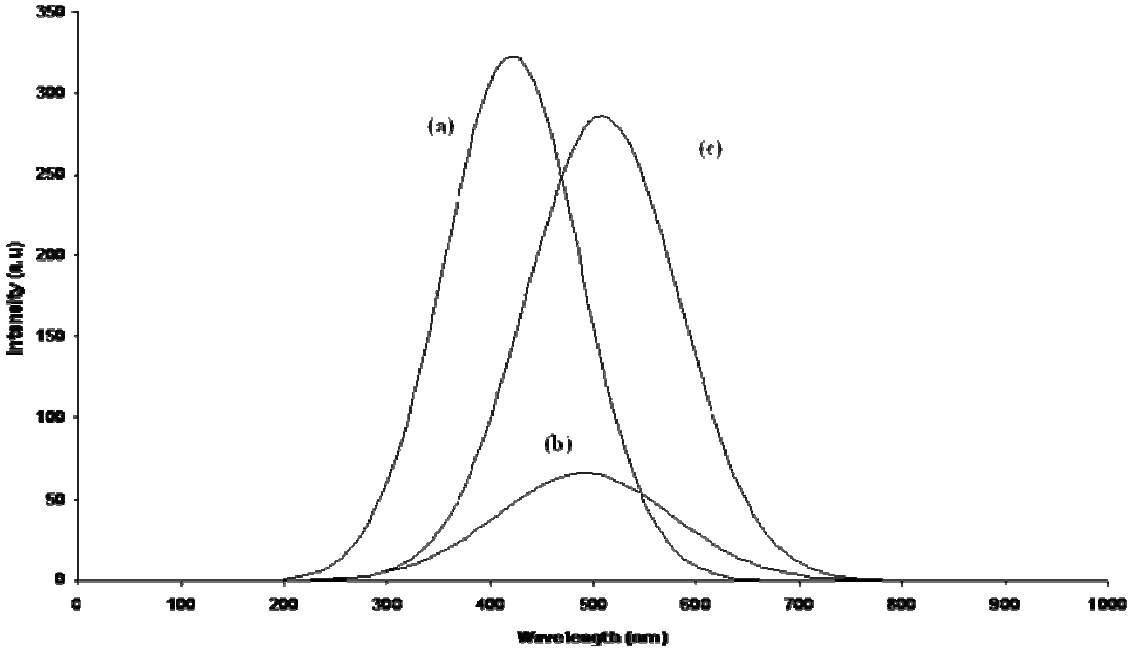


Figure 31: Emission spectra of HDA-capped CdS nanoparticles from complex IV at different temperatures 120 ℃ (a), 160 °C (b) and 200 ℃(c).

The photoluminescence spectra (Figure 31) show the emission maxima of HDA-capped CdS nanoparticles at different temperatures. The emission maxima obtained at lower temperature (120 °C) might be caused by a poor passivating ability of HDA at the lower temperature. As the temperature was increased from 160 °C to 200 ℃ red-shifted emission maxima of 484 nm and 508 nm respectively were observed.

3.3.1.2 HDA-capped NiS nanoparticles

Figure 32 shows absorption and emission spectra of HDA-NiS at 160 °C. The observed band edge of 3.66 eV (339 nm) which was blue shifted from the bulk NiS material, while the emission peak observed at 430 nm, displayed a red shift from the band edge. A comparing of absorption band edge of PAA-capped NiS and HDA-capped NiS, suggested low band edge in HDA-capped NiS might be caused by good capping ability of HDA at this temperature. The tailing absorption spectrum suggests poorly dispersed particles which are confirmed by the broad emission peak.

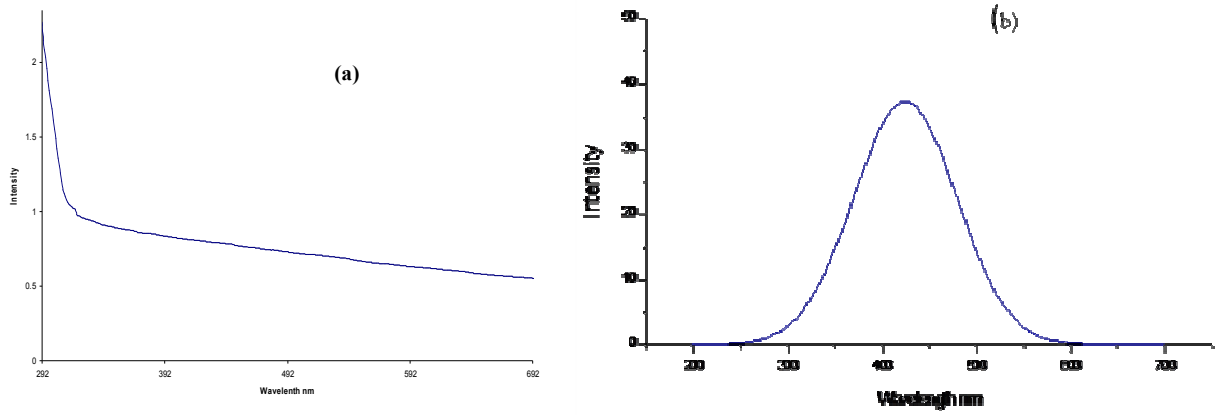


Figure 32: Absorption (a) and emission (b) spectra of HDA-capped NiS nanoparticles synthesized from complex VI at 160 °C.

3.3.2 Structural characterisation

The TEM images and corresponding particle size distribution histograms in Figure 33 show HDA-capped CdS nanoparticles prepared at 120 and 160 °C from complex IV. Figure 33 (a) and

(b) shows HDA-capped CdS at 120 °C with dots-shaped particles which have an average size of 19 nm which is indicated in its distribution curve. The particles are monodisperse which was shown by a sharp excitonic peak in its absorption spectrum. When the temperature was raised to 160 °C (Figure 33 (a)), morphology of particles changed to spheres, the average size of particles was about 19 nm. Temperature has proven to have an effect morphology of particles. The particle size distribution histogram is shown in Figure 33(b).

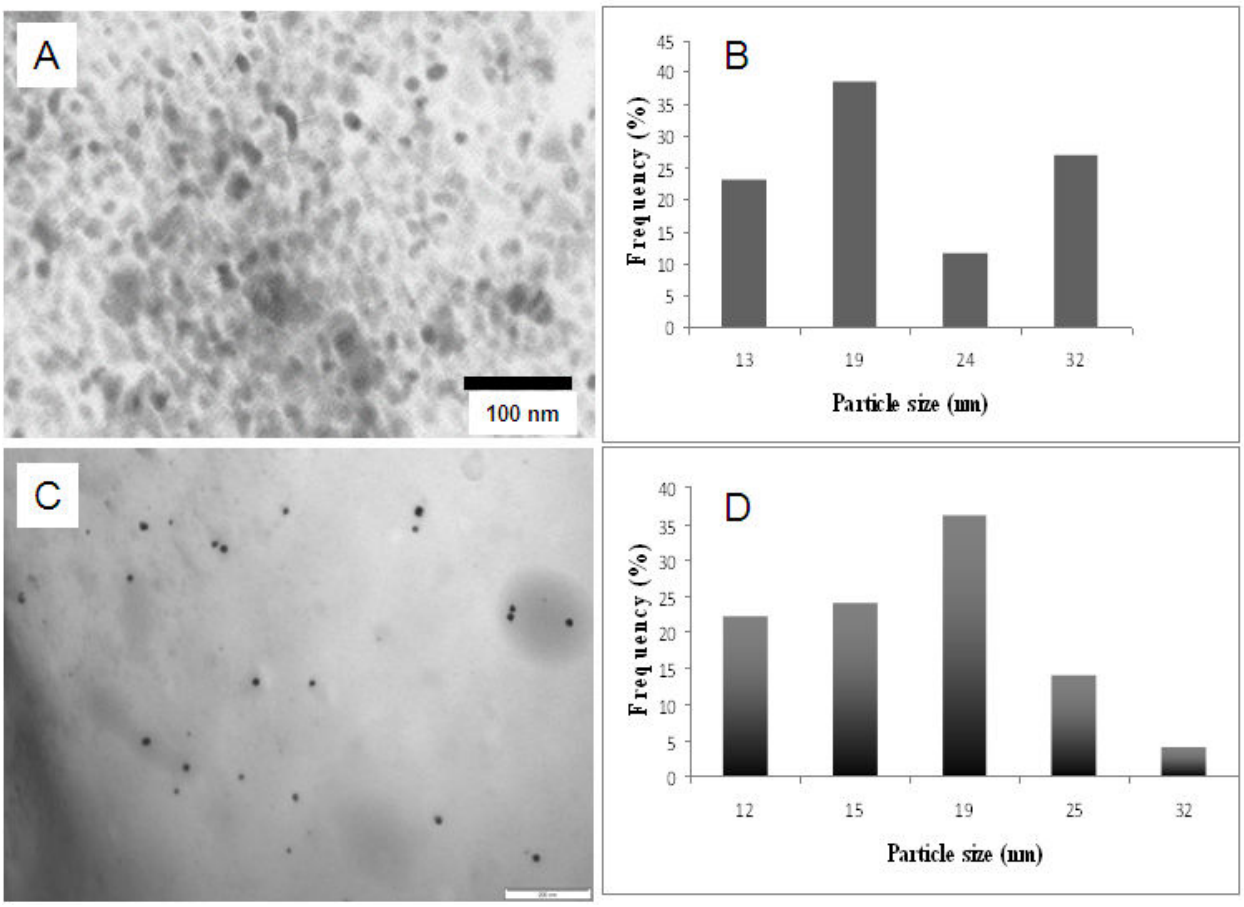


Figure 33: TEM images and corresponding particle size distribution histograms of HDA-capped CdS nanoparticles from complex IV, prepared at 120 °C (a), (b), and at 160 °C (c), (d).

The morphology of HDA-capped MnS nanoparticles at different temperatures are shown in Figure. 34. At 120 °C, HDA-capped MnS nanoparticles shows small polydispersed

nanoparticles with no definite shape. When the temperature was raised to 160 °C, needle-like nanoparticles of 8-9.4 nm of diameter range were obtained, which changed to rod-shaped at 200 °C of 11-14 nm size range. The effect of temperature on the morphology and size of HDA-capped MnS nanoparticles was observed which is in consistent with the findings of Furunuzo *et.al*[115]

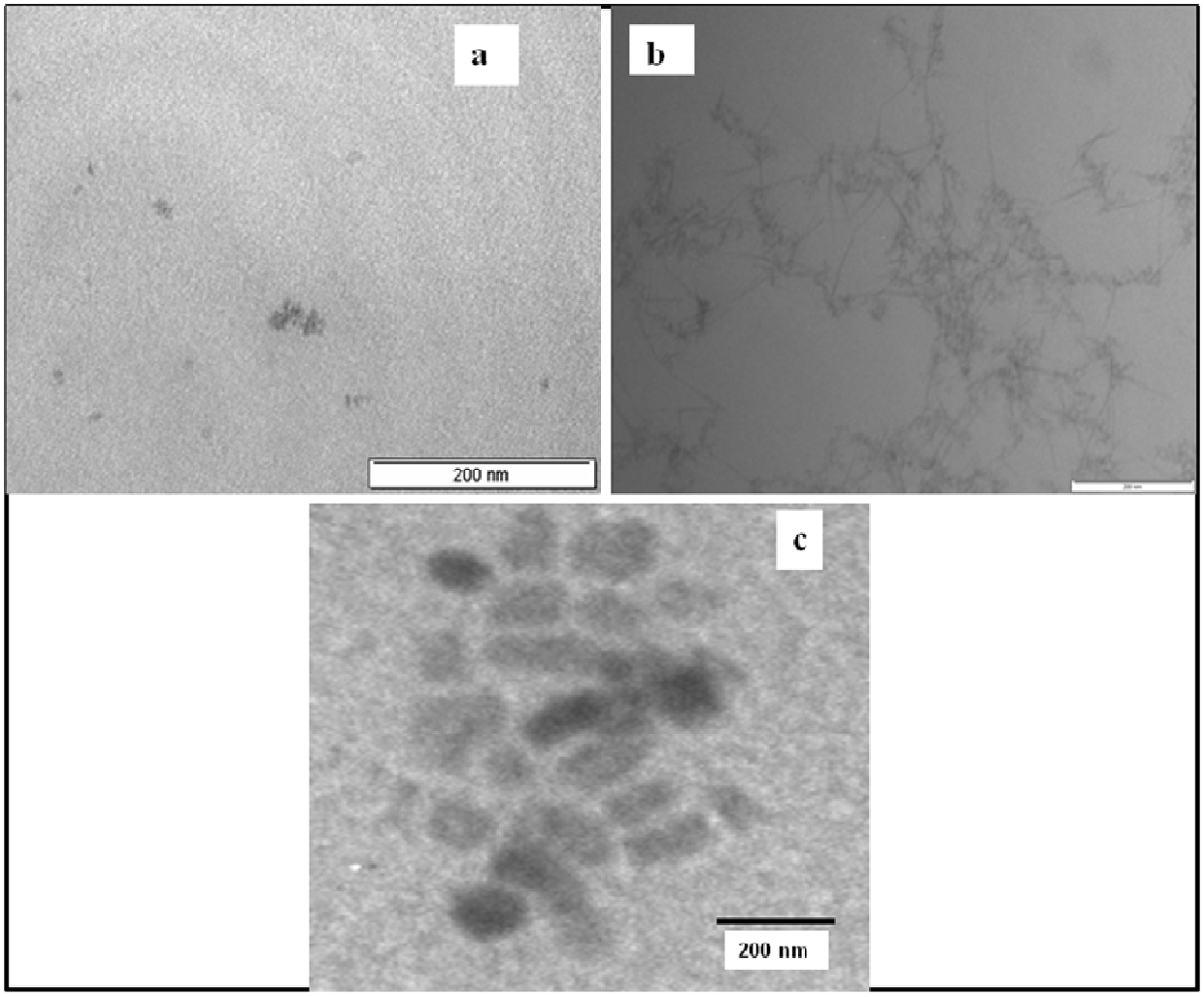


Figure 34: TEM micrographs of HDA-capped MnS nanoparticles from complex I, prepared at 120 °C (a), 160 °C (b) and 200 °C (c).

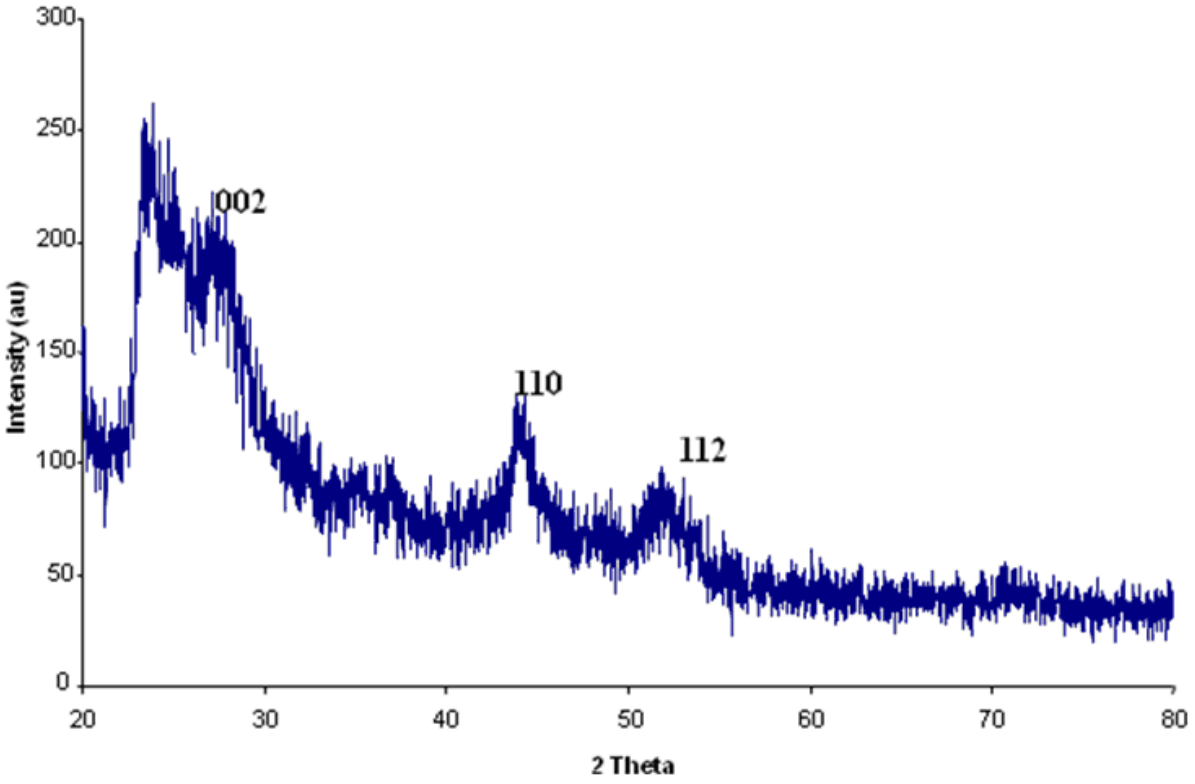


Figure 35: The XRD pattern of HDA-capped CdS nanoparticles from complex VI

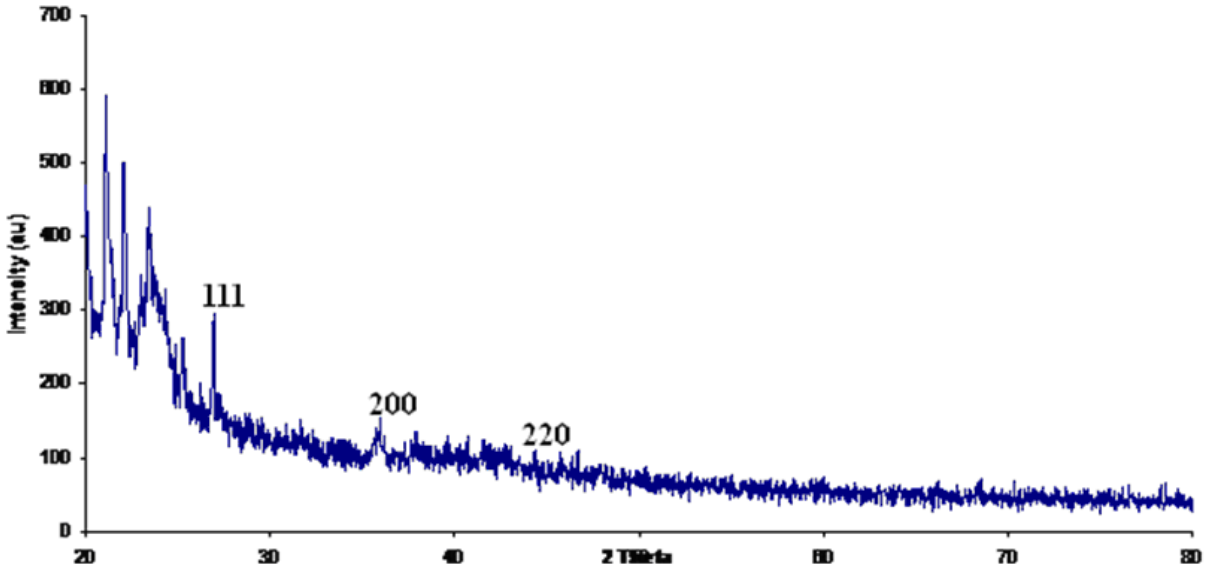


Figure 36: The XRD pattern of HDA-capped MnS nanoparticles from complex I

CdS nanoparticles can exist as either in the cubic, hexagonal or orthorhombic phases. The existence of the mixture of phases was reported by Bawendi *et al*[48] for CdSe nanoparticles. The XRD pattern of HDA- capped CdS nanoparticles prepared from complex IV is shown in Figure 35, with broad peaks confirming the small size of particles observed from TEM (Figure 33(a)). The CdS nanoparticles pattern can be indexed to a mixture of cubic and hexagonal phases, with 110 and 112 planes for a wurzite CdS clearly distinguishable in the diffraction pattern. The 002 plane confirm the existence of cubic phase. The XRD pattern of HDA-capped MnS nanoparticles is shown in Figure 36; the indexed peaks of 111, 200 and 220 clearly prove the existence of cubic phase.

3.4 PAA\TOPO-capped nanoparticles

3.4.1 Optical properties

The optical absorption and emission peaks of a tetrahydrofuran solution of the CdS nanoparticles obtained by the thermal decomposition of the precursor complex V, injected into a mixture of TOPO and PAA at 160 °C is shown in Figure 37. The sharp absorption edge shows a huge blue shift of 3.07 eV (403 nm) in relation of bulk CdS material which is in line with a blue shift observed by Nair *et al*[10]. Such a huge shift might be due to a co-capping of both PAA and TOPO.

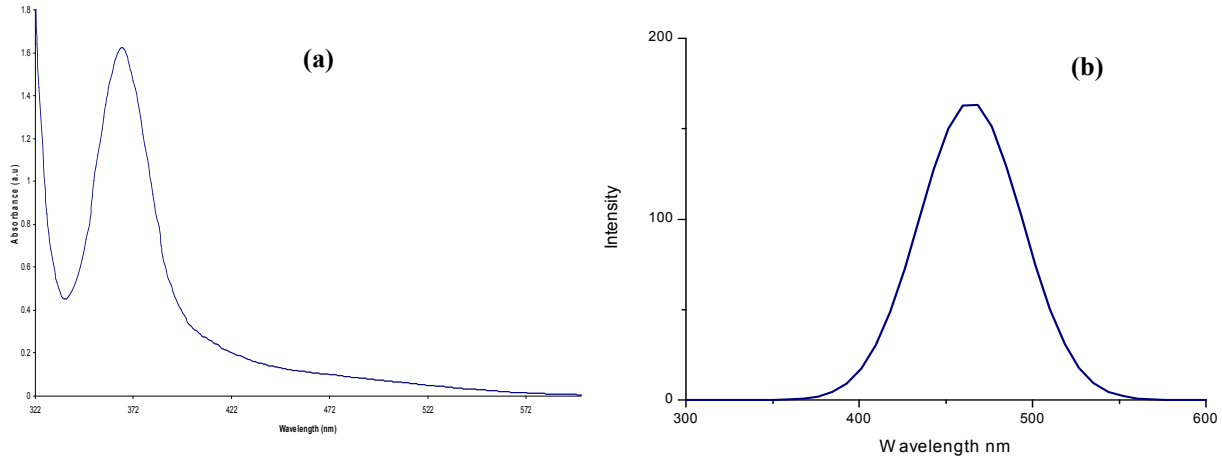


Figure 37: Absorption (a) and Emission (b) spectra of TOPO/PAA-capped CdS nanoparticles synthesized from complex V at 160 °C.

A shallow trap emission was observed with the close narrow emission peak of 410 nm to its material band edge of 403 nm. It is well known that the luminescence properties of nanoparticles are strongly dependent on the surface states, surface passivation and size distribution.[88, 116, 117] Thus the photoluminescence properties are environmentally condition-dependent. In this case two capping ligands are competing to interact with the surface of metal sulphide nanoparticles. PAA can provide P=O and COOH, while TOPO can provide a P=O. The competition of the two capping ligands creates a good environment for nanoparticles.

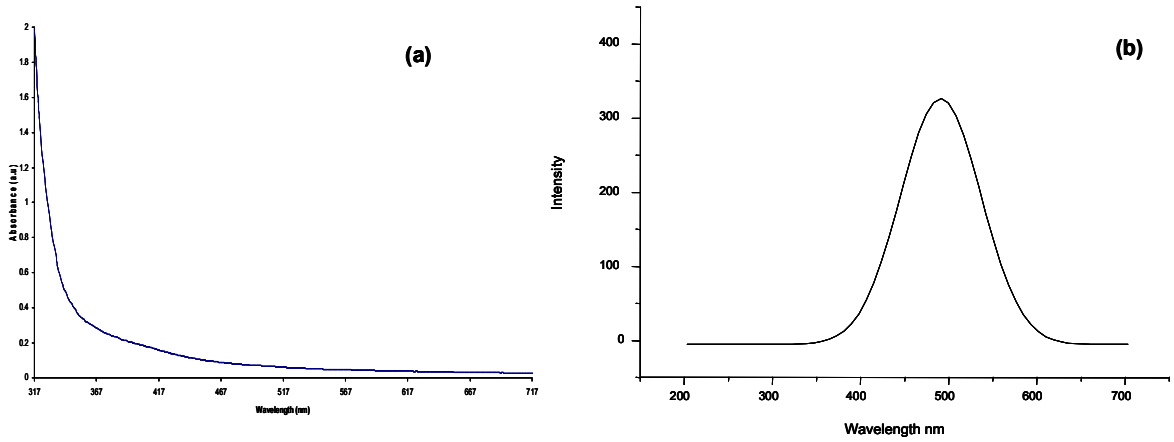


Figure 38: Absorption (a) and emission (b) spectra of TOPO/PAA-capped MnS nanoparticles synthesized from Complex II at 160 °C.

The absorption and the emission peak of TOPO/PAA capped MnS at 160 °C is shown in Figure 38. The prepared nanoparticles showed a band edge of 359 nm which is shifted to lower wavelength than its bulk counterpart of 3.1 eV (400 nm) and its emission peak was shifted to higher wavelength of its band edge. The shift confirms that the prepared material has a size in the nanoscale.

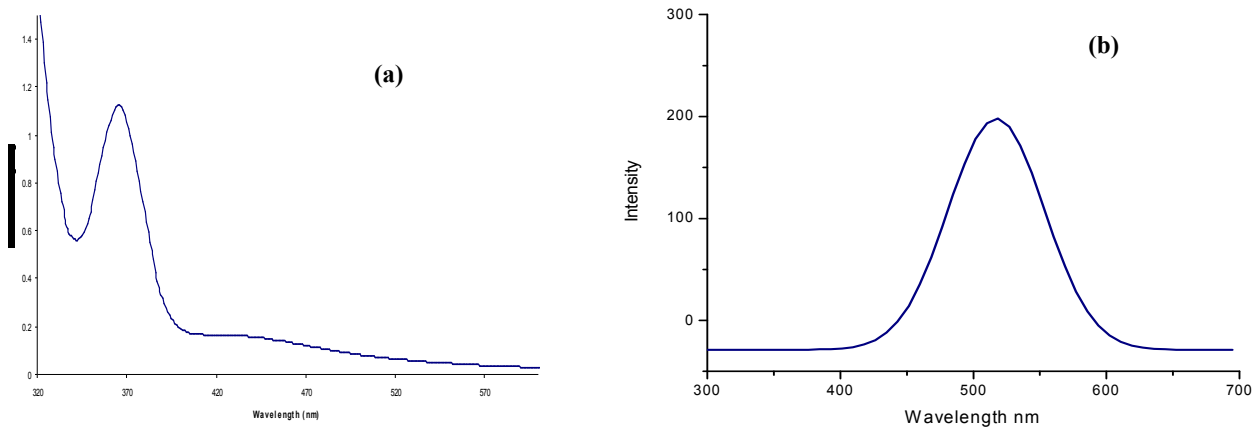


Figure 39: Absorption (a) and emission (b) spectra of TOPO/PAA-capped NiS nanoparticles synthesized from Complex VI at 160 °C.

The TOPO/PAA-capped NiS showed a band gap of 3.01 eV (412 nm) (Figure 39(a)) which was very close to the band gap observed in the PAA-capped NiS nanoparticles in (Figure 25(a)), this might suggest that PAA and TOPO/PAA are using the same functional group to interact or cap the surface of nanoparticles.

3.4.2 Structural characterisation

TEM image in Figure 40 shows nearly monodispersed spherical particles of TOPO/PAA CdS nanoparticles. The co-capping of the two ligands is also evident from the image with white spots observed at the centre of some particles. This indicate the presence of the two capping ligands are on the surface of the nanoparticles.

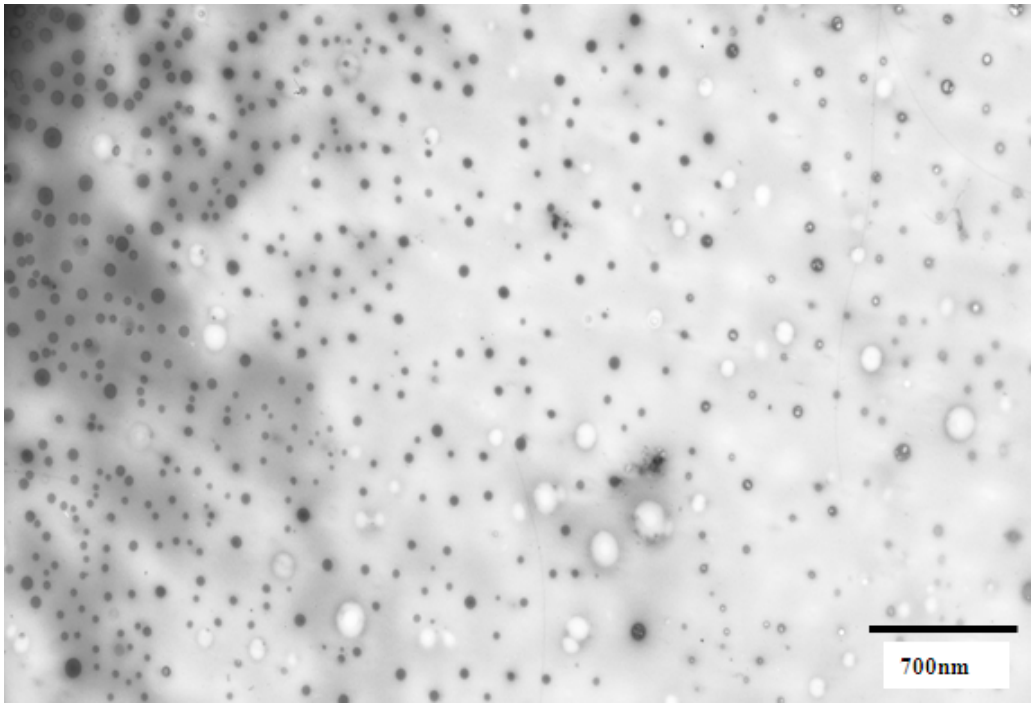


Figure 40: TEM image of TOPO\PAA-capped CdS nanoparticles from complex V at 160 °C

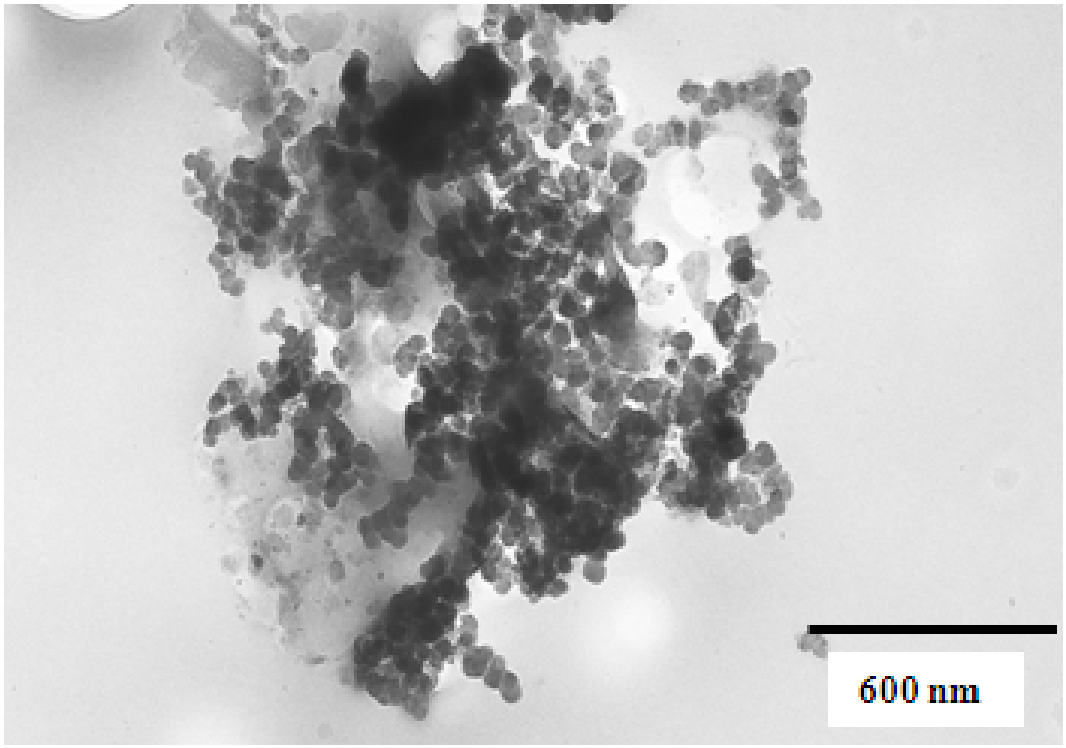


Figure 41: TEM image of TOPO\PAA-capped NiS nanoparticles from complex VI, at 160 °C.

The TEM image of TOPO\PAA NiS shown in Figure. 41 shows agglomerated particles which look like spherical in shape. This might also suggest that PAA and TOPO are using P=O to bind the surface of nanoparticles, that has a possibility of resulting in agglomerated particles because TOPO would have high affinity to interact with nanoparticles than PAA because of the long alkyl chain.

3.5 CONCLUSIONS

Trialkylthioureas and dialkylthioureas complexes of Cd, Ni and Mn were successfully synthesized for their use as single-source precursors for the preparation of metal sulphide nanoparticles. All the complexes were obtained in good yields, easy to prepare, air stable. The prepared complexes were subjected to a combination of spectroscopic techniques such as elemental analysis, infrared, NMR and TGA. All the complexes were used as precursors to synthesize metal sulphide nanoparticles.

The PAA-capped semiconductor nanoparticles were successfully synthesized varying the temperature. Although nanoparticles obtained from PAA as capping group displayed bigger sizes compared to other used organic capping groups, PAA shown an ability to be used as a capping group. The presence of COOH group could render this potential capping agent a suitable use in capping semiconductor nanoparticles for biological applications. The HDA and TOPO\PAA capped metal sulphide nanoparticles were prepared for the comparison reason with PAA-capped nanoparticles. HDA still showed good capping ability compared to TOPO\PAA and PAA. The morphology and size of nanoparticles were better in PAA and HDA (smaller rod-shaped) which showed an increase in size as temperature increased also forming long rods. While the mixture of PAA and TOPO showed bigger spherical particles.

3.6 RECOMMENDATIONS FOR FUTURE WORK

There are a number of properties that require special attention when one has to use a new capping agent in the preparation of nanoparticles using the single source precursor approach. The critical property of the ligand is its solubility, where the researcher has to look for the perfect solvent to precipitate the nanoparticles. The suitable solvent has to slightly solublize the capping group and nanoparticles must be insoluble. The XRD (X-ray diffraction) pattern was not used to analyze the PAA-capped nanoparticles because no precipitation was possible from the solvents such as THF, chloroform and methanol as the products tended to be oily and sticky. One of the solutions to this problem is to try PAA as a capping ligand with a different approach other than using the single source precursor method. Adding a long alkyl chain group to available binding site before capping can improve its capping ability and good results can be achieved.

The synthesis of complex based on one alkyl thiourea will provide comfort to compare the size and morphology of nanoparticles. An attempt to synthesize nanoparticles from a mixture of HDA and PAA was unsuccessful; firstly the two capping agents were mixed together in a three-necked flask and heated under nitrogen gas. The reaction produced a sticky whitish product, suggested that a condensation reaction occurred. The two capping agents were dissolved separately in THF, then mixed together and refluxed for 24 hours. The resulted white solid material was filtered and dried for characterization. The product melting point showed a huge difference in melting temperature range which suggested the presence of a mixture that contained starting reactants. It was concluded that the product contained two different compounds or that the two capping agents did not react at all. This requires further study where more characterization techniques will be used.

3.7. REFERENCES

1. S.E. Livingstone, in G. Wilkinson (Ed), Comprehensive Co-ordination Chemistry, vol 2, Section 16.6, Pergamon Press, Oxford, UK, 1987, pp. 639-640.
2. C. Sacht, M.S. Datt, S. Otto, A. Roodt, *J. Chem. Soc., Dalton Trans*. (2000), 727-733.
3. R.L. Zuckerman, R.G. Bergman, *Organometallic*s **19** (2000), 4795.
4. W. Henderson, R.D.W. Kemmitt, S. Mason, M.R. Moore, J. Fawcett, D.R. Russell, *J. Chem. Soc., Dalton Trans*. (1992), 59.
5. M. J. Moloto, N. Revaprasadu, P.O'Brien, M. A. Malik*, Materials in Electronics.,* **15**(5), 2004, p 313-316.
6. M. J. Moloto, N. Revaprasadu, G. A. Kolawole, P. O'Brien, M. A. Malik, *South African Journal of Science,* **101**(9/10), (2005), 463.
7. M. Krunks, J. Madarasz, L. Hiltunen, R. Mannonen, E. Mellikov, L. Ninisto*, Acta Chem. Scand.* **51** (1997) 294.
8. M. Krunks, T. Leskela, L. Ninisto, *Jpn. J. Appl. Phys.* **39** (Suppl. 39-1) (2000), 181.
9. N. Moloto , N Revaprasadu, M.J. Moloto, P. O'Brien, M. Heiwell*, Polyhedron ,* **26**, (2007), 3947-3955.
10. P.S. Nair, T Radhakrishnan, N Revaprasadu, G.A Kolawole, P. O'Brien, *Polyhedron,* **22**, (2003), 3129-3135.
11. E. Rodriguez-Fernandez, E. Garcia, M.R. Hermosa, A. Jimenez-Sanchez, M.M. Sanchez, E. Monte, J.J. Criado*, J. Inorg. Biochem.,* **75** (1999), 181.
12. L. Beyer, J.J. Garcia, E. Garcia, F. Lessman, M. Merdade, R. Richter, E. Rodriguez, *Tetrahedron.,* **15** (1996), 6233.
13. I. Dechamps-Olivier, E. Guillon, A. Mohamadou, J.P. Babier*, Polyhedron,* **15** (1996), 947.

14. R.D. Campo, J.J. Criado, E. Garcia, M.R. Hermosa, A.J. Sanchez, J.L. Manzano, E. Monte, E. Rodriguez-Fernandez, F. Sanz, *J. Inorg. Biochem.* **89** (2002), 74.

15. M. Dominguez, E. Antico, L. Beyer, A. Aghirre, S. Gracia-Granda, V. Salvado, *Polyhedron.* **21** (2001) 1429-1437.

16. R.D. Adams, M. Huang, J.H. Yamamoto, L. Zhang, *Chem. Ber.* **129** (1996), 137.

17. U. Bodensieck, Y. Carraux, H. Stoeckli-Evans, G. Suss-Fink, *Inorg. Chim. Acta* **195** (1992), 135.

18. P. Piraino, G. Bruno, G. Tresoldi, G. Faraone, G. Bombeiri, *J. Chem .Soc., Dalton Trans.* (1983), 2391.

19. P.L. Watson, J.A. Albanese, J.C. Calabrese, D.W. Overnal, R.G. Smith, *Inorg. Chem.* **30** (1991), 4638.

20. M. Lipowska, B.L Hayes, L. Hansen, A. Taylor Jr, L.G. Marzilli, *Inorg. Chem.* **35** (1996), 4227.

21. M. Lipowska, L. Hansen, A. Taylor Jr, L.G. Marzilli., *Inorg. Chem*. **35** (1996), 4484.

22. M.P. Coles, D.C. Swenson, R.F. Jordan, V.G. Young Jr., *Organometallics* **17** (1998), 4042.

23. L.A. Hoferkamp, G. Rheinwald, H. Stoeckli-Evans, G. Suss-Fink*., Organometallics* **15** (1996), 704.

24. S.D. Robinson, A. Sahajpal, J.W. Steed., *J. Inorg. Chim. Acta* **306** (2000), 205.

25. T. Phuong, t. Khac-Minh, N.T. Van Hal, H.T. Phuong, *Bioorg. Med. Chem. Lett.* **14** (2004), 653-656.

26. O.F. Huebhr, J.L. Marsh, R.H. Mizzoni, R.P. Mull, D.C. Schroeder, H.A. Troxell, C.R. Scholz, *J. Am. Chem. Soc*. **75** (1953), 2274-2275.

27. K. Ramadas, G. Suresh, N. Janarthanan, S. Masilamani, Pestic. Sci. **52** (1998), 145-151.

28. J.J. Criado, E. Rodriquez-Fenandez, E. Garcia, M.R. Hermosa, E. Monte*, J. Inorg. Biochem*. **69** (1998), 113-119.

29. D.C. Schroeder, *Chem. Rev.* **55** (1955), 181-228.

30. R.P. Rao, *Indian J. Appl. Chem.* **23** (1960), 110.

31. V.K. Madan, A.D. Taneja, *J. Indian Chem. Soc*. **68** (1991), 471.

32. S. Link, Z.L Wang and M.A. El-Sayed, *J. Phys. Chem B;* **103** (1999), 3529.

33. M. J. Hosteller, C. J. Zhong, B. K. H. Yen, J. Anderegg, S. M. Gross, N. D. Evans, M. Potter and R. W. Murray*, J Amer. Chem Soc.,* **120** (1998), 9396.

34. Y. Wang, H. Liu and H. Toshima*, J. Phys. Chem.,* **100** (1996), 19533.

35. M. T. Reetz, R. Breinbauer, and K. Wanniger, *Tetrahedron Lett.,* **37** (1996), 4499.

36. L. Z. Zhang, W. Sun, and P. Cheng, *Molecules.,* **211** (2003), 8, 220.

37. A. A. Bol, and A. Meijerink, *J. Lumin.,* **87** (2000), 315

38. X. Gong, W. J. Chen, P. F. Wu, W. K. Chan, *Appl. Phys. Lett.,* **73** (1998), 2875

39. R. N. Bhargava, D. Gallgher, X. Hong, A. Nurmiko*, Phys, Rev, Lett.,* **72**, (1994), 416

40. P. S Nair, T. Radhakrihsnan, N. Revaprasadu, G. A. Kolawole, and P. O'Brien*, Chem,. Commun;* (2002), 564

41. C. Mao, J. Qi, A. M. Belcher, *Adv. Funct. Mater.,* **13**(8), (2002), 421

42. J. Wu, Y Jiang, Q. Li, X.Liu, Y. Qian*, J. Cryst. Growth.,***235** (2002), 421

43. L. Spendel, H. Hasse, H. Weller, and A. Henglein, *J. Amer. Chem. Soc;* **109** (1987), 5649.

44. L. Spendel, H. Weller, and A. Henglein*, J. Amer. Chem. Soc*; **109** (1987)(b), 6632.

45. M. L. Steigerwald, L E. Brus*, Annual. Rev. Mater. Sci;* **19** (1989), 471.

46. C. Petit, P. Lixon, and M. P. Pileni, *Annual. Rev. Mater. Sci;* **18**, (1990), 319.

47. C. B. Murray, K. R. Kagan, M. G. Bawendi*, Ann. Rev. Mater. Sci;* **30** (2000), 545.

48. M. G. Bawendi, M. L. Steigerwald, L. E. Brus, *Ann. Rev. Phys. Chem.,* **41**, (1990), 477.

49. T. Trinidade, and P. O'Brien*, Adv. Mater.*, **8** (1996), 161.

50. T. Trinidade, and P. O'Brien, Chem. Mater. , 9 (1997), 523.

51. N. Revaprasadu, M. A. Malik, J. Cartens, and P. O'Brien, *J. Mater. Chem;* **9** (1999), 2885.

52. P. S Nair, T. Radhakrihsnan, N. Revaprasadu, G. A. Kolawole, and P. O'Brien, *Polyhedron;* **22** (2003), 3129.

53. W. Cai, Z. Li and J Sui, *Nanotechnology*, **19** (2008), 465 - 606

54. C.B Murray, D.J. Norris, M.G. Bawendi, *J. Am. Chem. Soc,* **115** (1993), 8706.

55. D.V Talapin, A.L. Rogach, A. Kornowski, M. Hasse, H. Weller, *Nano Lett,* **1** (2001), 207.

56. Y.L. Hao, J.F. Yu, A. Gao*, J Mater. Chem*, **13** (2003), 1983.

57.N.L Shipkowtz , R.R. Bower, R.N. Appell, C.W. Nordeen, L.R. Overby, W.R. Roderick, J.B. Schleicher, and A.M. Von Esch, *Appl, Microbiol*, **26** (1964), 264.

58. L.R Overby, R.G. Duff, and J.C.H. Mao, *Annals New York Acad. Sci*. **284** (1976), 310-366.

59. J. Hay, S.M. Brown, A.T. Jamieson, F.J. Rixon, H. Moss, D.A. Dargan, and J.H. Subak-Sharpe, *J. Antimicrob. Chemother*. **3 (Suppl.A)** (1977), 63

60. J.C.H. Mao, E.E. Robishaw, and L.R. Overby, *J. Virol,* **15** (1957), 1281.

61. Hans Stuzi and D.D. Perrin, *J. Inorg. Biochem.***10** (1979), 4.

62. M. Brust, J. Fink, D. Bethel, D. J. Schriffren, M. Kiely, *J. Chem. Soc. Chem. Commun*. (1995), 1655.

63. J. Tanori, M. P. Pileni, *Adv. Mater*. **7** (1995), 862.

64. R. A. Andrievckii, *Russ. Chem. Rev*.,**63** (1994), 411.

65. A. Kornowski, M. Giersig, M. Vogel, A. Chemseddine, H. Weller, *Adv. Mater*. **5** (1993), 634.

66. A. Fojtik, A. Henglein, *Chem. Phys. Lett*. **221** (1994), 363.

67. A. Henglein, *Pure Appl. Phys*. **56** (1984), 1215.

68. R. Rossetti, R. Hull, J. M. Gibson*, J. Chem. Phys*. **82** (1985), 552.

69. M. Green, P. O'Brien, *J. Chem. Soc. Chem. Commun.* (1998), 2459.

70. V. K. La Mer, R. H. Dinegar, *J. Am. Chem. Soc*. **69** (1950), 2459.

71. T. Johnson, V. K. La Mer, *J. Am. Chem. Soc*. **69** (1947), 1184.

72. R. J. Hunter, *Foundations of Colloid Science*, Oxford University Press, **6th ed**., Oxford, **vol. 1,** (1993), pp. 13.

73. Y Wang, N. Herron, *J. Phys. Chem***.91** (1987), 257.

74. T. Cassagneau, G. B. Hix, D. J. Jones, P. Maireles-Torres, M. Rhomari, J. Roziere, *J. Mater. Chem*. **4** (1994), 189.

75. T. Abe, Y. Tichibana, T. Uematsu, M. Iwamoto, *J. Chem. Soc. Chem*. *Commun*.(1995), 1617.

76. M. E. Brenchley, M. T. Weller, Angrew. *Chem. Int. Ed .Engl*. **32** (1993), 1663.

77. G. Blasse, C. J. Dirksen, M. E. Brenchley, M. T. Weller, *Chem. Phys. Lett*. **234** (1995), 177.

78. H. J. Watkze, J. H. Fendler, *J. Phys. Chem* **91** (1997), 854.

79. C. Petit, T. K. Jain, F. Billoudet, M. P. Pileni, *Langmuir*, **10** (1994), 4446.

80. A. Khan-Lodhi, B. H. Robson, T. Towey, C. Herramann, W. Knoche, U. Thesing, *In The Structure, dynamics and equilibrium properties of colloidal systems*; D. M. Bloor, E. Wyn-Jones, Eds.; London, (1990), 373.

81. T. F. Towey, A. Khan-Lodhi, B. H. Robinson*, J. Chem. Soc. Faraday Trans***. 86** (1990), 3757.

82. B. A. Korgel, G. Monbouquette*, J. Phys. Chem*. **100** (1996), 346.

83. K. M. Choi, K. J. Shea, *J. Phys. Chem*. **98** (1994), 3207.

84. K. M. Choi, K. J. Shea, *J. Am. Chem. Soc*. **116** (1994), 9052.

85. J. P. Carpenter, C. M. Lukehart, S. R. Stock, J. E. Wittig, *Chem. Mater*. **7**. (1995), 201.

86. Y. Wang, A. Suna, W. Mahler, R. Kasowski*, J. Chem. Phys*. **87** (1987),7315.

87. Gao, Y. Yang, B. Yang, F. Bian, J. Shen, *J. Chem. Soc. Chem. Commun*. (1994), 2779.

88. M. Nirmal, C. B. Murray, M. G. Bawendi, *Phys. Rev*. **B50** (1994), 2293.

89. R. Tassoni, R. R. Schrock, *Chem. Mater*. **6** (1994), 744.

89. D. L. Klein, R. Roth, A. K. L. Lim, A. P. Alivisatos, P. L. McEuen, *Nature* , **389 (1997),** 699.

90. M. A. Reed, C. Zhou, C. J. Muller, T. P. Burgin, J. M. Tour, *Science,*.**278** (1997), 252.

91. S. J. Tans, A. R. M. Verschueren, C. Dekker, *Nature* **49,** (1998), 393..

92. C. Bell, G. Burnell, D. J. Kang, R. H. Hadfield, M. J. Kappers, M. G. Blamire, *Nanotechnology* **14** (2003), 630.

93. N. A. Melosh, A. Boukai, F. Diana, B. Gerardot, A. Badolato, P. M. Petroff, J. M. Heath, *Science* **112** (2003), 300.

94. Fritz, M. K. Baller, H. P. Lang, H. Rothuizen, P. Vettiger, E. Meyer, H. J. Guntherodt, C. Gerber, J. K. Gimzewski *Science* **288** (2000), 316

95. C. R. Henry, *Appl. Surf. Sci*. **164 (**2000), 252.

96. D. J. C. Yates, J. H. Sinfelt, *J. Catal.* **8** (1967), 348.

97. C. Corrolleur, F. G. Gault, D. Juttard, G. Maire, J. M. Muller, *J. Catal.* 27 (1972), 466.

98. T. R. Thurston, J. P. Wilcoxon, *J. Phys. Chem.* **11** (1999), 103.

99. H. Shinojima, J. Yumoto, N. Uesagi, S. Omi, Y. Asahara, *Appl. Phys. Lett*. **55** (1989), 1519.

100. J.W. Robinson, 5th (Ed), Undergraduate Instrumental Analysis, Marcel Dekker Inc, Newyork, 1995, pp 662.

101.D.A. Skoog, D.M. West, T.J. Holler, 7th (Ed), Analytical Chemistry, Saunders College Publishing 7th (Ed).pg 506-523 and 601-608.

102. C. B. Murray, D. J. Norris, M. G. Bawendi, *J. Am. Chem. Soc*, **115** (1993), 8706

103. H. Akaiwa, H. Kawamoto and M. Abe, J. *Inorg. Nucl. Chem.***34**, (1972), 1763.

104. R. Farran and J. E. House, J. *Inorg. Nucl. Chem.* **34** (1972), 2219.

105. J. Zsako, Cs. Varhelyi and E. Kekedy, J. *Inorg. Nucl. Chem.***28,** (1966), 2637.

106. S. K. Awasthi, K. L. Chawla and D. M. Chackraburtty, J. *Inorg. Nucl. Chem.* **35** (1973), 3805.

107. P. S. Gomm, A. E. Underhill and R. W. A. Oliver, J. *Inorg.Nucl. Chem.* **36** (1974), 3699.

108. K. Akabori, H. Matsuo and U. Yamamoto, 3. *Inorg. Nucl.Chem.* **35** (1973), 2679.

109. C. F. Bell and R. E. Morcom, J. *lnorg. NucL Chem.* **36** (1974) 3689.

110. D. H. Brown and R. T. Richardson, J. *Inorg. Nucl. Chem.* **35**, (1973), 755.

111. R. A. Baily and W. J. Tangredi, *L inorg, nucl. Chem*., **38**,(1976), 2221-2225.

112. Y. Jun, J. Choi, J. Cheon, *Angew. Chem., Int Ed* **45,** (2006), 3414

113. S.M. Lee, S.N. Cho, and J.W.Cheon, *Adv. Mater.,* **15** (2003), 441.

114**.** S. Goodwin, B Witkop, *J. Am. Chem. Soc***, 76** (1954), 5599-5603.

115. F. Furunuzo, D. Walsh, K. Sato, K. Sonda and J. Tanaka, *J. Mater. Sci.Lett.,***20** (2001)**,** 111-114.

116 L.H. Qu and X.G. Peng,*J. Am. Chem. Soc.,***124** (2002), 2049.

117. C.M. Donega, S.G.Hickey, S.F. Wuister, D. Vanmaekelbergh and A. Meijerink, *J. Phys. Chem.B,* **107** (2003), 489.